

9-17-2015

# Modular Heat Dissipation Technique for a CubeSat

Melih Eken

Follow this and additional works at: <https://scholar.afit.edu/etd>

Part of the [Space Vehicles Commons](#)

---

## Recommended Citation

Eken, Melih, "Modular Heat Dissipation Technique for a CubeSat" (2015). *Theses and Dissertations*. 1927.  
<https://scholar.afit.edu/etd/1927>

This Thesis is brought to you for free and open access by the Student Graduate Works at AFIT Scholar. It has been accepted for inclusion in Theses and Dissertations by an authorized administrator of AFIT Scholar. For more information, please contact [richard.mansfield@afit.edu](mailto:richard.mansfield@afit.edu).



**MODULAR HEAT DISSIPATION TECHNIQUE FOR A CUBESAT**

THESIS

Melih Eken, Captain, Turkish Air Force

AFIT-ENY-15-S-73

**DEPARTMENT OF THE AIR FORCE  
AIR UNIVERSITY**

**AIR FORCE INSTITUTE OF TECHNOLOGY**

**Wright-Patterson Air Force Base, Ohio**

**DISTRIBUTION STATEMENT A.**  
APPROVED FOR PUBLIC RELEASE; DISTRIBUTION UNLIMITED.

The views expressed in this thesis are those of the author and do not reflect the official policy or position of the Turkish Air Force, Republic of Turkey Government, United States Air Force, Department of Defense, or the United States Government. This material is declared a work of the U.S. Government and is not subject to copyright protection in the United States.

AFIT-ENY-15-S-73

MODULAR HEAT DISSIPATION TECHNIQUE FOR A CUBESAT

THESIS

Presented to the Faculty

Department of Aeronautics and Astronautics

Graduate School of Engineering and Management

Air Force Institute of Technology

Air University

Air Education and Training Command

In Partial Fulfillment of the Requirements for the

Degree of Master of Science in Space Systems

Melih Eken, BS

Captain, TurAF

July 2015

**DISTRIBUTION STATEMENT A.**  
APPROVED FOR PUBLIC RELEASE; DISTRIBUTION UNLIMITED.

AFIT-ENY-15-S-73

MODULAR HEAT DISSIPATION TECHNIQUE FOR A CUBESAT

Melih Eken, BS

Captain, TurAF

Committee Membership:

Maj James L. Rutledge, PhD  
Chair

Eric D. Swenson, PhD  
Member

Richard G. Cobb, PhD  
Member

### **Abstract**

Due to their low cost, flexibility, short build-to-operations cycle and capabilities, CubeSats are a popular approach to gain access to space. In recent years, interest in larger scale CubeSats, such as 3U and 6U, has increased. This increased interest is resulting in new challenges including generating more power and correspondingly, radiating more waste heat from the CubeSat.

In this research, a modular approach was developed to dissipate heat from thermal energy generating components in a CubeSat in order to prevent excessive temperatures and meet responsive space needs. This research provides the details of the technique, which includes physical prototypes and implementation methodology. A box shape heat sink was designed, which is large enough to cover a common PC104 circuit board, with the purpose of dissipating the heat on the circuit board through thermal straps and various size radiators. The efficacy of the design was demonstrated using both computational and experimental methodologies.

To determine the heat transfer behavior of a 6U CubeSat, computational predictions were compared against experimental results collected in a Thermal Vacuum Chamber (TVAC). Subsequently, the validated CubeSat computational model was used to design a modular heat dissipater. Validation and performance experiments of the heat dissipater were conducted using prototypes of the design. All computational models used in this research were validated within steady state with  $T_{error} \leq 4$  °C. Finally, computational orbit performance predictions of the heat dissipater were made. These

predictions revealed that the temperature of a heat generating custom PC104 circuit board can be reduced from 116.8 °C to 12.2 °C on a sample hot case orbit with the design created in this research. Alternatively, it is possible to increase the power of the processors on the circuit board more than 400% without exceeding the temperature acquired without the heat dissipater design. Due to its modular approach, this design can be used in any CubeSat.

## **Acknowledgments**

I would like to thank my research advisor, Major James L. Rutledge, for his guidance and support. I would also thank Dr. Eric D. Swenson, Dr. Richard G. Cobb, Christopher A. Sheffield, Philip D. Smith, Captain Daniel M. Hatzung, Jorge Luis Urena Sarita, Jan LeValley, and Brian Crabtree for their continuous assistance and support during this research.

Finally, I would like to thank my wife and daughter. Nothing would have been possible without their love.

Melih Eken



## Table of Contents

	Page
Abstract .....	iv
Table of Contents .....	vii
List of Figures .....	ix
List of Tables .....	xii
List of Symbols .....	xiii
List of Acronyms .....	xiv
I. Introduction .....	1
Research Objective .....	3
II. Literature Review .....	5
Heat Transfer .....	5
Thermal Environment of the Earth Orbit .....	12
Spacecraft Thermal Design .....	13
Spacecraft Thermal Analysis .....	16
Spacecraft Thermal Testing .....	20
CubeSat Thermal Design Research Overview .....	22
Summary .....	24
III. Methodology .....	25
Experimental Test Methodology .....	25
Computational Simulation Methodology .....	30
Test Articles and Experiments .....	38
Baseline Experiments and Simulations .....	46
Heat Dissipater Design Process .....	52
Summary .....	72

IV. Analysis and Results.....	73
Results of Chassis Only Experiment and Simulation (ET-A and CS-A) .....	73
Results of Chassis with Heaters Experiment (ET-B) and Sample CubeSat Power Level Determination Experiment (ET-C).....	79
Results of Sample CubeSat Tests (ET-D and CS-D) .....	80
Experimental and Computational Results of the Heat Dissipater Design.....	86
Orbit Performance Simulation Results of the Heat Dissipater .....	95
Summary.....	99
V. Conclusions and Recommendations .....	101
Conclusions of Research .....	101
Recommendations for Future Research.....	106
Appendix A: Technical Drawing of the Heat Dissipater Box .....	108
References.....	111

## List of Figures

	Page
Figure 1: Spectral Blackbody Emissive Power (Evans et al., 2014) .....	9
Figure 2: Front View of TVAC .....	26
Figure 3: Open Door View of Chamber .....	27
Figure 4: Front View of Thermal Vacuum Control Enclosure and Main Screen.....	28
Figure 5: Pressure Control Screen .....	29
Figure 6: Temperature Control Screen .....	30
Figure 7: TD Thin Shell Data Dialog Box.....	31
Figure 8: Contactor Example .....	32
Figure 9: Heating Rate Case Manager Dialog Box and Orbit Dialog Box.....	34
Figure 10: Orbit Display .....	35
Figure 11: Set HR Dataset Properties Dialog Box.....	36
Figure 12: Editing Case Set Dialog Box.....	37
Figure 13: Two Views of the Chassis Hung from the Test Stand .....	39
Figure 14: Circuit Boards with Resistors.....	40
Figure 15: The Sample 6U CubeSat .....	40
Figure 16: Experiment Pictures and TD Screenshots of ET-A and CS-A.....	47
Figure 17: Photographs of ET-B.....	48
Figure 18: Photographs and TD Screenshots of the ET-D and CS-D.....	50
Figure 19: Three Views of the First Heat Dissipater Design in the Sample CubeSat .....	53
Figure 20: The First Heat Dissipater Design .....	54
Figure 21: The Final Design of the Heat Dissipater .....	56

Figure 22: Frequency Analysis Results of the Final Heat Dissipater Design.....	56
Figure 23: The Heat Dissipater Thermal Model.....	57
Figure 24: Thermal Conductive Pad on the Surfaces .....	59
Figure 25: The Thermal Straps Soldered to Heat Dissipater and the Radiator (ET-F).....	60
Figure 26: The Sample CubeSat with Black Photo Tape Covered 1U Radiator .....	61
Figure 27: Soldered Copper Braids Used in ET-F, ET-G, and ET-H.....	61
Figure 28: Photographs of ET-I and ET-J.....	63
Figure 29: The Heat Dissipater with a 1U Size Side Radiator and a 1U Size Deployable Radiator (ET-K) .....	64
Figure 30: Photographs of ET-K.....	65
Figure 31: The Heat Dissipater with 1U Size Radiator .....	65
Figure 32: Photographs of SHCB .....	66
Figure 33: Photographs of ET-M.....	67
Figure 34: Photographs of ET-O.....	69
Figure 35: Two views of the 0° Beta Angle Orbit, The Sample Cold Case .....	70
Figure 36: Two views of the 90° Beta Angle Orbit, the Sample Hot Case.....	71
Figure 37: Thermocouple Positions for ET-A and CS-A .....	74
Figure 38: Temperature Color Post-processing Figures of the -10 °C CS-A.....	75
Figure 39: Temperature Color Post-Processing Figures of the 30 °C CS-A.....	76
Figure 40: Temperature Color Post-Processing Figures of the 60 °C ET-A and CS-A....	77
Figure 41: Thermal Image of the Circuit Board in Ambient Pressure and Room Temperature .....	81
Figure 42: Steady State Test Result Comparisons for the 1.8W ET-D and CS-D.....	83

Figure 43: Steady State Test Result Comparisons for the 4.5W ET-D and CS-D.....	84
Figure 44: The Temperature Color Post-Processing Figures of CS-H .....	94
Figure 45: Temperature Color Post-Processing Figures of CS-P, CS-Q, and CS-R .....	96
Figure 46: Temperature Color Post-Processing Figures of CS-S, CS-T, and CS-U.....	98
Figure 47: Technical Drawing of the Heat Dissipater Box.....	110

## List of Tables

	Page
Table 1: Test Specifications and Explanations .....	42
Table 2: T= -10 °C ET-A and CS-A Steady State Temperature Result Comparison.....	75
Table 3: T= 30 °C ET-A and CS-A Steady State Temperature Results Comparison.....	76
Table 4: T= 60 °C ET-A and CS-A Steady State Temperature Results Comparison.....	78
Table 5: Temperature Errors of the ET-A and CS-A for All Steady State Test Points ....	78
Table 6: Steady State Result Comparison of the ET-B and ET-C .....	80
Table 7: 1.8W ET-D and CS-D Steady State Result Comparison.....	85
Table 8: 4.5W ET-D and CS-D Steady State Result Comparison.....	86
Table 9: Steady State Temperature Results of the Heat Dissipater Validation Experiments with THCB .....	87
Table 10: The Comparison of ET-D and ET-H for Different Power Levels .....	90
Table 11: Steady State Temperature Results of ET-L, ET-M and ET-N.....	91
Table 12: Steady State Temperature Result Comparison of ET-H and CS-H.....	94
Table 13: Steady State Temperature Predictions of CS-P, CS-Q, and CS-R .....	97
Table 14: Steady State Temperature Predictions of CS-S, CS-T, and CS-U.....	99

### List of Symbols

$A$	area, $m^2$	$T_s$	surface temperature, K
$C_p$	specific heat, $J/kg \cdot K$	$T_\infty$	fluid temperature, K
$C_o$	speed of light in vacuum, $2.998 \times 10^8$ m/s	$\alpha$	absorptivity
$E$	emissive power per area, $W/m^2$	$\varepsilon$	emissivity
$E_b$	blackbody emissive power per area, $W/m^2$	$\lambda$	wavelength, $\mu m$
$\dot{E}_g$	rate of energy generation, W	$\rho$	mass density, $kg/m^3$ ; reflectivity
$\dot{E}_{st}$	rate of increase of energy stored within a control volume, W	$\sigma$	Stefan-Boltzmann constant, $5.67 \times 10^{-8} W/m^2 \cdot K^4$
$G$	irradiation, $W/m^2$	$\tau$	transmissivity
$G_{abs}$	absorbed incident radiation heat flux, $W/m^2$		
$h$	convection heat transfer coefficient, $W/m^2 \cdot K$ ; Planck constant, $6.6256 \times 10^{-23}$ J·s		
$I$	radiation intensity, $W/m^2 \cdot sr$ ;		
$k$	thermal conductivity, $W/m \cdot K$ ; Boltzmann constant, $1.381 \times 10^{-23}$ J/K		
$L$	length, m		
$q$	heat transfer rate, W		
$\dot{q}$	rate of energy generation per unit volume, $W/m^3$		
$q''$	heat flux, $W/m^2$		
$T$	temperature, K		

## List of Acronyms

AFIT	Air Force Institute of Technology
AO	Atomic Oxygen
CR	Computational Result
CT	Computational Simulation
CSRA	Center for Space Research and Assurance
DoD	U.S. Department of Defense
ET	Experimental Test
ER	Experimental Result
FDM	Finite Difference Method
FEM	Finite Element Method
GEVS	General Environmental Verification Standard, NASA
GMM	Geometric Math Model
IR	Infrared
LDEF	Long Duration Exposure Facility
LEO	Low Earth Orbit
MLI	Multilayer Insulation
NASA	National Aeronautics and Space Administration
SHCB	Single-Heater Circuit Board
TD	C&R Thermal Desktop®
THCB	Ten-Heater Circuit Board
TMM	Thermal Mathematical Model
TVAC	Thermal Vacuum Chamber System



U.S.	United States
UV	Ultraviolet
VUV	Vacuum Ultraviolet



# **MODULAR HEAT DISSIPATION TECHNIQUE FOR A CUBESAT**

## **I. Introduction**

Spacecraft analyses and tests are extremely important for exposing potential failures before launch and ensuring successful on-orbit operation. Environmental tests validate that space systems can survive in the harsh space environment and operate even in the worst cases during their lifetime. Thermal testing, a part of environmental testing, demonstrates the performance of the space system and its components in expected and stressing thermal environments.

The Air Force Institute of Technology (AFIT) Center for Space Research and Assurance (CSRA) has a Thermal Vacuum Chamber System (TVAC) with a solar simulator sized for thermal testing small satellites such as CubeSats. CubeSats are the new generation of small satellites, developed by a number of universities and organizations to accelerate small and low cost space experiment platforms [Heidt, 2000]. Between 2003, the first year CubeSats were launched, and 2012, 112 CubeSat-class missions were flown [Swartwout, 2013]. In addition to this, 197 CubeSat-class spacecraft were launched in 2013 and 2014 [Swartwout, 2015]. These data show that, CubeSats are gradually providing increased access to space. Today, due to their advantages, CubeSats are recognized for their potential utility by space and research agencies around the world including United States (U.S.) National Aeronautics and Space Administration (NASA), U.S. Department of Defense (DoD), National Science Foundation, and the U.S. National Reconnaissance Office [Asundi and Fitz-Coy, 2013].

However, Swartwout's analysis on CubeSats shows that the failure rate is almost 40% of all attempted launches. In addition to this, launch failures are also 20% in the years between 2000 and 2012 and the failure percentage approaches to 50% in university-led missions [Swartwout, 2013]. It can also be deduced from the analysis that on-orbit failures of University-CubeSats are approximately four times that of industry mission failures. Swartwout concluded that, one of the main reasons of high failure rate was lack of testing. Through analysis and testing of the CubeSats could doubtless reduce these failure rates.

To improve thermal analysis and validation techniques of the AFIT's future CubeSats, a computational model of the TVAC environment was generated by Hatzung at AFIT in 2014 [Hatzung, 2014]. However, this model was validated only by using a 10 in x 10 in. aluminum plate because of time constraints. Since the TVAC model was used in this research, the first element of this thesis is to provide a greater validation for Hatzung's model by using a more realistic test article, a 6U CubeSat chassis, for experiments and computational simulations with a steady state temperature error below 4 °C for selected set points. In experiments,  $dT/dt < 0.5 \text{ }^\circ\text{C/hr}$  was determined as thermal equilibrium and steady state criterion.

Another fact in Swartwout's analysis is that larger-scale CubeSats are becoming more popular, because of the need for larger payloads. Even though most of the CubeSats have been 1U-scale, most industry-built CubeSats have been 3U-size in recent years [Swartwout, 2013]. This increased interest in larger-scale CubeSats is resulting in new challenges including generating and storing more power. Correspondingly, dissipating

the heat from the high power components in the CubeSat becomes a challenge for thermal control.

Removing the waste heat from the components is critical, because it provides the opportunity to increase on-board processing, improves the reliability of the processor and increases the expected lifetime. The current processors on satellites are operating at 10% of their capability because of insufficient thermal management [Air Force Small Business, 2015]. Efficient thermal management may reduce processor temperatures and increase processing capability 10 times or more.

### **Research Objective**

The objective of this research is to develop a modular approach to dissipate heat from thermal energy generating sources on a circuit board by using thermal control hardware in a CubeSat. This approach can reduce time spent on design, building and testing of the CubeSat. The tasks created to accomplish this objective are presented below.

- Task 1: Provide further validation for the previously generated TVAC environment computational model by conducting experiments with more realistic test articles, because it was validated only by using a 10 in x 10 in. aluminum plate as explained previously. Conduct initial experiments with a 6U CubeSat chassis. All models need to be validated within steady state with  $T_{error} \leq 4$  °C compared to the experimental measurements.

- Task 2: Perform computational simulations of the heat transfer behavior on a sample 6U CubeSat within TVAC and compare predictions against TVAC experiment results for validation.

- Task 3: Create and analyze a modular heat dissipater design using the validated thermal model of the sample CubeSat.
- Task 4: Conduct validation and performance experiments of the heat dissipater.
- Task 5: Create orbit performance predictions of the heat dissipater, using the validated heat dissipater computational model.

This heat dissipation technique was designed to prevent excessive temperatures for the heat-generating component with a *plug-and-play* approach. Due to its modularity, this design can be used in any 1U stack in a CubeSat and reduce the design to launch period.

In the remainder of this thesis, Chapter 2 provides a theoretical basis by presenting background to heat transfer, thermal environment of the earth orbit, spacecraft thermal design and spacecraft thermal analysis and testing. Chapter 3 describes the computational and experimental methodologies were used. Chapter 4 examines the data and analyzes the results. Finally, Chapter 5 summarizes the results and offers recommendations for further research.

## **II. Literature Review**

The purpose of this chapter is to describe the theoretical basis for the research. First, heat transfer and the modes of it: conduction, convection, and radiation, are explained. Second, an overview of thermal environment of the Earth orbit is presented to provide a basic understanding of the terms direct solar, albedo, and Earth infrared (IR). Third, spacecraft thermal design process is expressed and some commonly used thermal control hardware is described. Fourth, spacecraft thermal analysis is introduced and spacecraft thermal testing is briefly expressed. Finally, an overview of CubeSat thermal design and analysis research in the last decade is provided.

### **Heat Transfer**

As it is well known, energy can be neither created nor destroyed. It can, however, be transferred by interactions of a system with the system's surroundings. These interactions are called heat and work. While thermodynamics, the science of energy, deals with the end states of the process, heat transfer provides information concerning the nature of the interaction or time rate at which it occurs. A general definition of heat transfer is thermal energy in transit due to a temperature difference. There are three modes of heat transfer: conduction, convection, and radiation [Ozisik, 1985].

#### ***Conduction***

Conduction is summarized based on the Incropera et al. text [Incropera et al., 2006]. This heat transfer mode is transfer of energy from the more energetic to the less energetic particles of a substance due to interactions between particles. It occurs in a solid or a stationary fluid. Rate equations quantify heat transfer process and may be used to

compute the amount of energy being transferred per unit time. Fourier's law is the rate equation for heat conduction and is expressed in three dimensions as

$$\mathbf{q}'' = -k\nabla T = -k\left(\frac{dT}{dx}\mathbf{i} + \frac{dT}{dy}\mathbf{j} + \frac{dT}{dz}\mathbf{k}\right) \quad \text{Equation 2.1}$$

where:

- $\mathbf{q}''$  Heat flux (W/m<sup>2</sup>)
- $k$  Thermal Conductivity (W/mK)
- $T$  Temperature (K)

Vector quantities are represented as bold letters. The heat flux vector  $\mathbf{q}''$  is the heat transfer rate in three directions per unit area.  $\frac{dT}{dx}$ ,  $\frac{dT}{dy}$ ,  $\frac{dT}{dz}$  are the temperature gradients. The parameter  $k$  is a thermophysical material property referred to as a transport property. For a prescribed temperature gradient, increasing thermal conductivity increases the conduction heat flux. The minus sign indicates that heat is always transferred in the direction of decreasing temperature gradient.

In case of a thermal energy generation within the system, the energy source term can be expressed as

$$\dot{E}_g = \dot{q} dx dy dz \quad \text{Equation 2.2}$$

where  $\dot{q}$  is the rate at which energy is generated per unit volume (W/m<sup>3</sup>). In addition, the energy storage term is represented as

$$\dot{E}_{st} = \rho c_p \frac{\partial T}{\partial t} dx dy dz \quad \text{Equation 2.3}$$

where  $\rho c_p \frac{\partial T}{\partial t} dx dy dz$  is the time rate change of the sensible (thermal) energy per unit volume. From the conservation of energy law and the first law of thermodynamics, energy is always conserved. From the conservation of energy requirement, the heat equation can be obtained.



$$\frac{\partial}{\partial x} \left( k \frac{\partial T}{\partial x} \right) + \frac{\partial}{\partial y} \left( k \frac{\partial T}{\partial y} \right) + \frac{\partial}{\partial z} \left( k \frac{\partial T}{\partial z} \right) + \dot{q} = \rho c_p \frac{\partial T}{\partial t} \quad \text{Equation 2.4}$$

Equation 2.4 is the general form of the *heat diffusion equation* and it is often referred to as the *heat equation*. This equation is the basic tool for heat conduction analysis in Cartesian coordinates.  $\dot{q}$  Is the energy generation term,  $(\rho c_p \frac{\partial T}{\partial t})$  is the energy storage term as explained before. The spatial and temporal temperature distribution  $T$  can be obtained from the solution of Equation 2.4.

### **Convection**

Convection is the energy transfer between a surface and a fluid moving over the surface. This mechanism of heat transfer takes place because of the motion of fluid relative to surface [Ozisik, 1985]. The equation

$$q'' = h(T_s - T_\infty) \quad \text{Equation 2.5}$$

where:

- $q''$  Convective heat flux (W/m<sup>2</sup>)
- $h$  Convection heat transfer coefficient (W/m<sup>2</sup> K)
- $T_s$  Surface Temperature (K)
- $T_\infty$  Fluid Temperature (K)

is the appropriate equation for the convection and referred to as *Newton's law of cooling*.

Convection heat transfer coefficient depends on conditions in the boundary layer such as surface geometry and thermophysical properties of fluid [Incropera et al., 2006].

Convective heat flux increases with increasing difference between surface and fluid temperature.

## ***Radiation***

Radiation heat transfer mode is summarized based on the Incropera et al. text in this chapter [Incropera et al., 2006]. Thermal radiation is electromagnetic radiation generated by thermal motion of charged particles in matter. Radiation is emitted by matter at a nonzero Kelvin temperature. Unlike conduction and convection, radiation energy transfer does not require the presence of a material medium. In fact, vacuum is the most efficient medium for radiation.

To evaluate the radiation, introducing the concept of the blackbody is necessary. A blackbody is an idealized physical body that absorbs all incident radiation, regardless of wavelength and direction. Additionally, no surface can emit more energy than a blackbody for a prescribed wavelength and temperature. *The Stefan-Boltzmann law* expresses the upper limit to the emissive power as

$$E_b = \sigma T_s^4 \quad \text{Equation 2.6}$$

where  $E_b$  is blackbody emissive power, energy is released per unit area ( $\text{W}/\text{m}^2$ ),  $T_s$  is the absolute temperature (K) of the surface, and  $\sigma$  is the Stefan-Boltzmann constant ( $\sigma = 5.67 \times 10^{-8} \text{ W}/\text{m}^2 \cdot \text{K}^4$ ). The spectral distribution of a blackbody is represented as

$$I_{\lambda,b}(\lambda, T) = \frac{2hc_0^2}{\lambda^5 [\exp((hc_0)/\lambda kT) - 1]} \quad \text{Equation 2.7}$$

where  $h = 6.6256 \times 10^{-34} \text{ J}\cdot\text{s}$  is the Planck constant,  $k = 1.3805 \times 10^{-23} \text{ J}/\text{K}$  is the Boltzmann constant,  $c_0 = 2.998 \times 10^8 \text{ m}/\text{s}$  is the speed of light in vacuum and  $T$  is the

absolute temperature of the blackbody (K). Blackbody spectral emissive power is known as *Planck distribution* and represented by the equation below.

$$E_{\lambda,b}(\lambda, T) = \pi I_{\lambda,b}(\lambda, T) \quad \text{Equation 2.8}$$

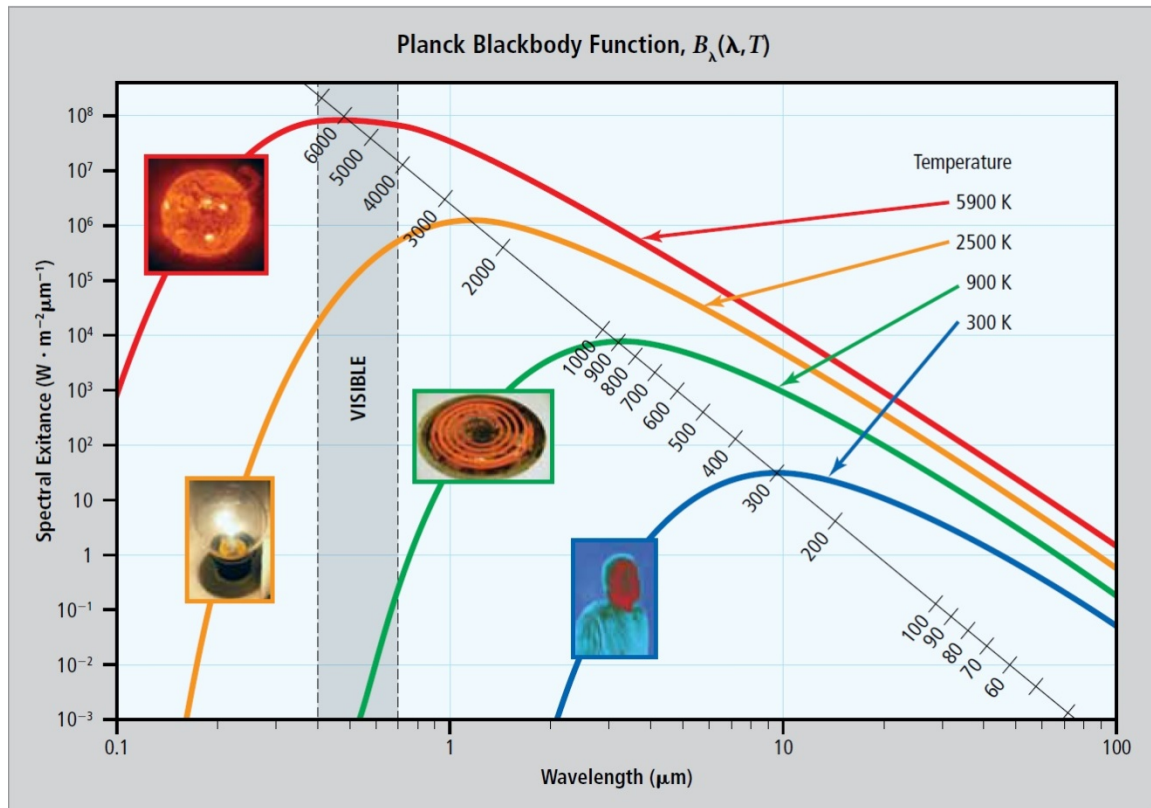


**Figure 1: Spectral Blackbody Emissive Power (Evans et al., 2014)**

A plot of Equation 2.8 for selected temperatures is shown in Figure 1. It can be noted that emitted radiation increases with increasing temperature at any wavelength and the sun may be approximated as a blackbody at 5800 K with its emission peak in the visible region. It can also be seen from the plot that, for any given temperature, Planck's

function has a peak wavelength. This relationship is expressed by *Wien's displacement law* as

$$\lambda_{max}T = 2897.8 \mu\text{m}\cdot\text{K} \quad \text{Equation 2.9}$$

and it can be deduced that with increasing temperature, shorter wavelengths become more prominent. Whereas a blackbody at 5800 K has its peak at 0.5  $\mu\text{m}$  in the visible region, for a blackbody at 300 K, peak emission occurs at 9.7  $\mu\text{m}$ , which is in the long wave infrared region.

A real surface emits less heat flux than a blackbody at the same temperature and this property is represented by the equation

$$E = \varepsilon \sigma T_s^4 \quad \text{Equation 2.10}$$

where  $\varepsilon$  is emissivity, a radiative property of a surface, which provides a measure of how efficiently the surface emits energy relative to a blackbody, with values in the range  $0 \leq \varepsilon \leq 1$ .

Absorptivity ( $\alpha$ ), a surface radiative property of a material is used to evaluate the rate at which radiant energy is absorbed per unit surface area. This rate is expressed as

$$G_{abs} = \alpha G \quad \text{Equation 2.11}$$

where  $G_{abs}$  is absorbed incident radiation ( $\text{W}/\text{m}^2$ ),  $G$  is irradiation ( $\text{W}/\text{m}^2$ ), and  $\alpha$  is surface absorptivity with values in the range  $0 \leq \alpha \leq 1$ . Reflectivity ( $\rho$ ) determines the fraction of the incident radiation reflected by a surface, and transmissivity ( $\tau$ ) is used to determine the fraction of the incident radiation transmitted by a semi-transparent surface. Each surface absorbs, reflects or transmits the incident energy. This can be represented mathematically as

$$\alpha_\lambda + \rho_\lambda + \tau_\lambda = 1 \quad \text{Equation 2.12}$$

It is obvious that, if the surface is opaque, it either absorbs or reflects the irradiation, so

$$\alpha_{\lambda} + \rho_{\lambda} = 1 \quad \text{Equation 2.13}$$

Additionally *Kirchhoff's law* states that, for real surfaces at a particular temperature, emission is equal to absorption at any particular wavelength, which can be expressed as

$$\varepsilon_{\lambda} = \alpha_{\lambda} \quad \text{Equation 2.14}$$

The thermal laws, stated in this chapter, are used by engineers to control the temperatures in spacecraft. Direct solar energy, which is mostly in the visible spectrum, is the most significant heat source on most spacecraft in Earth Orbit [Gilmore, 2002]. Spacecraft's outer surfaces generally emit in infrared region due to their temperatures as expressed by *Wien's displacement law*. Thus, absorptance in the visible spectrum and emittance in the IR region determine the temperature of the spacecraft. Designers select materials, surface finishes and coatings of exterior surfaces of the spacecraft with respect to solar absorptivity and IR emissivity values to set the desired temperature of the spacecraft.

Thermal absorption and emission of all inner and outer surfaces of the spacecraft can be selected for thermal management. IR emittance and solar absorptance are the two main surface properties for surface finishes as explained above. Since the main heat sources in the space environment, discussed below, are mainly in the visible region of the spectrum, materials on the outer faces with high solar absorptivity increase the

temperature of the spacecraft. On the other hand, outer surfaces with high IR emissivity radiate more heat to deep space and decrease the temperature of the spacecraft and vice versa. Thus, the designer can control the temperature using the advantage of the optical property differences of surface finishes between visible and IR regions.

### **Thermal Environment of the Earth Orbit**

Environmental heating plays a major role in spacecraft thermal control and the principal forms of environmental heating in Earth orbit are direct sunlight, sunlight reflected from the Earth (albedo), and IR energy emitted from the Earth [Gilmore, 2002]. For orbits with an altitude below 180 km, free molecular heating is also a significant form of environmental heating which is a result of bombardment of the vehicle by individual molecules in the outer reaches of atmosphere. Because of the fact that free molecular heating affects the space systems especially during launch ascent, most of the CubeSats are assumed to be thermally safe in the launch vehicles due to the launch vehicle shroud. An overview of direct solar, albedo, and Earth IR environmental heating forms follows.

#### ***Direct Solar***

Direct solar is usually the most significant heat source in spacecraft thermal control. The sun is a very stable energy source, which emits the radiation remaining constant within a fraction of 1% at all times in spite of the 11-year solar cycle. However, Earth has an elliptical orbit. The intensity of sunlight reaching Earth varies between 1322 and 1414 W/m<sup>2</sup> (approximately  $\pm 3.5\%$ ), depending on Earth's distance from the sun. Earth's average distance from the sun is 1 AU. The solar constant is the intensity of sunlight at 1 AU and equals 1367 (W/m<sup>2</sup>) [Gilmore, 2002].

### *Albedo*

Albedo is the fraction of the incident sunlight reflected back to space by Earth. Usually, reflectivity is greater over continental regions than oceanic regions and varies with local solar elevation angles, cloud coverage, or ice coverage. For a spacecraft in LEO, the orbital average albedo varies from about 24 to 42% of direct solar, depending on orbital inclination [Birur et al., 2014].

### *Earth IR*

Earth reflects some sunlight as albedo and rest of the sunlight is absorbed by the Earth and eventually reemitted as IR energy. IR energy emitted by Earth varies with factors such as local temperature of Earth's surface and the amount of cloud cover. For a spacecraft in LEO, the orbital average Earth IR varies somewhat depending on orbital inclination, but is generally about  $251 \text{ W/m}^2$  [Birur et al., 2014]. It must be noted that, since albedo is the reflection of sunlight, it is mostly in the visible spectrum. However, the IR energy emitted by Earth is approximately at the same wavelength with the energy emitted by spacecraft [Gilmore, 2002]. For this reason, Earth IR loads incident on a spacecraft cannot be reflected away radiators with special coatings, because the same coating would prevent to radiate waste heat away from the spacecraft.

### **Spacecraft Thermal Design**

Spacecraft thermal design is a process to control the thermal energy flowing throughout the spacecraft system in such a way that thermal requirements are met during the entire life of the mission. Furthermore, thermal designers should make the optimum use of resources such as mass, power, cost, and labor [Birur et al., 2014]. A thermal design process starts in the early conceptual phase of the design and proceeds through

various stages such as simple heat balance calculations, preliminary designs, more detailed computer analysis, detailed designs, integration of the hardware and finally thermal testing [Birur et al., 2014]. The main purpose of all efforts is to set and maintain all of the components within the allowable temperature range during the mission lifetime. Establishing a thermal design for a spacecraft is usually a two-part process. The first step is select a thermal design for the body, or basic enclosures, which serves as a thermal sink for all internal components, and the second step is to select thermal designs for various components located both within and outside the body [Gilmore, 2002].

Besides spacecraft thermal design challenges, CubeSat thermal design presents additional challenges such as less power, less volume for thermal control hardware, and smaller surface area compared to larger spacecraft. Although a wide range of thermal control hardware and techniques is available, to minimize weight, cost, and test complexity and due to power and volume restrictions, usually active thermal control components are avoided and the thermal control system for CubeSats is kept as simple as possible. To provide a basic understanding of spacecraft thermal design, this chapter introduces the common thermal control hardware.

### ***Thermal Control Hardware***

A wide range of hardware can be used to design the thermal subsystem and meet thermal requirements. The most common thermal hardware components used on any spacecraft are multilayer insulation (MLI) blankets, radiators, coatings, and heaters [Birur et al., 2014].

*MLI blankets* are used on the outer surfaces to prevent both excessive heat loss from a component and excessive heating from environmental fluxes, rocket plumes, and



other sources [Gilmore, 2002]. MLI blankets are typically made of several 0.25 mil thick metalized sheet layers separated by a mesh made of a low thermal conducting material [Birur et al., 2014].

*Radiators* reject waste heat to space by IR radiation, and occur in several different forms such as spacecraft structural panels, flat-plate radiators mounted to the side of the spacecraft, and panels deployed after the spacecraft is on orbit [Gilmore, 2002].

*Heaters* are active thermal control hardware, which protect components from cold temperatures and keep them within allowable temperature limits. Heaters are required when passive thermal techniques are not sufficient. The most common type of heater used on spacecraft is the patch heater, which consists of an electrical resistance element sandwiched between two sheets of flexible electrically insulating material such as Kapton [Wertz et al., 2011]. The patch heaters used on the spacecraft have some sort of control or switch. The most common control type is the thermostatic on-off control using a bimetallic mechanical thermostat, which opens or closes the heater circuit at a preset temperature [Birur et al., 2014].

*Surface finishes* are one of the most common thermal control components. Various materials with specific wavelength-dependent absorptivity and emissivity properties are used as thermal control coatings with different purposes. IR emittance and solar absorptance are the two main surface properties for surface finishes as discussed on page 11. In the Gilmore text considering these properties, thermal control surfaces are fallen into four basic categories with respect to their surface properties: solar reflector, solar absorber, flat reflector, and flat absorber [Gilmore, 2002]. Solar reflectors have a very low  $\alpha/\epsilon$  ratio (solar absorptivity / IR emissivity) such as white paint and second-

surface mirrors. On the contrary, solar absorbers have a high  $\alpha/\varepsilon$  ratio such as polished aluminum alloys and polished gold. Flat reflectors reflect energy throughout the spectral range in both the solar and IR regions. Aluminum paint and polished silver are examples for this type of surface. Flat absorbers absorb throughout the spectral range such as black paint.

### **Spacecraft Thermal Analysis**

The thermal design process is a combination of design selection and supporting analysis as emphasized before. Detailed thermal analysis is required to verify and refine the selected thermal design. The thermal engineer starts the thermal management process with establishing thermal design requirements, obtaining spacecraft design and details, determining heat dissipation, and identifying environmental and boundary conditions [Gilmore, 2002]. The first analysis can consist of simple calculations such as computing orbit average temperatures and power dissipation in the spacecraft. However, as the design progresses and becomes more detailed, computer simulations are needed for analysis. The thermal engineer needs to construct a detailed thermal model of the spacecraft to predict all subsystem temperatures under all expected environmental conditions. A description of a typical thermal model is included in this chapter to provide a basic understanding of thermal software calculations.

#### ***Thermal Model***

The thermal model development is introduced based on the text *Spacecraft Thermal Control Handbook* by Gilmore [Gilmore, 2002]. A detailed thermal analysis involves constructing a geometric mathematical model (GMM) and a thermal mathematical model (TMM), which serve different purposes. GMM is a mathematical

representation of the physical surfaces and is used to calculate radiation couplings between all surfaces in the model, as well as heating rates to each surface from external flux sources such as direct solar, albedo, and Earth IR. In this research, Autodesk's Thermal Desktop (TD) is used to construct the GMM of the 6U CubeSat. TMM is directly analogous to an electrical resistance-capacitance network and is used to predict instrument temperatures. The most common TMM code is Systems Improved Numerical Differencing Analyzer (SINDA), and as discussed in the next section, it is also used as a thermal analyzer by thermal desktop.

Thermal analysis software requires the user to define a thermal network system analogous to an electrical circuit. To achieve this requirement, the user subdivides the thermal system into finite subvolumes called *nodes*. The central nodal point of each subvolume is considered to represent the concentrated thermal properties of that node. Each node has two thermal-network elements: a temperature that is analogous to electrical potential, and a thermal mass that is analogous to electrical capacitance. Thermal analyzers, such as SINDA, usually use three types of nodes to define a thermal network:

- Diffusion node (finite thermal mass) has a finite capacitance, therefore, store and release energy over time. Thus, the temperature of the material can change because of heat flow into or out of the nodes.
- Arithmetic node (zero thermal mass) is a physically unreal quantity but its effective use with numerical solutions can often be helpful in interpreting results in such applications as surface temperatures, bondline temperatures, and node-coupling temperatures

- Boundary node (infinite thermal mass) is used to represent a boundary whose temperature is set and will not change such as deep space.

The placement of the nodes depends on some factors such as the points where temperatures are desired, the expected temperature distribution, and ease of computation. Usually, a minimum number of nodes is desired to verify design. The nodes also need to be spaced closely enough that the grid resolution becomes acceptable, particularly for unsteady or multi-dimensional heat transfer.

The objective of all thermal analysis codes, such as SINDA, is to solve the general heat equation (Equation 2.4). The two commonly used numerical solution approaches of heat transfer problems are the finite difference method (FDM) and the finite element method (FEM).

The FDM approximates the physical objects and makes some assumptions such as the nodes are isothermal and physical properties are constant within a node. Each finite difference node is located at the center of the mass. The heat equation is converted into a system of finite difference equations from an FDM mesh. The FDM is based on the Taylor series approximation. The numerical error associated with the calculation can be estimated through knowledge of the order of the Taylor series expansions.

The FEM is based on discretizing the structure or system into numerous elements. Even though each finite element model includes hundreds of elements similar to finite difference models, finite element models depend on geometry and application. Element nodes are typically located at the elements' corners. Parameter values, such as temperatures, are known or calculated at element nodes. Variations within the element

are calculated by interpolation functions. Thus the properties, such as temperatures, can vary across the element.

The FDM is extensively used for building spacecraft-system thermal models. Heat transfer problems that are primarily driven by radiation can be easily solved using the FDM. On the other hand, the FEM is generally used in structural analysis and it is excellent for solving thermal/stress problems. For example, using the FEM in thermal analysis of rocket nozzles is common.

Energy absorbed on surfaces of spacecraft and radiation interchange factors between surfaces are calculated by codes that use either the gray diffuse assumption or the Monte Carlo method. The codes using gray diffuse assumption assume that the emittance, absorptance, and transmittance of a surface are independent of wavelength and direction, and all energy from a surface is emitted and reflected diffusely. On the other hand, codes using Monte Carlo technique are not limited to these assumptions. Although Monte Carlo method can handle complex geometries, large detailed thermal models can greatly increase the execution time of the Monte Carlo software [Gilmore, 2002].

### ***Thermal Desktop***

Autodesk's thermal desktop (TD) is a thermal modeling program that allows a user to build, analyze, and post-process thermal models [C&R Technologies, 2013]. TD does thermal calculations using abstract network, finite difference, and finite element modeling methods. TD runs as an AutoCAD® application and CAD techniques for generating geometry can be used for generating thermal models. Monte-Carlo ray-tracing algorithm is used by TD to compute radiation exchange factors and view factors. SINDA/FLUINT, SINDA/G and ESATAN are thermal analyzer options.

SINDA/FLUINT is used as the analyzer in this research. The user can assign optical properties to thermal model surfaces. TD also provides a complete external heating environment definition and viewing facility, which allows users to do on-orbit analyses. Detailed usage information about TD is presented in Chapter 3.

### **Spacecraft Thermal Testing**

In a spacecraft thermal management process, selected thermal design is validated and thermally successful operation of the spacecraft is ensured by ground thermal tests. These tests simulate the expected flight environments for the spacecraft. Test facilities with vacuum are used to minimize non-flight thermal influences and simulate on-orbit environments. Test categories and test types for spacecraft are introduced in this chapter based on *Spacecraft Thermal Control Handbook* by Gilmore [Gilmore, 2002].

There are three test categories: development, qualification, and acceptance tests. *Development tests* are used to validate the design concepts and to reduce of risk in committing designs to hardware fabrication. Development test requirements are unique to test objectives and are not specified in military and commercial standards. These tests are also known as engineering tests. *Qualification tests* are conducted to demonstrate that the design and manufacturing process meet the requirements. Qualification tests simulate more severe conditions than expected and because of the severity of the test environment, qualification hardware is typically not flown. The test item for these tests is produced from the same drawings using the same materials. *Acceptance tests* provide quality control assurance against workmanship and material deficiencies. These tests are conducted after qualification tests and they prove the flightworthiness of the space system.

The test categories explained above include different types of tests such as thermal cycle tests, thermal vacuum tests, burn-in tests, and thermal balance tests. *Thermal cycle tests* subject the test article to a number of cycles of hot and cold temperatures in an ambient air or gaseous nitrogen environment whereas *thermal vacuum tests* do the thermal cycle tests in a vacuum environment. Thermal cycle tests' primary purpose is to screen environmental stress and reveal workmanship or material defects. On the other hand, thermal vacuum tests' primary purpose is performance verification, because these are conducted without convection and the most realistic ground simulation of the space environment. *Burn-in tests* are typically part of unit thermal cycle tests in which additional test time is applied. The unit is either held or cycled at an elevated hot temperature. *Thermal balance tests* have two purposes: verification of the thermal control subsystem and correlation of thermal analytic models. Correlation within 1 and 5 °C is typically desired depending on sensitivity [Birur et al., 2014]. Test phases simulate hot and cold flight conditions to gather steady-state temperature data. These data are compared to model predictions and they verify all aspects of the thermal hardware and software.

There are a series of documents which specify and describe the requirements for spacecraft thermal testing. *MIL-STD-1540D* is the document for US military applications. It was published in 1999. This document provides a guideline including expected methodologies and acceptance testing requirements without specifically directing test practices and procedures [Gilmore, 2002]. *GSFC-STD-7000A*, General Environmental Verification Standard (GEVS), document provides requirements and guidelines for environmental verification programs and describes methods for implementing those

requirements for NASA applications [NASA GEVS, 2013]. GSFC-STD-7000A directs thermal test practices and procedures in detail.

Even though CubeSats do not have long mission lives, thermal tests can certainly increase operational lifetime and reduce failure rates [Swartwout, 2013]. Various tests, such as qualification and acceptance tests, are typically conducted to verify the thermal design and to qualify the CubeSat for the mission.

### **CubeSat Thermal Design Research Overview**

Even though the interest in CubeSats has increased over the past decade, there is little publicly released research about thermal design and analysis of the CubeSats. The following paragraphs present some of the researches conducted in this area.

In 2004, Czernik at the University of Applied Sciences in Aachen, Germany, did a thermal design and the computational analysis of a 1U CubeSat called *Compass-1*, which is designed for a sun-synchronous LEO orbit [Czernik, 2004]. Active thermal control hardware, such as heaters, was included as well as passive hardware in the design. ANSYS software, which uses FEM to calculate nodal temperatures, was chosen for computational analysis, but experimental analysis was not performed to validate computational analysis in the research.

In 2009, Diaz-Aguado et al. at NASA Ames Research Center in Moffett Field, California designed the thermal control system of 3U CubeSat named *PharmaSat* [Diaz-Aguado et al., 2009]. The thermal design included active and passive thermal control hardware such as heaters, MLI, and low thermal conductance materials. Computational analysis was performed in TD and experimental tests conducted in a thermal vacuum chamber. Worst hot case and worst cold case results of the experimental



tests were validated with computational simulations with  $\pm 5$  °C error acceptance. However, Diaz-Aguado et al. provide little information about the thermal model.

Elhady, at National Authority for Remote Sensing & Space Science NARSS in Cairo, Egypt, did a thermal design and analysis of a 740 mm x 740 mm x 722 mm micro satellite in 2010 [Elhady, 2010]. The effect of thermal contact resistance on the satellite was also analyzed. An in-house developed software package was used for computational analysis. However, the research did not include the experimental analysis.

Smith conducted a thermal analysis of a CubeSat called *NPS-SCAT* at the Naval Postgraduate School (NPS) in 2011 [Smith, 2011]. For computational analysis, NX-6 I-DEAS software was used with FEM for predictions. Experimental test results of TVAC were used to validate computational models. There were significant temperature differences during the cold soak caused by some effects such as simplification of the model compared to the complexity of the satellite and inaccuracies in the TVAC temperature profile. These effects were discussed in research and some recommendations were provided for future work.

In 2012, thermal design and computational analysis of a 1U CubeSat were performed by Dinh at San Jose State University in California [Dinh, 2012]. Dinh used TD and ANSYS Icepak as thermal software; however, the research did not include experiments for validation of the models.

Different from all researches discussed above, this presented thesis provides a modular thermal design for the CubeSats. This design was created using both experimental and computational methodologies. All computational models were validated using experimental data in this thesis effort.

Finally, Hatzung's research is briefly discussed in this chapter to provide a background for the first task, provided on page 3, of this presented research [Hatzung, 2014]. At AFIT in 2013, Hatzung used TD to create a computational thermal model of the AFIT's TVAC. The purpose of the TVAC model is to validate AFIT's future CubeSat thermal models by comparing with experimental test results. Hatzung did experiments to validate his model using a 10 in x 10 in aluminum plate and demonstrated that the model is valid for use in steady state temperature predictions for model validation. Due to time considerations, he could not conduct experiments with another test article for greater validation.

### **Summary**

This chapter provided a theoretical basis through an overview of heat transfer and Earth orbit thermal environment. Thermal design process and commonly used thermal control hardware were described. As emphasized before, the design process is a combination of design selection and validation tests. Both experimental and computational thermal analyses are crucial parts of the thermal design process. Computational and experimental tests provide validation not only for the selected design but also for each other. Finally, to contribute to basic understanding of the thermal design and analysis effort of CubeSats in the past decade, a research overview was provided.

### **III. Methodology**

The purpose of this chapter is to describe the methodologies used in this research. First, the experimental test system of the thesis, Abbess produced TVAC test system, is introduced. Second, an overview of Thermal Desktop software is provided as the computational methodology and a brief thermal model design and test process is presented to provide a basic understanding of the software logic. Third, test articles and procedures are discussed. Fourth, validation process is discussed. Finally, the heat dissipater design process is presented.

#### **Experimental Test Methodology**

AFIT's TVAC was used for experimental tests in this research. The TVAC system is described and a brief operation process is introduced below.

##### ***TVAC***

TVAC approximates specific thermal, vacuum pressure, and illumination conditions in order to observe articles under test, which may experience similar conditions in actual use [Thermal/Vacuum Solar, 2012]. Vacuum and temperature conditions are established using on board controls. These controls activate thermal system components and turbo molecular pumping system to set the desired conditions within the chamber. A front view of the TVAC is shown in Figure 2. Some of the major components of the TVAC are introduced below.

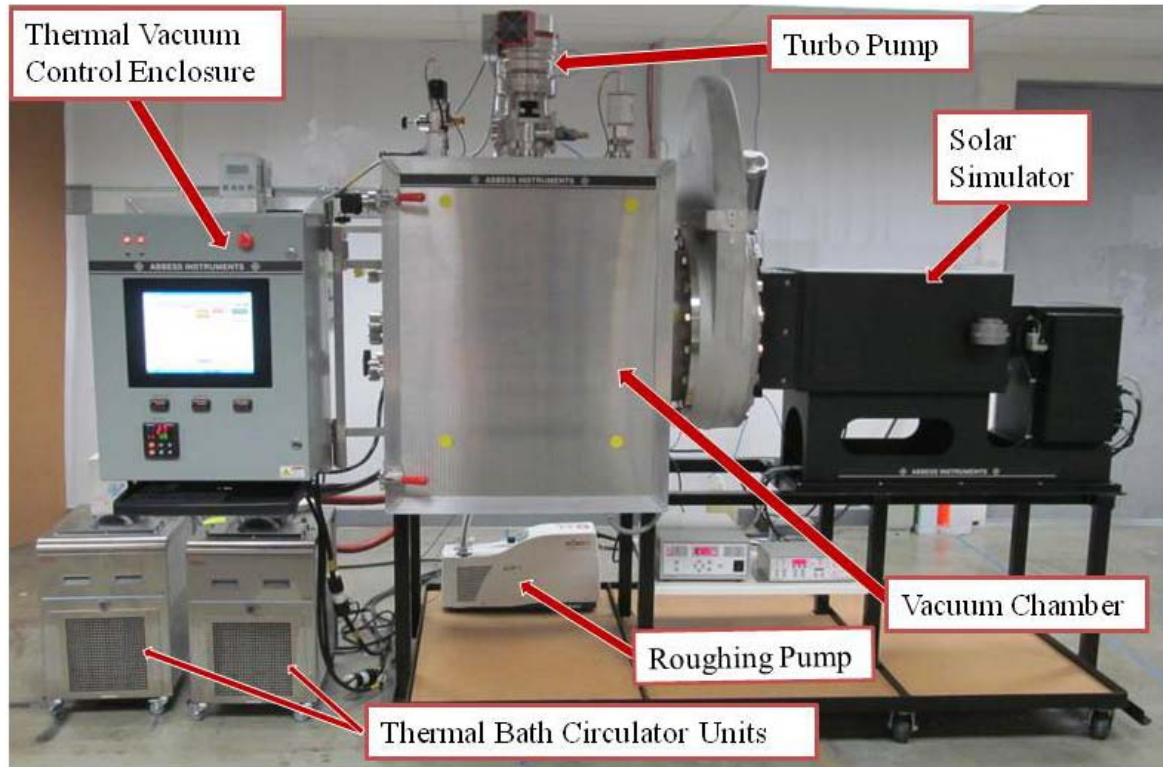


**Figure 2: Front View of TVAC**

The vacuum chamber is a front-loading, insulated stainless steel chamber, which serves to condition the chamber for high vacuum performance down to  $1 \times 10^{-5}$  Torr. Temperature within the chamber is measured by built-in temperature sensors, which are located on the platen and the shroud. The chamber has process ports, which were used for thermocouple and power connections in experiments.

The thermal platen/shroud assembly consists of a copper thermal platen and a shroud mounted in vacuum chamber with engaged heating/cooling loop as shown in Figure 3. The platen and shroud facilitate heating/cooling profiles ( $-40^{\circ}\text{C}$  to  $125^{\circ}\text{C}$ ) in the chamber under vacuum. These profiles are controlled by an integrated control interface provided by a touch screen PC. The platen is gold plated and the shroud is

Aeroglaze black paint coated. They are each heated and cooled individually by an engaged thermal media loop piping from a thermal bath circulator system manufactured by Thermo Fisher Scientific. The front wall of the shroud is removable and is not actively heat controlled. Conduction with the other walls of the shroud mainly determines the temperature of the front wall during test profiles.

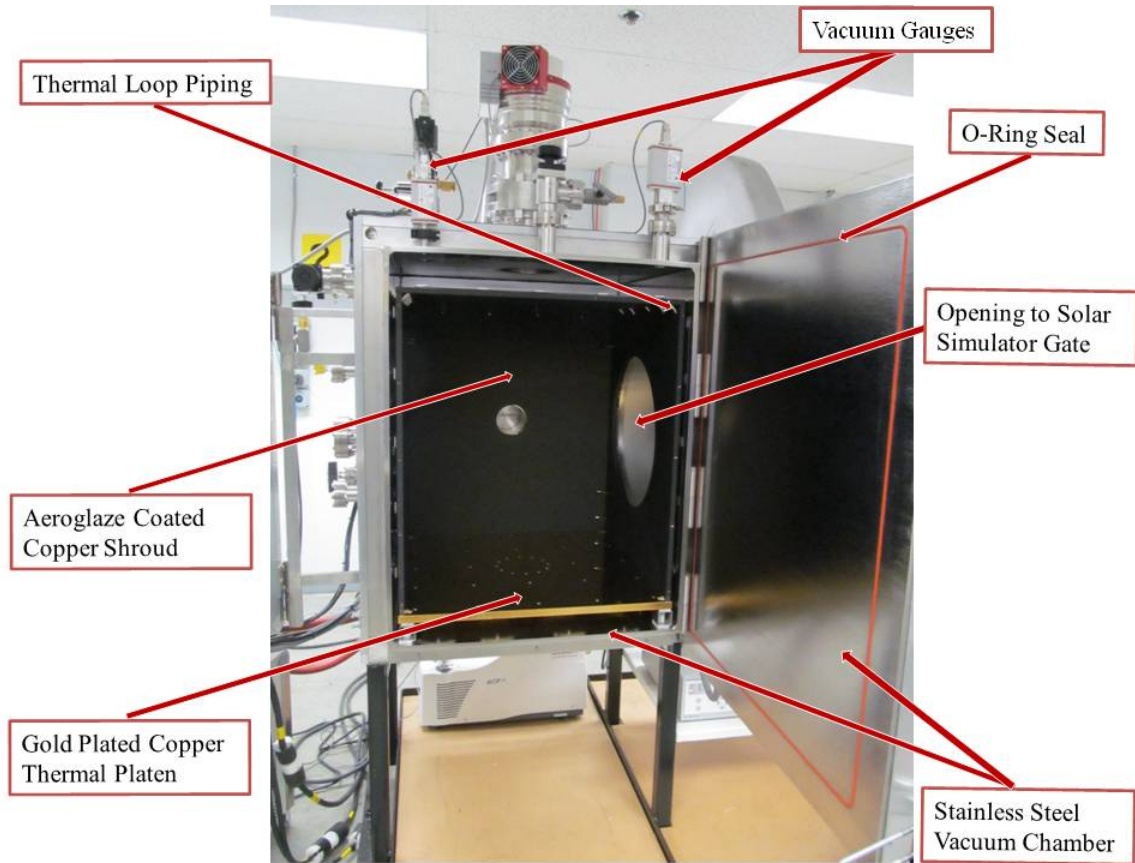


**Figure 3: Open Door View of Chamber**

The vacuum system consists of a roughing pump and a turbo pump. The roughing pump removes the bulk of gas from the chamber from atmosphere down to a mid-level vacuum range. The turbo pump is a 6,000 to 49,000 RPM pump used to achieve high and ultra high vacuum pressure in chamber ( $P \leq 1 \times 10^{-5}$  Torr). This pump system is powered

by a digital control unit with pressure data provided by two separate digital vacuum gauges.

The solar simulator is designed to achieve one sun equivalent illumination with three-degree collimation over a 12 in x 12 in area. A 1.6 kW lamp is used for the illumination and managed by an arc lamp power supply and digital exposure controllers. The solar simulator was unnecessary for this research.

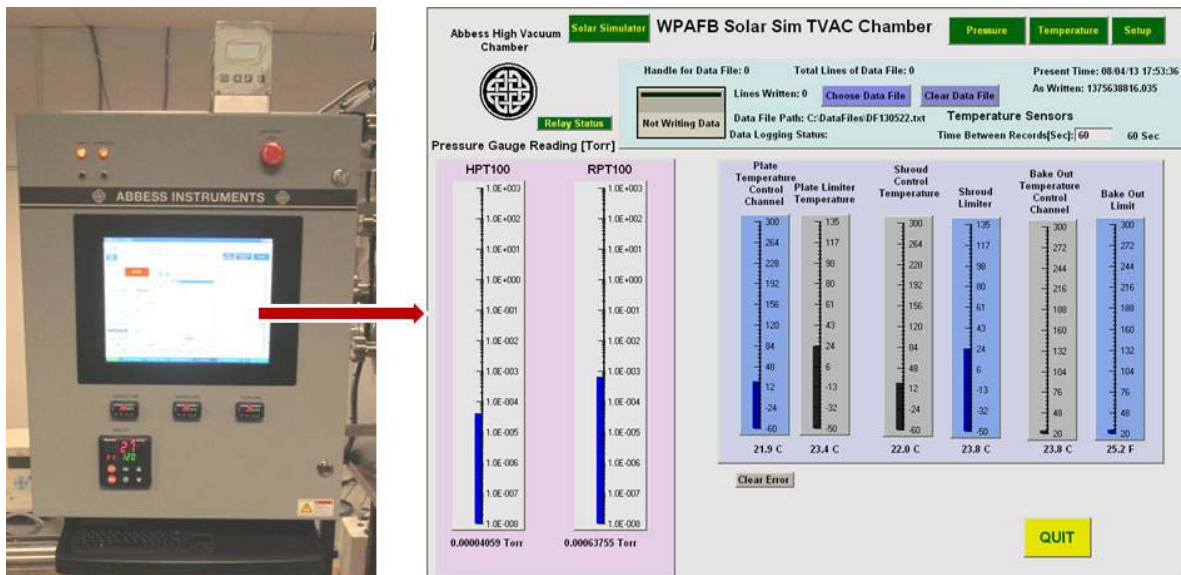


**Figure 4: Front View of Thermal Vacuum Control Enclosure and Main Screen**

The TVAC is controlled by an integrated control interface provided by a touch screen PC as expressed above. The main screen of PC is as shown in Figure 4. Real time plate, shroud, and bake-out control and limit temperatures are displayed on this screen. On the left, chamber pressure, in Torr, is displayed according to two digital vacuum gauges, which are shown in Figure 4. A user is able to navigate the Pressure Control, Temperature Control, and Solar Simulator interfaces as well as the Setup and Relay Status screens using the buttons on main screen. The user can also create or select a file

to record experiment data using buttons at the top center of the main screen. The data file is a text file, which can be opened in Notepad or Excel format.

To conduct an experiment, when the chamber is loaded with a properly prepared test article, the user secures all chamber doors and decreases the pressure using the Start/Stop button on the pressure control screen shown in Figure 5. On the left, chamber pressure in Torr is displayed according to two digital vacuum gauges in digital data format. On the right half of the screen, a graphic display charting chamber pressure against time is shown with color-coded traces of the two gauges in real time.

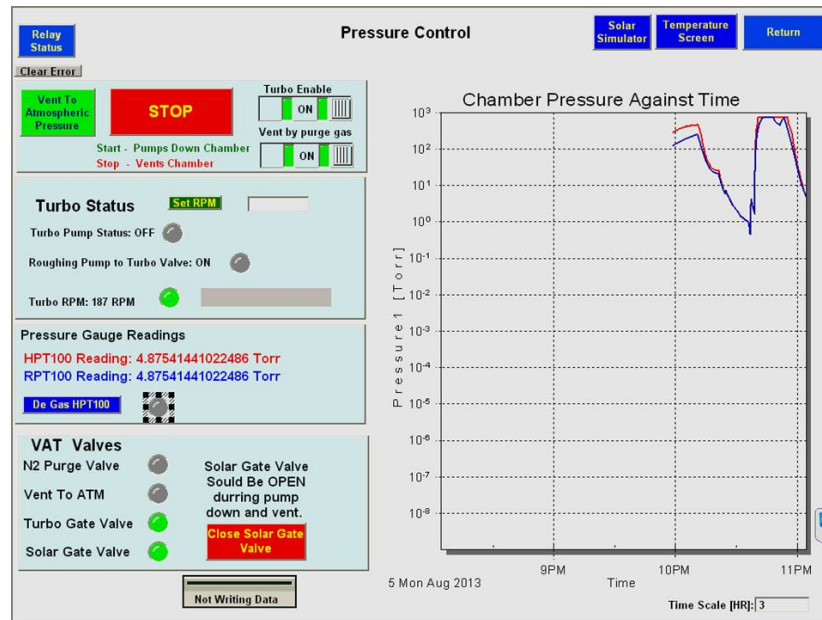


**Figure 5: Pressure Control Screen**

When the chamber is under vacuum, the user may individually enter a temperature value for plate and shroud using the temperature control screen, which is shown in Figure 6. The center of this screen is devoted to graphic display charting temperature vs. time with color-coded trace of plate, shroud, and bakeout temperatures in real time.

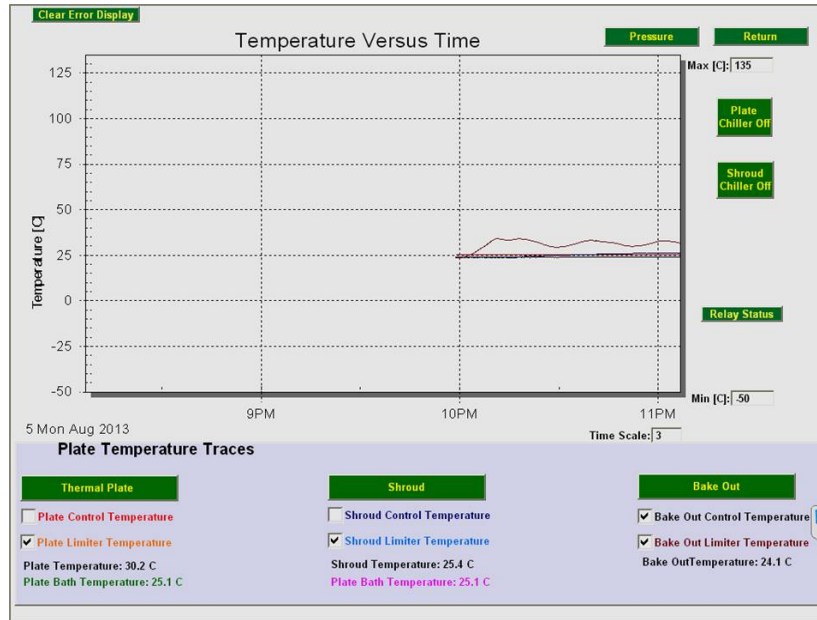


**Figure 6: Temperature Control Screen**

When the experiment is finished, the user can start the controlled depressurization process using the Start/Stop button on pressure control screen after returning the chamber to room temperature.

## Computational Simulation Methodology

As discussed in the previous chapter, Thermal Desktop (TD) was used for computational simulations in this research. Even though the manual [C&R Technologies, 2013], which is available online, provides very detailed information, a brief thermal model design and test process is presented here to assist reader in future discussion.

### *Thermal Desktop*

C&R Thermal Desktop® is a program that allows the user to build, analyze, and post-process thermal models [C&R Technologies, 2013]. TD runs as an AutoCAD application and can import some other models, such as TRASYS, NEVADA, TSS, and



NASTRAN, and I-DEAS. Every new object is associated with a layer, and layers are used to organize the design as in AutoCAD.

TD objects are generated using thermal-specific surface types such as rectangle, disc, cylinder and solids such as brick, solid cylinder. CAD surfaces created by built-in CAD construction techniques can be converted to TD surfaces as well. Starting the drawing process with defining materials and their thermophysical and optical properties may be timesaving for a modeling process. Units of thermophysical properties can be changed by the user. The SI unit system (W/m/K for conductivity, J/kg/K for specific heat, and kg/m<sup>3</sup> for density) was used for this thesis effort.

When a surface or solid is created, the Thin Shell Data dialog box appears as shown in Figure 7.

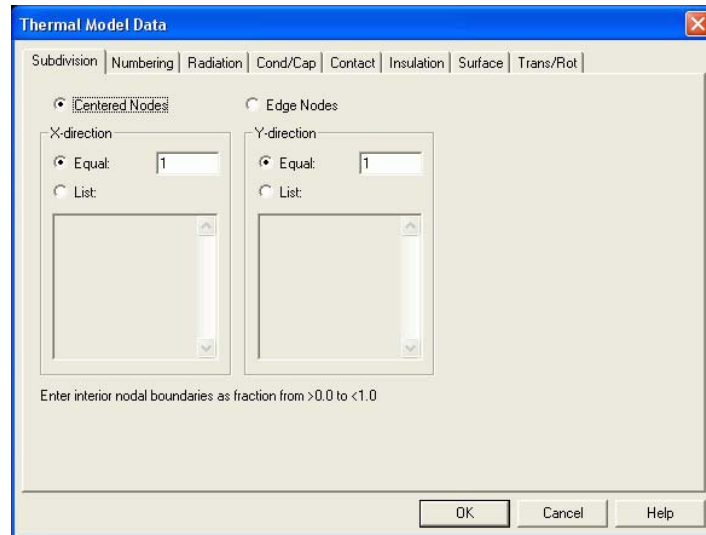


**Figure 7: TD Thin Shell Data Dialog Box**

The user selects the node type and the number of the nodes in each direction from the Subdivision tab. The user selects *Centered Nodes* button for finite difference objects and *Edge Nodes* button for finite element objects. If the processing speed and minimizing the

number of the nodes are important (for large models), the user may consider finite difference objects when the shape of the geometry fits one of the built-in finite difference surfaces and solids. When creating complex models with irregular curves, finite element objects are preferable. However, the user should expect increased processing time with increased complexity of the model when using finite element objects. Furthermore, care must be taken when selecting edge or centered nodes, particularly in the case of creating conduction between separate surfaces using a contactor, which is described below. The contactors do not calculate the conduction within any nodal breakdown in an object. When conduction created from the lower two objects, shown in Figure 8, to upper object, the contactor functionality calculates the conduction from the lower objects' surfaces to upper object's near surface. This means, in Figure 8, conduction between *Point 1* and *Point 2* (conduction within any nodal breakdown) are not calculated. If that conduction is important, edge nodes should be used. Using small finite element objects in a large finite difference model does not create a serious effect on the precision of the model. A few objects were created with edge nodes, such as circuit board and 1U stack rods, in this research.

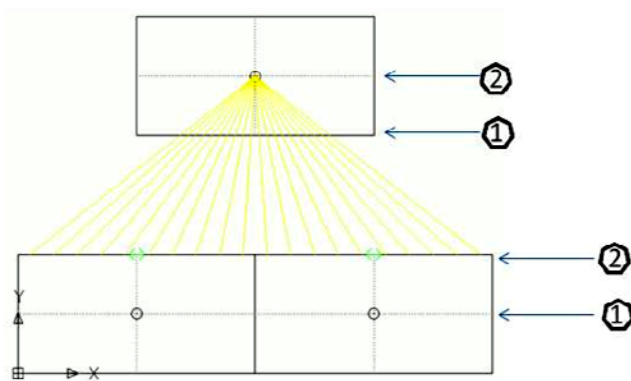


**Figure 8: Contactor Example**

The object material is selected using the Cond/Cap tab. Optical properties of the surfaces are selected on the Radiation tab for radiation calculations. All surfaces and solids can be modified (moving, rotating, stretching etc.) by using built-in AutoCAD commands.

Since no fluid was used for heat dissipation, convective heat transfer was ignored in this research. TD uses optical properties and physical locations of the objects to calculate radiation. Nevertheless, conductive heat transfer should be created by the user on TD using conductors, contactors or merge nodes.

A conductor can be created using one of the three choices: Node-to-Node, Node-to-Nodes, or Node-to-Surface Conductor. In this conduction type, the user should select a single node to determine the *from object* of conduction. Conductors allow specifying the conductivity value of the intervening material as a function of time or temperature difference. Since heat transfer calculations from an individual node were not necessary in this research, the conductor was not use as a conduction type.

The contactors are created to model conduction between two or more high level objects, such as 2D surfaces or 3D solids. For finite conductions between surfaces and solids, the contactors are the best option and widely used in this thesis. The contactor divides the conductive heat transfer into a  $k \cdot A / L$  or  $h \cdot A$  term, where  $k$  is the conductivity,  $A$  is the area,  $L$  is the thickness of the interface and  $h$  is the heat transfer coefficient. To create the contactor, the user can provide a fixed heat transfer coefficient and the contacted area is calculated by the contactor. Alternatively, use of the material option allows the user to choose an intervening material. With this option, the contactor takes the conductivity value from the thermophysical properties and calculates the area values

from the geometry. The user needs only to input the thickness of the interface. The contactor also allows the user to pick the Ray Trace Algorithm, which shoots rays perpendicular to the “from surface” and deems the closest node to be whatever node the ray first encounters. Since this is a very fast algorithm, it was used in this research for the contactors created between parallel surfaces.

For very large conductances value or perfect contact, merging nodes should be considered. Merging nodes, where possible, increases the processing speed of the model instead of creating the contactors with large conductances. As an example, nodes at the edges are merged when the aluminum chassis of the CubeSat was created using a small piece of aluminum solids to simulate large conductances. However, the contactors were used to create conduction between the chassis and its covers to simulate relatively smaller conductances.

When the model is created, using the techniques explained above, the user can simulate an orbit using Heating Rate Case Manager dialog box as shown in Figure 9.

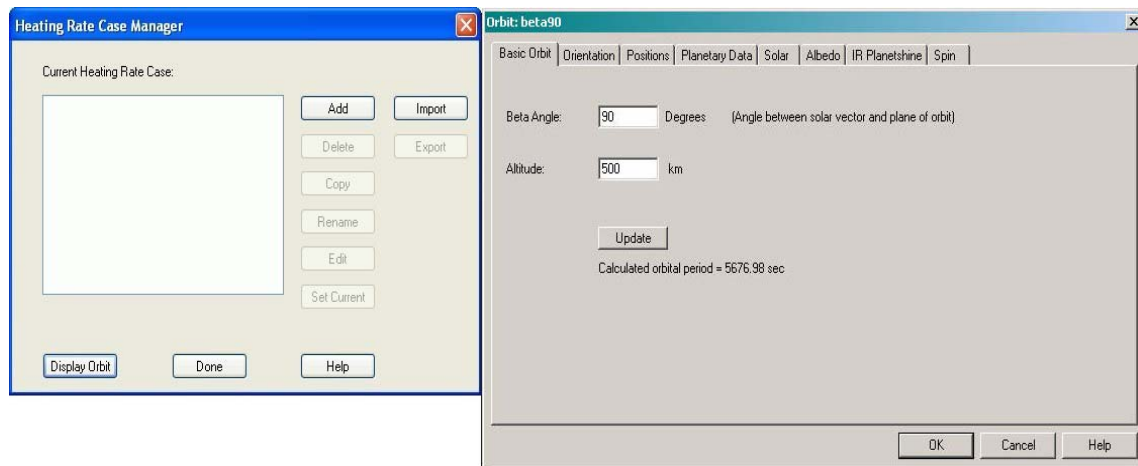


**Figure 9: Heating Rate Case Manager Dialog Box and Orbit Dialog Box**

The Create New External Heating Environment dialog box appears when selecting the Add button. TD allows the user to define many external heating environments such as basic orbit, Keplerian orbit, and free molecular heating with a reference orbit. A basic orbit was used in this research to get the orbit performance of the heat dissipater design. The basic orbit constellation allows the user to define the altitude and beta angle of a circular orbit as shown in Figure 9. The Orbit dialog box also allows user to specify the orientation of the spacecraft, the locations (positions) in orbit for which heating rates will be calculated, planetary data which the satellite orbits such as earth, sun, moon, and orbital heating rate data such as direct solar, albedo and IR emittance of the planet. The orbit and selected positions can be displayed as shown in Figure 10.

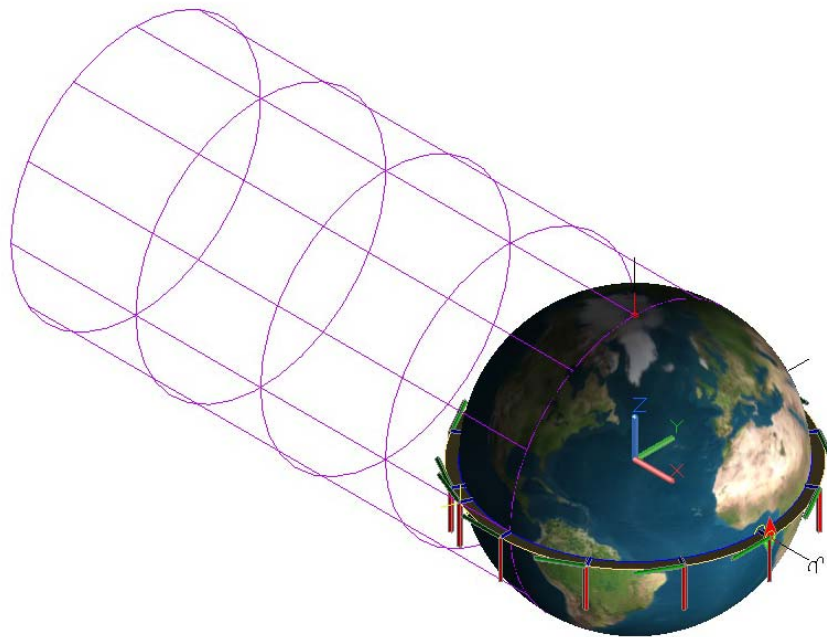


**Figure 10: Orbit Display**

Color-coded coordinate systems (XYZ axes) on the orbit display depict the spacecraft's orientation at each position with respect to the celestial coordinate system, which is at the

center of the Earth (X-red, Y-green, and Z-blue). Purple cylinders show the shadow zone of the Earth.

After defining the orbit and the satellite orientation, the user can compute heating rates for solar albedo and IR planetshine using a Monte Carlo method. The user can also compute orbital heating rates individually or get the error rate in calculations by using Set HR Dataset Properties dialog box as a post-processing as shown in Figure 11.

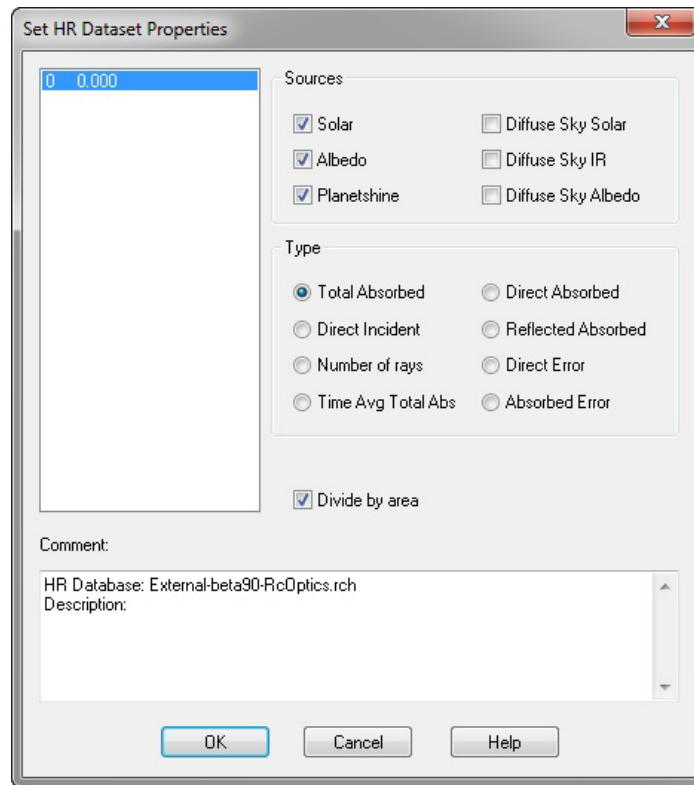


**Figure 11: Set HR Dataset Properties Dialog Box**

When the model and external heating environment (orbit) are created, the Case Set Manager is used to conduct a simulation. The Case Set Manager's primary purpose is to set up different thermal analysis cases and to make temperature calculations from radiation calculations. First, it performs the radiation and heating rate tasks of the current

case, computes and outputs the node temperature values and node-to node radiation conductor data, builds and runs a SINDA model, and finally displays the temperature results mapped on the thermal model. A case can be added or the current case can be edited by Case Set Manager dialog box. The Editing Case Set dialog box appear as shown in Figure 12, when add or edit button is selected on Case Set Manager dialog box.

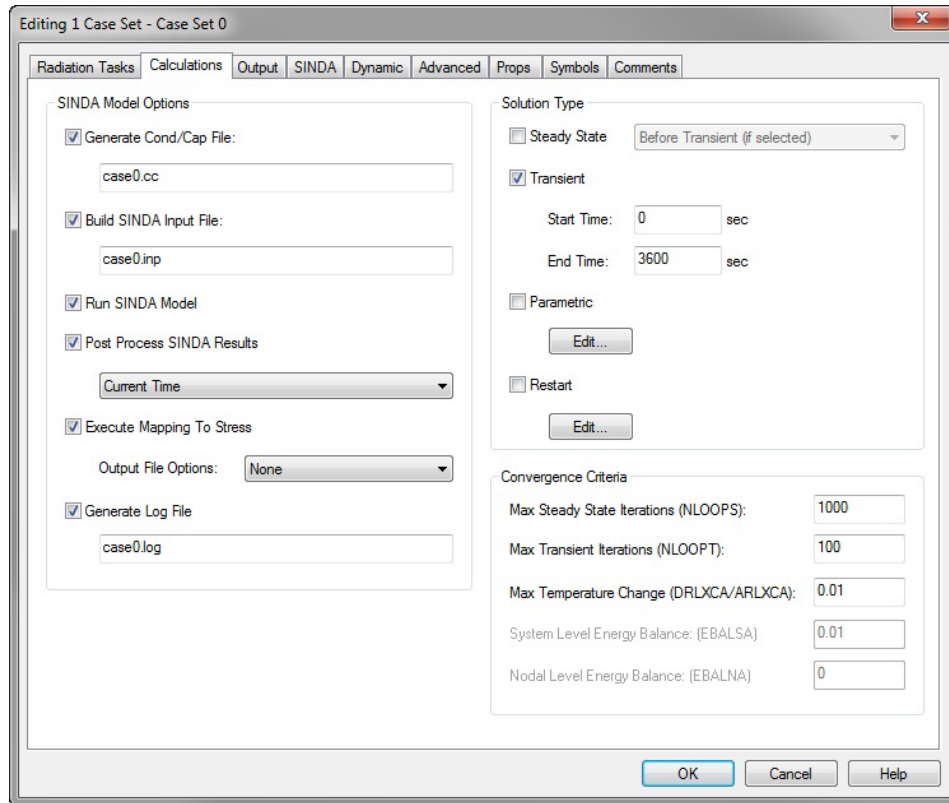


**Figure 12: Editing Case Set Dialog Box**

New radiation tasks can be added or the current ones can be edited on the Radiation Tasks tab. The user defines solution types such as transient or steady state on the Calculations tab and selects type of output data on Output tab. The selected type of data is written on the output files such as temperatures, capacitances or radiation data (e.g.,

radiation calculation results such as number of rays shot for each node and weighted error).

When the calculations are performed, calculation results can be examined by post-processing such as color post-processing (displaying calculation values on graphical object as colors), X-Y plotting (as a function of time), query node (by selecting graphical objects), and results queries (generating summary files based on one or more result files). Temperature color post-processing figures are provided for the computational simulations conducted in this research in Chapter 4.

### **Test Articles and Experiments**

A simple test article, a 6U CubeSat Chassis, was used for the initial tests to achieve the first task of the thesis, which is to provide further validation for the previously generated TVAC environment computational model [Hatzung, 2014]. The Chassis is entirely made from T-6061 aluminum. The Chassis was instrumented with thermocouples and hung from the test stand using a monofilament fishing line as shown in Figure 13 to minimize conductive heat transfer.



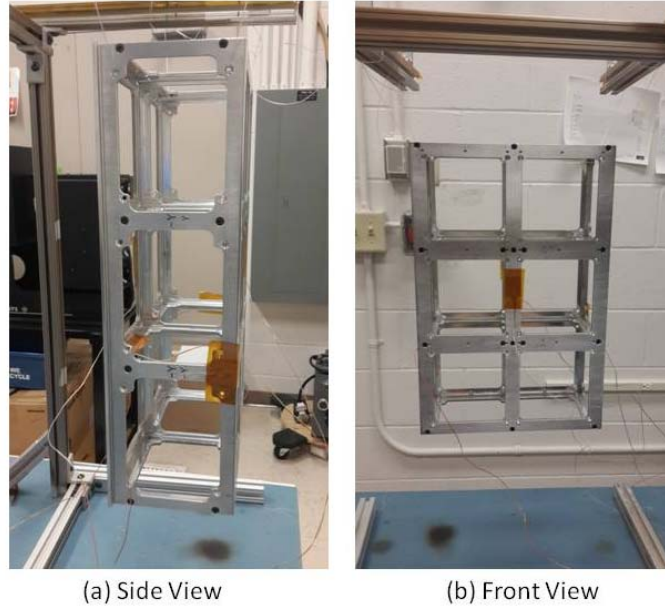
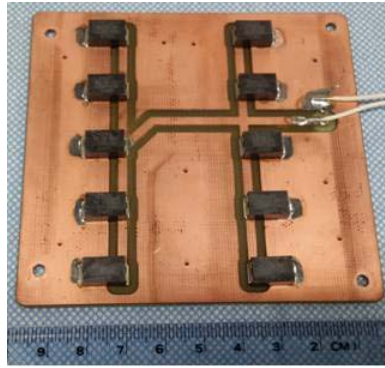
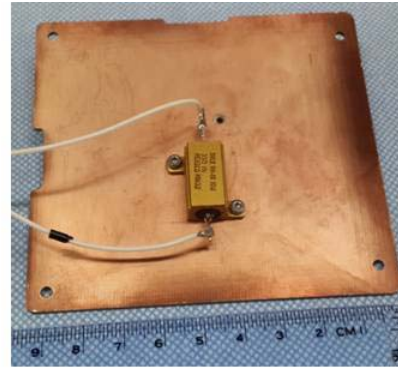


**Figure 13: Two Views of the Chassis Hung from the Test Stand**

Two circuit boards with resistors were used in experiments in this research. The first one was a custom PC104 circuit board with ten resistors, as shown in Figure 14 (a), which was named as ten-heater circuit board (THCB). Ten Vishay WSC4527 wirewound resistors, each capable of dissipating 2W of power, were mounted on the Isola FR402 circuit board to simulate processors in a CubeSat. The second circuit board was built with a Vishay 10W Resistor as shown in Figure 14 (b) and named as single-heater circuit board (SHCB) for this research.



(a) The Ten-Heater Circuit Board, THCB



(b) The Single-Heater Circuit Board, SHCB

**Figure 14: Circuit Boards with Resistors**

The chassis was covered with aluminum plates for succeeding experiments to simulate a fully enclosed 6U CubeSat as shown in Figure 15. The covered chassis including heat sources was named as sample CubeSat in this research. The covers were made of T-6061 aluminum. A small gap was cut on the cover to allow thermocouple and power connections between the TVAC and CubeSat interior as shown in bottom right corner of Figure 15.

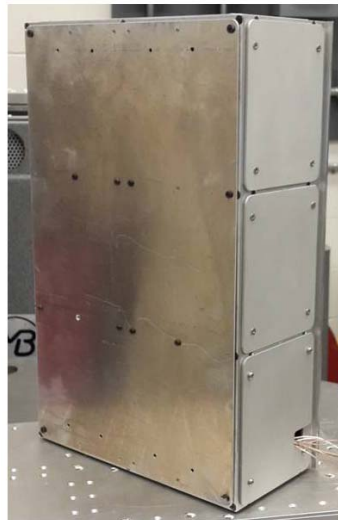


**Figure 15: The Sample 6U CubeSat**

All experiments are named with a letter to reduce confusion in this research. For example, chassis-only experiment, which is discussed below, is named as experimental test-A (ET-A). In case of an experiment is also modeled computationally in TD, the computational simulation is also named with the same method. For example, chassis-only computational simulation is named as computational simulation-A (CS-A). All experiments and computational simulations conducted in this research are presented in Table 1. Even though many items in Table 1, such as radiators or heat dissipater configuration, have not been introduced at this point, the table is presented before experiment and simulation discussions to give the reader a big picture.

**Table 1: Test Specifications and Explanations**

<b>Experimental Test Name</b>	<b>Computational Simulation Name</b>	<b>Explanation</b>	<b>Purpose</b>	<b>Heater</b>	<b>Heat Dissipater</b>	<b>Radiator Size</b>	<b>TVAC Test Point (°C)</b>	<b>Power (W)</b>
ET-A	CS-A	Chassis-Only	Provide greater validation for previously created TVAC computational model	-	-	-	-10 30 60	-
ET-B		Chassis with Heaters	Acquire thermal behavior of the heaters in vacuum	THCB	-	-	-15	1.8 2.7 4.5 6.3
ET-C		Sample CubeSat Power Level Determination	Power level determination for subsequent experiments	THCB	-	-	-15	1.8 2.7 4.5
ET-D	CS-D	Sample CubeSat	Acquire thermal behavior of the sample CubeSat and computationally model it	THCB	-	-	-15	1.8 4.5
ET-E		Sample CubeSat	Determine thermal behavior of test article with heat dissipater box and radiator when there is no connection between the box and the radiator	THCB	Box and Radiator (No thermal strap connection)	1U (Bare Copper)	-15	1.8 4.5
ET-F		Sample CubeSat	Determine the performance of the heat dissipater with bare copper radiator (no surface finish)	THCB	Box, straps and radiator (Poor Conduction in Braid Connections)	1U (Bare Copper)	-15	1.8 4.5

Experimental Test Name	Computational Simulation Name	Explanation	Purpose	Heater	Heat Dissipater	Radiator Size	TVAC Test Point (°C)	Power (W)
ET-G		Sample CubeSat	Determine the effect of surface finish of the radiator in the heat dissipater design (with comparison of ET-F)	THCB	Box, straps and radiator (Poor Conduction in Braid Connections)	1U (Black Tape)	-15	1.8 4.5
ET-H	CS-H	Sample CubeSat, Basic Configuration of the Heat Dissipater	Determine the importance of thermal strap connection quality in the heat dissipater design (with comparison of ET-G)	THCB	Basic Configuration (Thermal Straps with High Temperature Soldering)	1U (Black Tape)	-15	1.8 4.5 11
ET-I		Sample CubeSat	Determine the effect of radiator size in the heat dissipater design	THCB	Basic Configuration	3U (Bare Copper)	-15	1.8 4.5
ET-J		Sample CubeSat	Determine the effect of radiator size and radiator surface finish in the heat dissipater design	THCB	Basic Configuration	3U (Black Tape)	-15	1.8 4.5 7.2
ET-K		Sample CubeSat	Determine the effect of a deployable radiator in the heat dissipater design	THCB	Basic Configuration	1U Side + Deployable	-15	1.8 4.5
ET-L		Sample CubeSat	Acquire the thermal behavior of the CubeSat with SHCB	SHCB	-	-	-15	3.3

Experimental Test Name	Computational Simulation Name	Explanation	Purpose	Heater	Heat Dissipater	Radiator Size	TVAC Test Point (°C)	Power (W)
ET-M		Sample CubeSat	Determine the effectiveness of the heat dissipater design, when there is indirect contact between the heat source and the heat dissipater	SHCB	Full Configuration (Basic + Aluminum Edges)	1U (Black Tape)	-15	3.3
ET-N		Sample CubeSat	Determine the effectiveness of the basic configuration of heat dissipater, in case of an concentrated heat source	SHCB	Basic Configuration	1U (Black Tape)	-15	3.3
ET-O		Sample CubeSat	Determine the effectiveness of the heat dissipater's box shape in comparison with ET-H	THCB	Basic Configuration w/o Bottom Face	1U (Black Tape)	-15	1.8 4.5
	CS-P	0° Beta Angle Orbit	Acquire the thermal behavior of the sample CubeSat in the cold case orbit	THCB	-	-	-	4.5
	CS-Q	0° Beta Angle Orbit	Determine the effectiveness of the heat dissipater in the sample cold case orbit	THCB	Basic Configuration	1U (Black Tape)	-	4.5 13.5
	CS-R	0° Beta Angle Orbit	Determine the effect of the radiator size in the sample cold case orbit	THCB	Basic Configuration	3U (Black Tape)	-	4.5 19

Experimental Test Name	Computational Simulation Name	Explanation	Purpose	Heater	Heat Dissipater	Radiator Size	TVAC Test Point (°C)	Power (W)
	CS-S	90° Beta Angle Orbit	Acquire the thermal behavior of the sample CubeSat in the sample hot case orbit	THCB	-	-	-	4.5
	CS-T	90° Beta Angle Orbit	Determine the effectiveness of the heat dissipater in the sample hot case orbit	THCB	Basic Configuration	1U (Black Tape)	-	4.5 15.5
	CS-U	90° Beta Angle Orbit	Determine the effect of the radiator size in the sample hot case orbit	THCB	Basic Configuration	3U (Black Tape)	-	4.5 22

In experiments,  $dT/dt < 0.5 \text{ }^\circ\text{C} / \text{hr}$  was determined as thermal equilibrium and steady state criterion as explained in Chapter 1. Even though the thermal equilibrium was achieved approximately in 15-18 hours in experiments, all experiments were conducted 24 hours to provide greater confidence to data. Due to some failures of the thermocouples, i.e., detachment from the surface, some experiments were conducted repeatedly to acquire dependable data throughout this research. As an example, in some experiments two thermocouples were used to acquire temperatures from the circuit board top surface, expecting to show the same results, because the circuit board has roughly uniform heat dissipation on its surface (uniformity of the heat dissipation of the circuit board surface will be discussed in the next chapter). When different results were collected from the thermocouples, tests were repeated. Furthermore, thermal images of the circuit

board were acquired when the heaters are active to ensure that there is a uniform heat distribution on the circuit board. Since TVAC does not allow use of a thermal camera due to lack of an observation window, IR images were acquired in ambient pressure and temperature.

### **Baseline Experiments and Simulations**

Experiments conducted and simulations created to acquire a validated CubeSat model were named as *baseline* in this research. Baseline experiment and simulations consist of chassis-only experiment (ET-A), chassis-only simulation (CS-A), chassis with heaters experiment (ET-B), CubeSat with heater experiment (ET-C), sample CubeSat experiments (ET-D), and sample CubeSat simulations (CS-D). Even though the test article is the same in ET-B and ET-C, they were named separately, because the purposes of the experiments were different from each other.

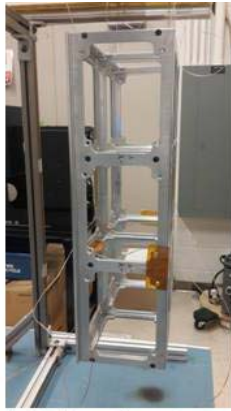
#### ***Chassis-Only Experiment and Simulation (ET-A and CS-A)***

The purpose of the chassis only experiment and simulation was to provide further validation for the previously generated TVAC environment computational model using a 6U CubeSat chassis [Hatzung, 2014]. The chassis only experiment (ET-A) was conducted with three steady state temperature set points, -10, 30, and 60 °C. Set points were selected within the TVAC's temperature envelope to be able to perform the TVAC model validation at cold, hot, and room temperatures. Five thermocouples were used to obtain temperature data from the chassis.

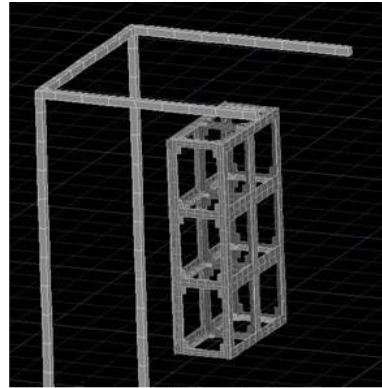
In the chassis only computational simulation (CS-A), an analogous computational model of the chassis was created in TD and located in TVAC computational model at the



same position and orientation with ET-A. Photographs and TD screenshots of ET-A and CS-A are shown in Figure 16.



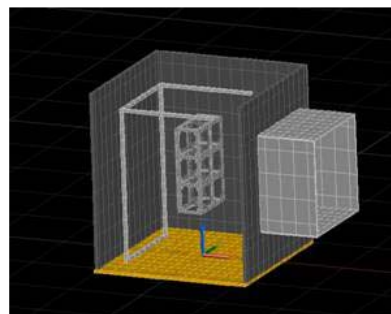
(a) The Chassis, Hung from the Test Stand



(b) Thermal Model of the Chassis, Hung from the Test Stand



(c) The Chassis inside TVAC



(d) Thermal Model of the Chassis inside TVAC

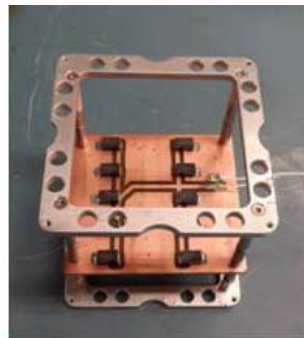
**Figure 16: Experiment Pictures and TD Screenshots of ET-A and CS-A**

***Chassis with Heaters Experiment (ET-B) and Sample CubeSat Power Level Determination Experiment (ET-C)***

The purpose of ET-B was to determine the thermal behavior of the heaters under vacuum. The purpose of ET-C was to determine two power levels for subsequent experiments to reduce the experiment time. Additionally, the data collected from ET-C was compared with ET-B and this information was used to examine the thermal behavior

of the heaters when their open view to TVAC shroud was obstructed with aluminum plates.

The circuit board with the heaters was connected to an external power supply through a feed-through port of TVAC. The power level was set using the external power supply. Since the cables between the power supply and the circuit board were relatively long and had electrical resistance, power loss in the cables was measured and calculated as 10%. For this reason, the power levels dissipated at the circuit board were used to name the tests, even though the power levels measured at the power source were higher (i.e., the power at the power source was 2W in 1.8W tests; and it was 5W in 4.5W tests). Thus, the THCB model was run with the power matching the power applied on the heaters, not the power supplied by the power supply. Figure 17 shows the photographs ET-B.



(a) 1U Stack including the Circuit Board



(b) The Chassis including Heaters in TVAC

**Figure 17: Photographs of ET-B**

In chassis with heaters experiment, the TVAC shroud temperature was set to -15 °C and the power level of the heaters was gradually increased. Experiments were

started with 1.8W power level, and the power was increased to 2.7W, 4.5W, and 6.3W allowing sufficient time for steady state to be achieved at each power level. The top face of the circuit board was measured at each test point. Experiment terminated at the 6.3W power level, which had a temperature of 92.2 °C on the circuit board. Since the maximum operating temperature of the circuit board was 130 °C, greater power levels were not pursued.

ET-C was conducted with three steady state test points, 1.8W, 2.7W and 4.5W, which are the same with the previous test. The circuit board reached to 97.6 °C steady state temperature at the 4.5W power level. Greater power levels were not pursued to prevent damage. These data were used to determine two steady state test points for the subsequent tests to reduce experiment time, because reaching steady state temperatures in sample CubeSat experiments required at least 24 hours at each step.

ET-B and ET-C also allowed making a comparison between uncovered and covered (with aluminum plates) chassis thermal behavior when using the same heat sources with the same power levels, as explained above.

#### ***Sample CubeSat Experiments and Simulation (ET-D and CS-D)***

The purpose of the Sample CubeSat experiments (ET-D) was to determine the thermal behavior of a sample CubeSat within the TVAC and gather enough data to model the CubeSat computationally. In ET-D, THCB was used in aluminum plate covered 6U chassis (sample CubeSat). In CS-D, the sample CubeSat was modeled in TD and the correlated model was used to design a modular heat dissipater. Photographs and TD screenshots of the ET-D and CS-D are shown in Figure 18.

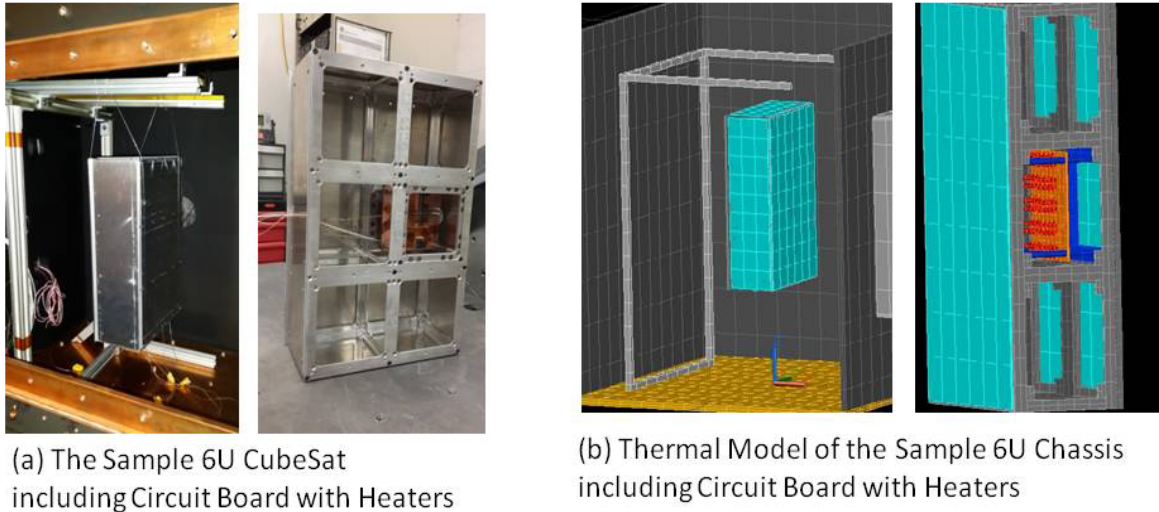


**Figure 18: Photographs and TD Screenshots of the ET-D and CS-D**

ET-D includes six experiments in  $-15\text{ }^{\circ}\text{C}$  TVAC at the power levels 1.8W and 4.5W using seven thermocouples in each test. The temperature was measured at particular points (e.g., circuit boards, heaters, stack rods) repeatedly to acquire comparable data. Some uncontrolled effects caused changes at the temperatures in successive experiments. For example, the temperature of TVAC platen and TVAC shroud did not stay at the same level in every experiment. There were some power fluctuations at the power source of the heaters. The sample CubeSat was disassembled before each experiment to place the thermocouples on different points. It is a possibility that, the gaps between the surfaces, such as between 1U stack and chassis or circuit board and 1U stack, have changed in consecutive experiments, and cause conductive heat transfer deviations due to contact resistance changes. This effect might also change the temperatures throughout the CubeSat. As explained above, the temperature of particular points was measured repeatedly in successive experiments to acquire dependable data. In the case of acquiring different temperature values on the same point, the most frequently

occurring temperature was assumed to be the reference value for thermal model design. Deviated temperatures from the reference value on a particular point were neglected taking into account the effects expressed above. For example, the circuit board temperature was measured in five Sample CubeSat 4.5W experiments. The results were 89.5 °C, 93.2 °C, 81 °C, 92.5 °C and 93.3 °C. It is evident that there was an anomaly in the third measurement, so that outlying value was ignored. The reference value was selected as 93 °C for the circuit board. All reference values for selected points and their comparisons to computational data are presented in Chapter 4.

In CS-D, the thermal model of the CubeSat was created using built-in finite difference objects. Published optical properties were used for all surfaces except the aluminum covers of the CubeSat. The CubeSat covers were made of T-6061 commercial sheet aluminum with a published IR emissivity value of 0.1. However, since some oxidation occurred on the covers, the IR emissivity value of the covers was assumed to be 0.15. This value provided improved agreement between the experimental results and computational model predictions. For modeling conduction through chassis, the adjacent nodes of each part were merged to behave as a solid body. All other conductions were modeled using the previously explained the contactor method.

Heaters were created using TD's Heater command, which allows the user to apply a heat load to an object such as a surface, a solid or a single node. Thermoplastic rectangular boxes were created using Solid Brick, which are the same size as Vishay Resistors. Detailed information about TVAC computational model is provided by Hatzung [Hatzung, 2014].

## **Heat Dissipater Design Process**

The experiments and simulations, ET-A through CS-D, established baseline conditions for a hypothetical CubeSat without explicit thermal control hardware. Since the goal of this research is to create a modular heat dissipation technique, the design should function over a large range of CubeSat missions. To achieve this goal, a heat sink was designed to cover a PC104 circuit board. PC104 printed circuit board mounting scheme is widely used in CubeSats, because it leaves a considerable area for circuitry on the board and has a simple scheme [Pumpkin, 2013]. Assuming there are high power processors on the circuit board, the heat sink's main purpose is conducting the processors' heat to a radiator, while minimizing the heat flow into other regions within the CubeSat. Since it was measured in ET-C experiments that the temperature of the bottom face of the circuit board is very close to the temperature of the processor, the heat sink was designed to conduct heat from the bottom face of the heat dissipater too. The heat sink connects to a copper radiator with soldered copper thermal straps. Since the IR emissivity of the copper is very low, a black paint surface finish was employed for the outside face of the radiator (3M 235 Black Photo Tape was used to simulate black paint in experiments). The inner faces were left as bare copper, because it was aimed to radiate heat out of the CubeSat, while avoiding radiating heat to inner surfaces and other components. The design was first modeled computationally. Then the prototype was built and validation experiments were conducted in the TVAC. Finally, orbit performance simulations of the validated heat dissipater model were conducted in TD.

### *Computational Design of the Heat Dissipater*

First, a copper heat sink was modeled using finite difference objects to cover the PC104 circuit board. The first heat sink design is shown in Figure 19. Some layers of the CubeSat thermal model are turned off in each image to get a better view below.

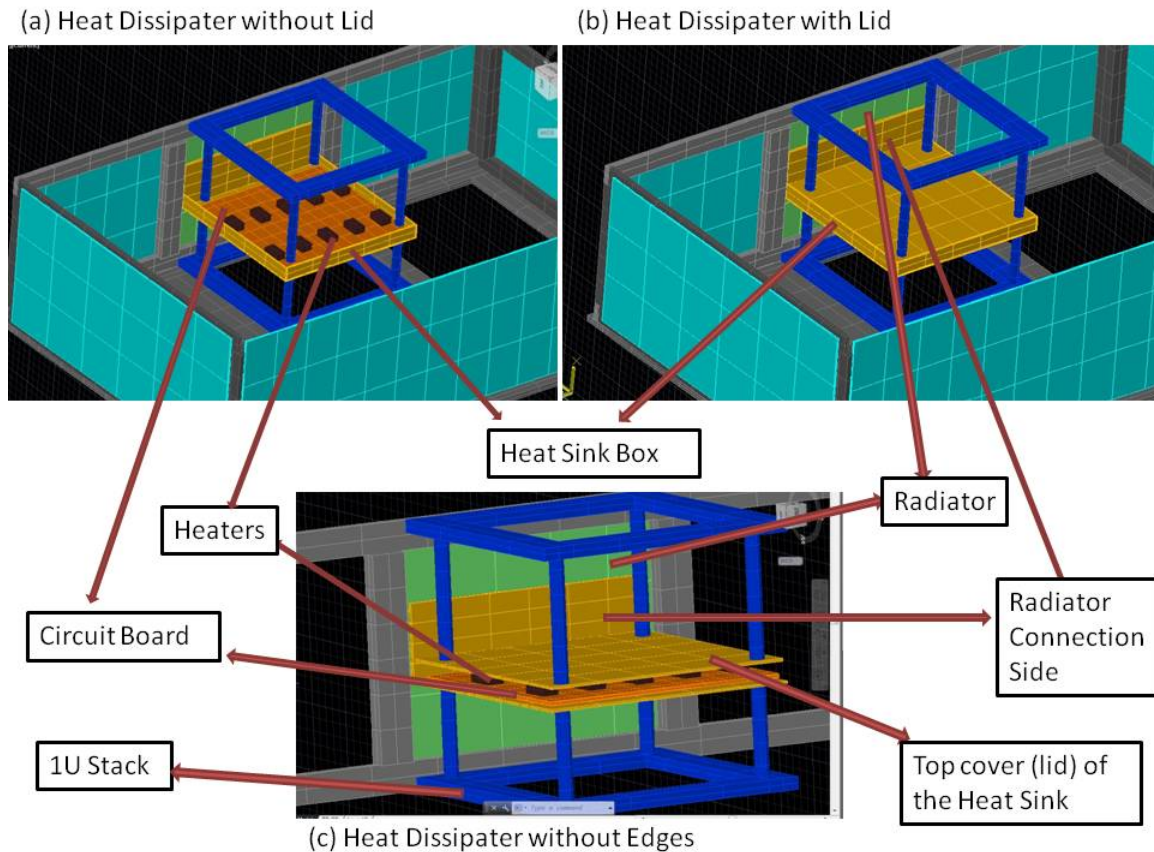
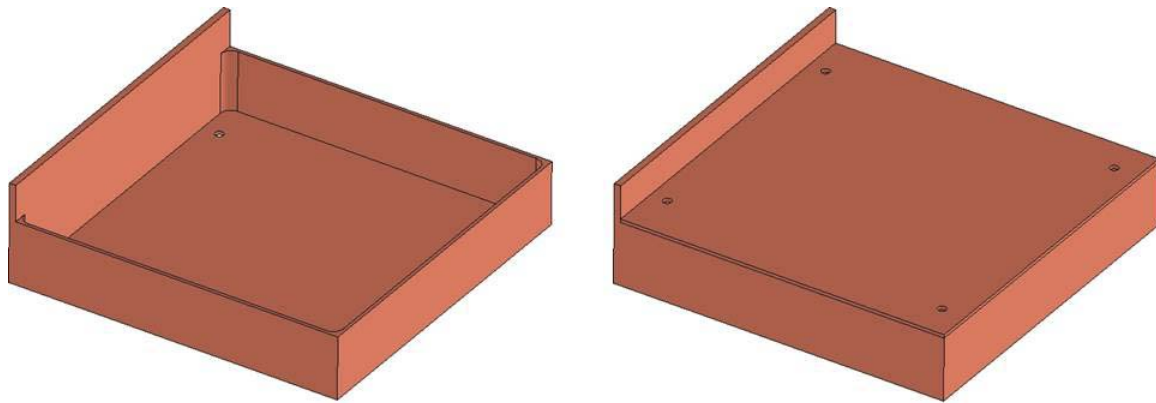


**Figure 19: Three Views of the First Heat Dissipater Design in the Sample CubeSat**

The first design was a copper box sitting in the 1U stack, which holds the circuit board. The heat sink was designed slightly longer in the radiator side to be in direct contact with the radiator. The connection was made with a relatively large edge of the heat dissipater, which is labeled as *radiator connection side* in Figure 19. A thermal conductive pad was designed between the heat sink and the radiator to reduce contact

resistance. The box was designed as one piece solid except the lid (the top cover of the box) as shown in Figure 20 (a).



(a) First Heat Dissipater Design without Lid

(b) First Heat Dissipater Design with Lid

### **Figure 20: The First Heat Dissipater Design**

Four conductions were modeled using the contactor method between the circuit board and the heat dissipater. The first one is between the heaters and the top cover. The second one is between the circuit board and the bottom face of the box. The third one is between the box and the radiator, and the final one is between the box and the 1U stack rods. For the first three, the conductions were modeled using  $12 \text{ W/m}\cdot\text{K}$  conductivity value, which is a common value for thermal conductive pads, which were modeled between the circuit board and the heat dissipater to decrease the contact resistance. To model conduction between the box and the 1U stack rods, plastic was used as the interfacing material because of the plastic washers used at the experiments to minimize the heat flow through chassis. Thickness of the each side of the box was determined taking into consideration the fact that, even though thermal performance is getting better, the weight of the box also increases with increasing thicknesses.



After the box dimensions are decided, the heat dissipater was modeled in SOLIDWORKS® and frequency analysis was conducted computationally by Mr. Philip D. Smith. He conducted simulations with various materials for mechanical comparison. Although this baseline geometry was not particularly problematic in terms of rigidity, opportunities were identified for improvement from the frequency analysis. Since the main purpose of the edges of the box is supporting the faces of the heat dissipater, instead of removing heat from the heat source, aluminum was selected for edge material instead of copper to decrease the weight and increase the stiffness.

To increase the manufacturability and provide even greater rigidity, the material and the dimensions of the box were redesigned. The dimensions of the box were reduced to the size of the circuit board as shown in Figure 21. The results of Mr. Smith's frequency analysis are shown in Figure 22 . The technical drawing of the heat dissipater box is presented in Appendix A: Technical Drawing of the Heat Dissipater Box.

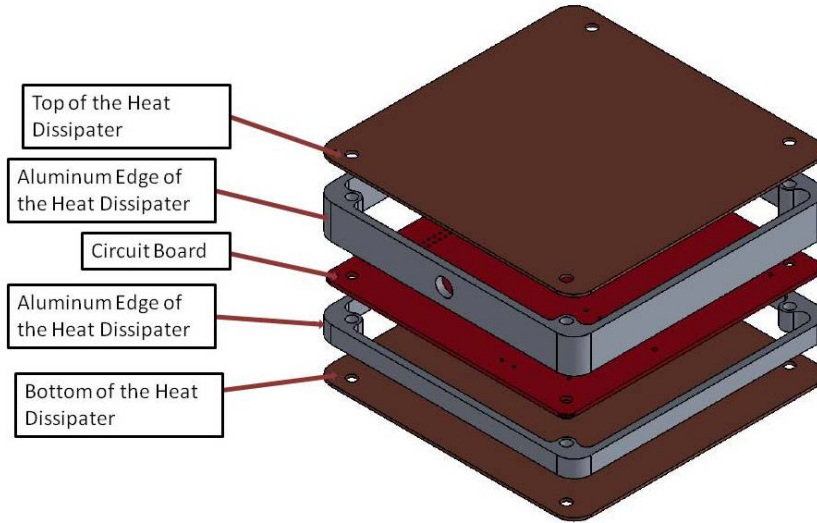


**Figure 21: The Final Design of the Heat Dissipater**

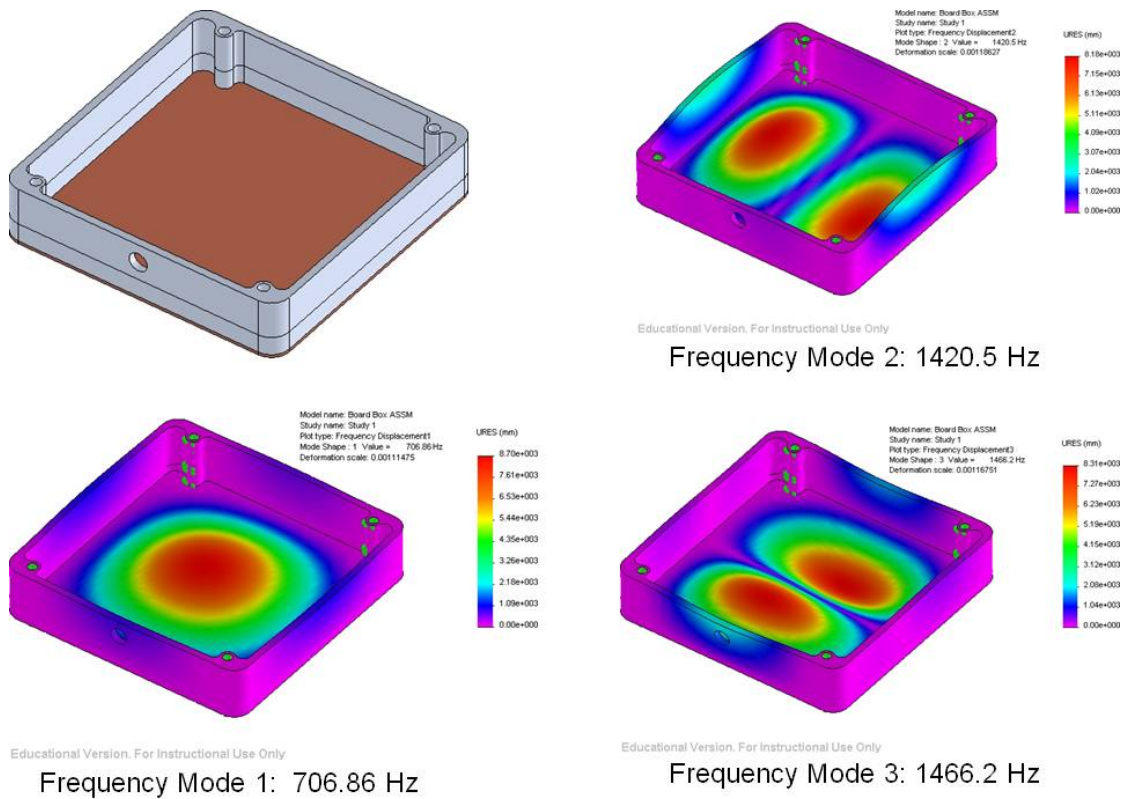


**Figure 22: Frequency Analysis Results of the Final Heat Dissipater Design**

In the new design, the edges were designed as aluminum due to its weight and stiffness advantages compared to copper, as explained above. Furthermore, separate edges, which allow for various configurations of the box with different thicknesses, increase the modularity of the design. Both faces of the heat dissipater and the radiator were designed as copper. Thicknesses of the top face, bottom face, aluminum edges and the radiator were set as 1mm. Two conductions were modeled between the box and the radiator. First conduction was modeled between the top face of the dissipater and the radiator, and the second one was between the bottom face and the radiator. Since this design did not have a direct connection between the heat dissipater box and the radiator, thermal straps were employed between the radiator and the both faces (top and bottom) of the box as shown in Figure 23.

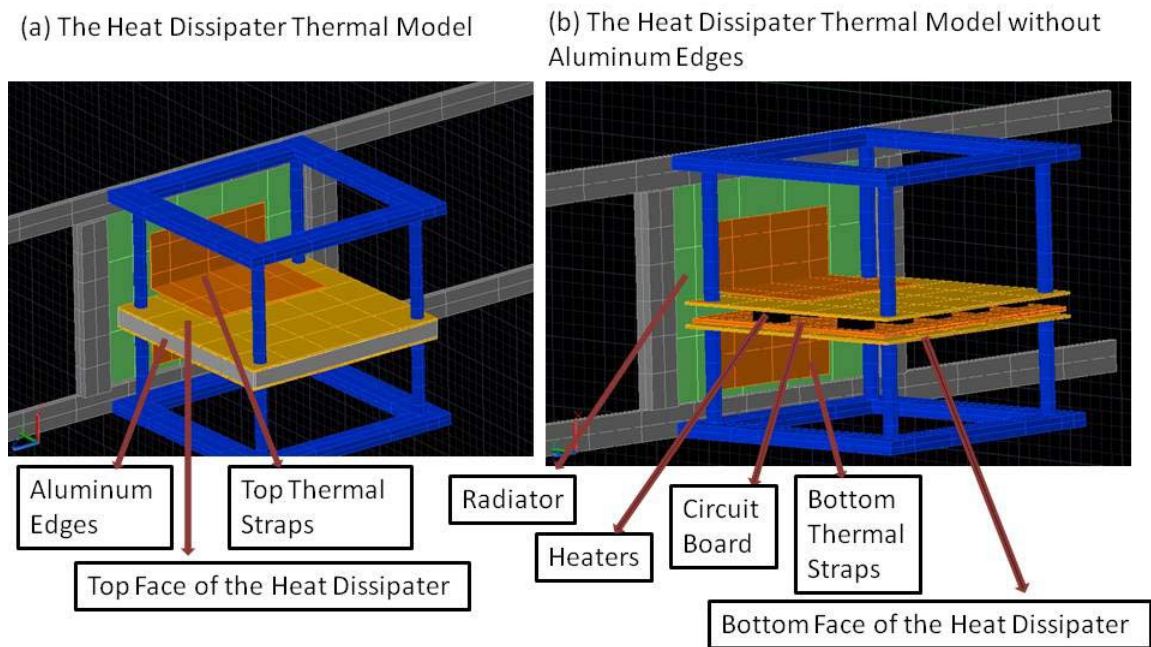


**Figure 23: The Heat Dissipater Thermal Model**

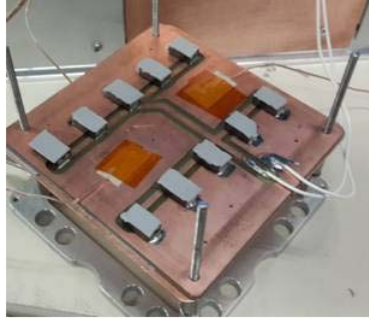
The contactor method was used to model soldering of the thermal straps. Four conduction paths were modeled through the straps: between the top face of the dissipater and the top straps, between the top straps and the radiator, between the bottom face of the dissipater and the bottom straps, and finally, between the bottom straps and the radiator.

### ***Experimental Validation of the Design***

A prototype of the heat dissipater was built when satisfactory results were obtained with the computational simulations. First, a thermal image of the circuit board was taken using a FLIR thermal imaging camera. The camera provides a visual map of test article temperatures using infrared thermography, which can be explained as detection of radiation in the long-infrared range of the electromagnetic spectrum. The purpose was to ensure the uniformity of heat distribution on the circuit board. After ensuring the uniformity, the experimental validation experiments were started with ET-E. The heat dissipater was placed in the sample CubeSat with the THCB heater. The TVAC was set to -15 °C and two power levels were (1.8W and 4.5W) applied to heaters, which are the same conditions used with ET-D. In the experiments conducted with THCB, aluminum edges, shown in Figure 21, were not used because the heaters had the same thickness. The reason was to create a direct contact between the heaters and the top face of the heat dissipater. This adjustment increased the conduction and simplified the validation process. A TGX Ultra Soft Thermal Conductive Pad was used between the heaters and the top face of the heat dissipater and between the bottom face and the circuit board in all experiments with THCB as shown in Figure 24.



(a) Thermal Conductive Pad Used between the Heat Dissipater Bottom Face and the Circuit Board



(b) Thermal Conductive Pad Used between the Resistors and the Top Face of the Heat Dissipater

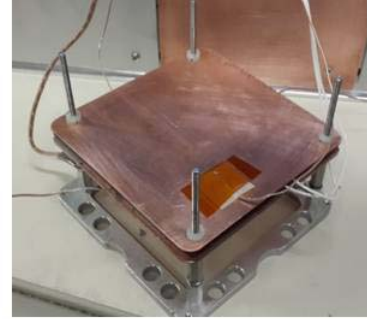


### **Figure 24: Thermal Conductive Pad on the Surfaces**

ET-E was conducted with a bare copper 1U size (10 cm x 10 cm) radiator. Thermal straps were not used in this experiment. The reason was to with prevent a direct conductive heat transfer between the heat dissipater and the radiator, therefore, to be able to observe the effectiveness of the straps in the following experiments.

In ET-F, conduction between the heat dissipater and the radiator was created using copper thermal straps. The comparison of ET-F and ET-E provided the effectiveness of the thermal straps. The straps soldered to both surfaces using a soldering iron as shown in Figure 25.

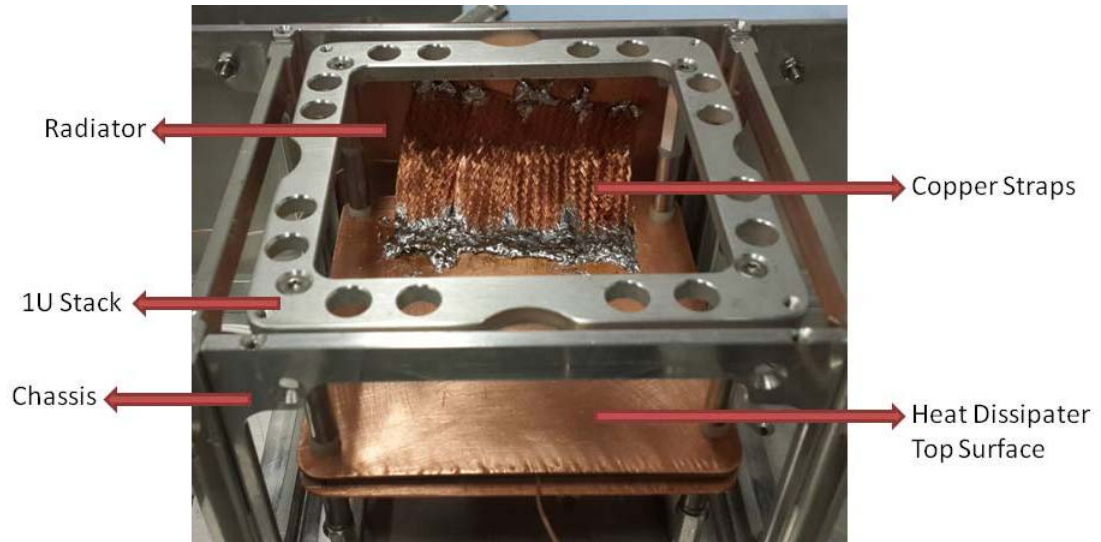


**Figure 25: The Thermal Straps Soldered to Heat Dissipater and the Radiator  
(ET-F)**

These thermal straps consisted of 15 mm wide Flat Bare Copper Braid, which is widely used in ground wire applications. Each of them has the dimensions of 1 mm x15 mm x 70 mm. Four straps were used between each heat dissipater surface and the radiator. Even though the braids are 1 mm thick, the effective thickness of the braids was calculated as 0.34 mm, because a 12.4 cm x 1.5 cm braid piece weighs 5.7g, however a solid copper with 1mm thickness should weigh 16.6g.

In ET-G, 3M 235 Black Photo Tape was used to cover the radiator to increase its radiative heat transfer with TVAC. The purpose was to determine the effectiveness of the surface finish of the radiator. Photographs of ET-F and ET-G are shown in Figure 26.



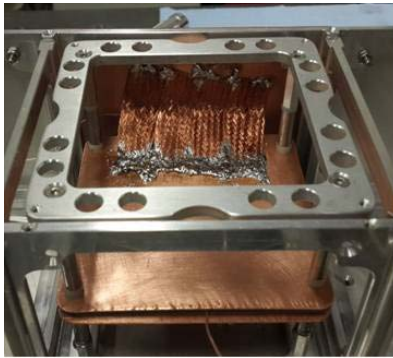
(a) The Sample CubeSat with 1U Radiator (ET-F)



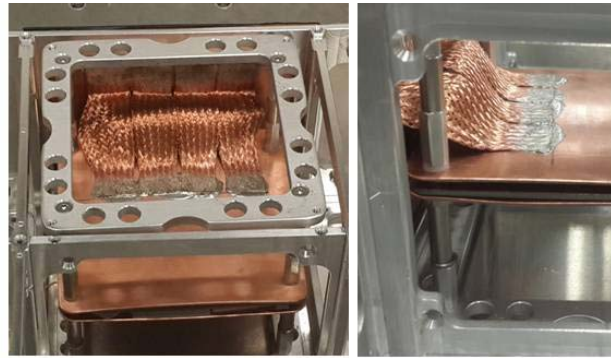
(b) The Sample CubeSat with Black Photo Tape Covered 1U Radiator (ET-G)

**Figure 26: The Sample CubeSat with Black Photo Tape Covered 1U Radiator**

In ET-H, ET-G configuration re-conducted with new soldered straps shown in Figure 27 (b). The purpose was to observe the effectiveness of the strap connection.



(a) Soldered Copper Braids Used in ET-F and ET-G



(b) Two Views of Soldered Copper Braids Used in ET-H

**Figure 27: Soldered Copper Braids Used in ET-F, ET-G, and ET-H**

The braids were soldered using a soldering iron for ET-F and ET-G. To increase the conduction, a blowtorch was used to solder the braids in ET-H. It can be seen in Figure 27(a) that, ET-F soldering technique did not create a connection between the braids and the dissipater as good as the technique in ET-H. ET-H heat dissipater configuration, which includes the heat dissipater box without aluminum edges, total eight 7 cm long copper soldered braids, and 1U size black tape covered radiator, was named as basic configuration of the heat dissipater in this research. Since it is assumed as the basic configuration of the heat dissipater, ET-H results were used to validate computational model of the heat dissipater on TD. Conduction values of ET-H were used to model the conductions through braids using the contactor method. In CS-H, TVAC computational model was set to same conditions with ET-H and the same power levels were applied.

In ET-H, an additional power level, 11W, was applied to heaters different from the other experimental validation tests. The purpose was to determine maximum power level to reach to 93 °C on the circuit board, which was the temperature measured without the heat dissipater in ET-D.

In ET-I, a 3U size (10 cm x 30 cm) radiator was used. The results were compared with ET-H to determine the effect of the radiator size. In ET-J, the 3U size radiator was covered with black tape to increase its radiative heat transfer within the TVAC. Figure 28 shows the photographs of the CubeSat used in the fifth and the sixth experiments.





(a) 3U Size Radiator Connected to the Heat Dissipater Using Soldered Thermal Straps



(b) The CubeSat with 3U Size Radiator, ET-I



(c) The CubeSat with Black Tape Covered 3U Size Radiator, ET-J

### Figure 28: Photographs of ET-I and ET-J

In ET-K, a black tape covered 1U size deployable radiator was used in addition to a 1U size side radiator, as shown in Figure 29, to determine the effect of a deployable radiator. The ruler in Figure 29 is in inches. Two straps were soldered to create the conduction between the top face of the dissipater and the deployable radiator. Two braids were used between the top face and the side radiator and four straps were used between the bottom face and the side radiator.

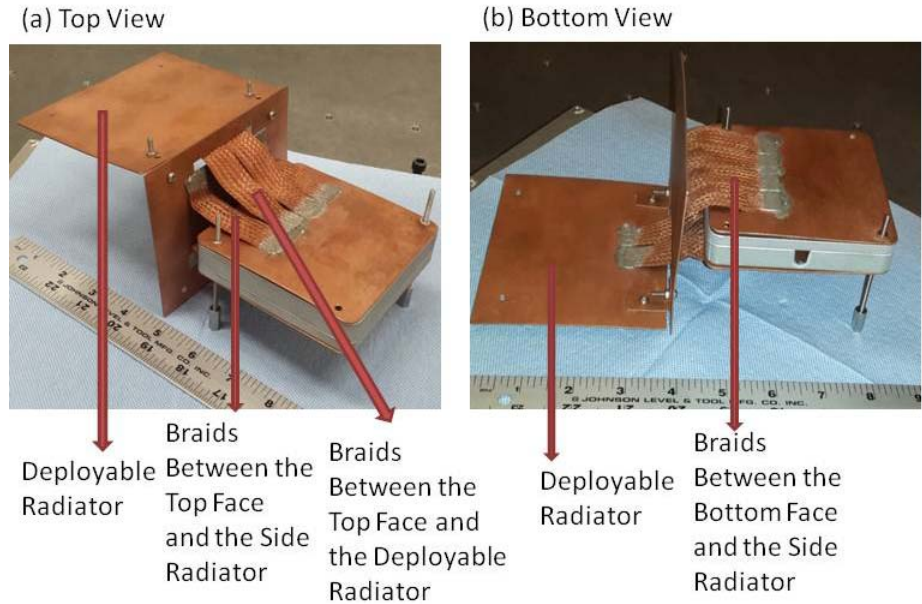


**Figure 29: The Heat Dissipater with a 1U Size Side Radiator and a 1U Size Deployable Radiator (ET-K)**

Both faces of the deployable radiator and the outside face of the side radiator were covered with black tape to be able to make a comparison with ET-H and determine the effect of the deployable radiator. Two L shaped copper fixed hinges were used to mount the deployable radiator to the side radiator. Since the hinges are poor conductors in actual use, black tape, kapton tape, and plastic washers were placed between the hinges and the deployable radiator to reduce conduction between the deployable radiator and the CubeSat as shown in Figure 30 (b). Photographs of ET-K are shown in Figure 30.

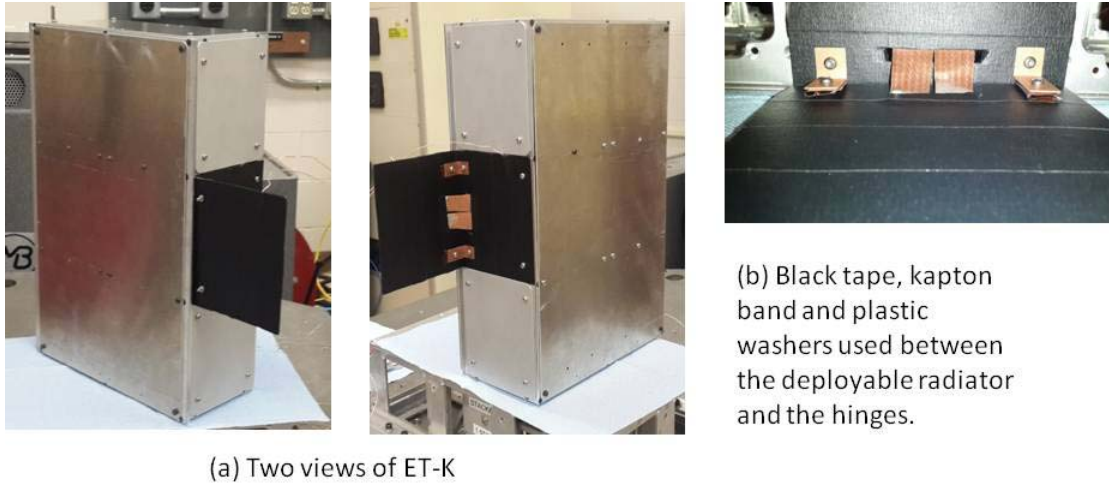


**Figure 30: Photographs of ET-K**

The design allows the user to add or remove aluminum edges, shown in Figure 21 and Figure 31 , with respect to circuit board components. The ruler in Figure 31 is in inches. The weight of all parts (heat dissipater box, radiator and soldered braids) is 360 grams.

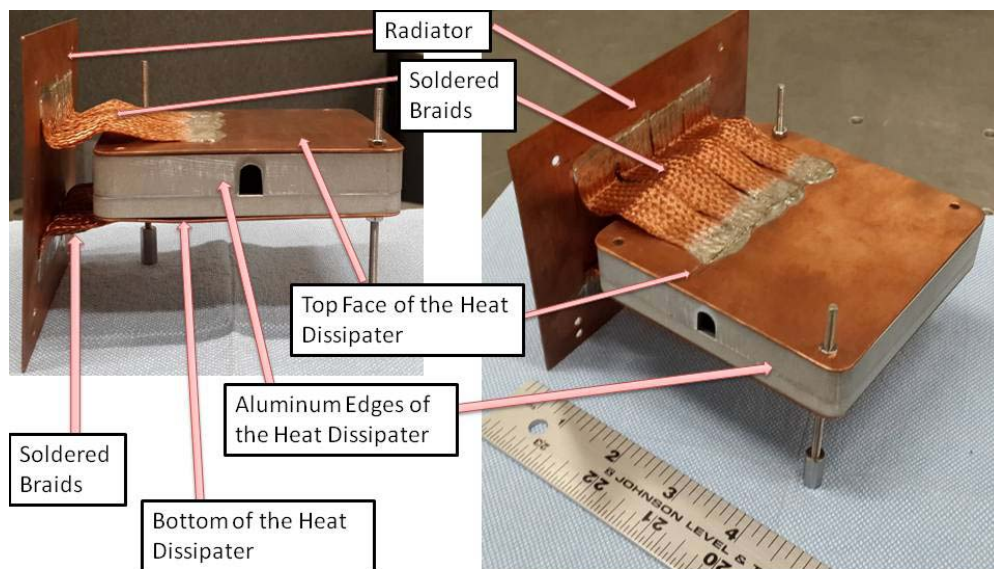
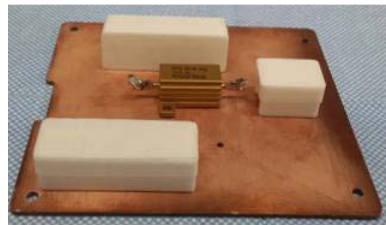


**Figure 31: The Heat Dissipater with 1U Size Radiator**

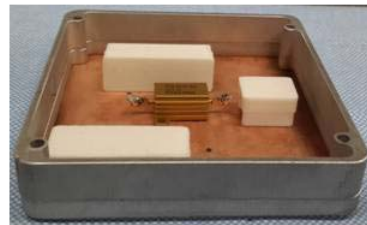
Since the thickest components of the circuit board were the heaters, which are at the same height, in the experiments with THCB, the aluminum edges were not mounted as shown in Figure 25, Figure 27, and Figure 28 (a). The top and bottom faces of the heat dissipater were placed directly on the circuit board. This configuration allowed for a direct contact and a good conduction between the processors and the heat dissipater's top surface. However, a direct contact may not be available in many applications. For example, there may be thicker components than the main heat source as shown in Figure 32 (b). In this case, aluminum edges of the heat dissipater must be used, as shown in Figure 32 (c), and the heat must be conducted from the high power processor to the top face of the heat dissipater, which sits on the aluminum edges. To simulate this configuration, two experiments, ET-L and ET-M, were conducted to get further verification for the design. SHCB, shown in Figure 14 (b) and Figure 32(a), was used in these experiments.



(a) SHCB (The Circuit Board with a Vishay 10W Capacity Resistor)



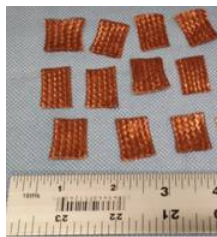
(b) SHCB with Sample Components



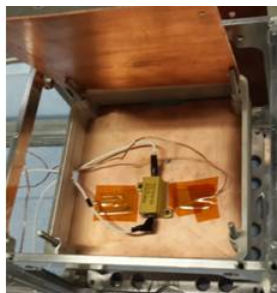
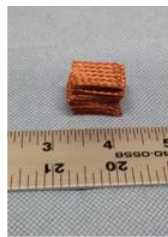
(c) SHCB with Aluminum Edges of the Dissipater

**Figure 32: Photographs of SHCB**

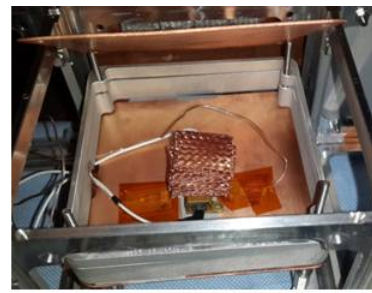
In ET-L, the sample CubeSat was tested in the -15 °C TVAC with 3.3W power. The purpose of the ET-L was to get the thermal behavior of the sample CubeSat with SHCB. In ET-M, the heat dissipater with aluminum edges was placed to cover the circuit board as shown in Figure 33, assuming there are thicker (higher) components than the heater (high power processor) on the circuit board and a direct contact between the heat source and the heat dissipater's top surface is not possible. The purpose of ET-M was to determine the effectiveness of the heat dissipater, when a direct contact between the heat source and the heat dissipater is not possible.



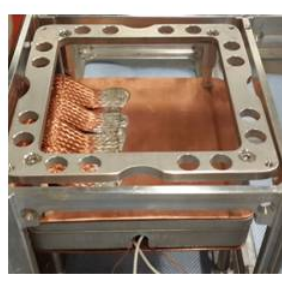
(a) The Copper Braids Used between the Heater and the Top Face of the Heat Dissipater (The ruler is in inches)



(b) The Heat Dissipater Covered the SHCB (Top Face is Open)



(c) The Braids Are Placed between the Heat Dissipater and the Single Heater (Top Face is Open)



(d) Two views of the ET-M (Top Face is Closed)

### Figure 33: Photographs of ET-M

Conduction was created using copper braids between the heater and the top face of the heat dissipater. The braids used in this experiment are shown in Figure 33(a). (The

ruler in the picture is in inches.) The braids were placed and pressed between the single heater and the top face of the heat dissipater as shown in Figure 33. In ET-M, TVAC was set to  $-15\text{ }^{\circ}\text{C}$  and 3.3W power applied to heater, which is the same condition with ET-L.

In ET-N, SHCB was used again in  $-15\text{ }^{\circ}\text{C}$  TVAC with 3.3W power. However, this time the basic configuration of the heat dissipater (without aluminum edges) was used. The purpose of this test was to compare results with ET-M and determine the heat transfer effectiveness of the copper braid pieces used in ET-M.

As discussed previously, since ET- D results showed that the temperature on the bottom face of the circuit board is very close to the temperatures of the heaters, the shape of the heat dissipater design was determined as a box. The first reason was to be able to dissipate the heat using the bottom face of the circuit board in addition to the top face. The second reason was to minimize or eliminate the heat source's thermal effect on the CubeSat's overall thermal management with covering the heat source with a box shape heat sink. In ET-O, only the top face of the heat dissipater was used with THCB in  $-15\text{ }^{\circ}\text{C}$  TVAC. The photographs of ET-O are shown in Figure 34. The same two power levels with the other THCB experiments, 4.5W and 1.8W, were used. The purpose of this test was to determine the effectiveness of the heat dissipater's box shape with a comparison between ET-O and ET-H.

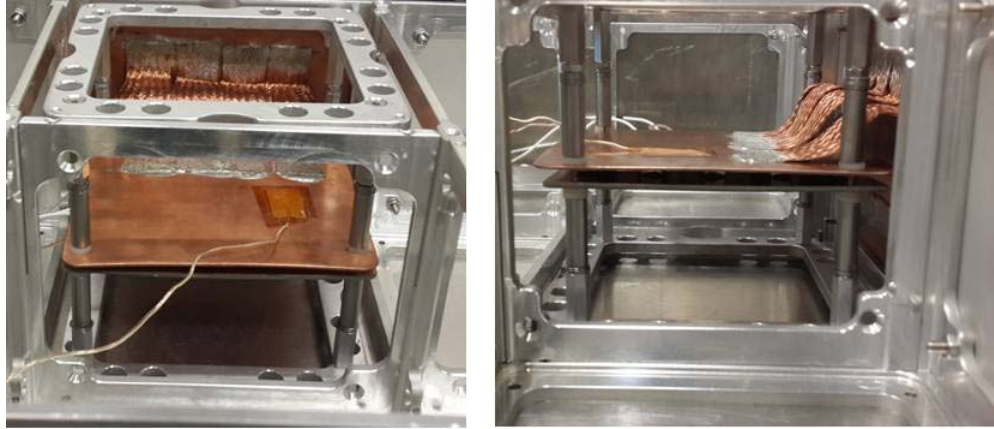


**Figure 34: Photographs of ET-O**

### *Computational Orbit Performance Simulations of the Design*

While it is able to simulate the space environment, a TVAC cannot reach actual deep space vacuum and temperature conditions. The main purpose of TVAC testing is to validate a thermal design so that one may conduct dependable further computational experiments such as orbit performance simulations.

Two orbits were modeled with TD for these simulations. The validated model created in CS-H was used in orbit performance simulations. Both orbits were modeled with 500 km circular orbits. It needs to be emphasized that, the most important assumption of these simulations was allowing radiators to face deep space continuously. The first orbit had a  $0^\circ$  beta angle to simulate a sample cold case as shown in Figure 35.

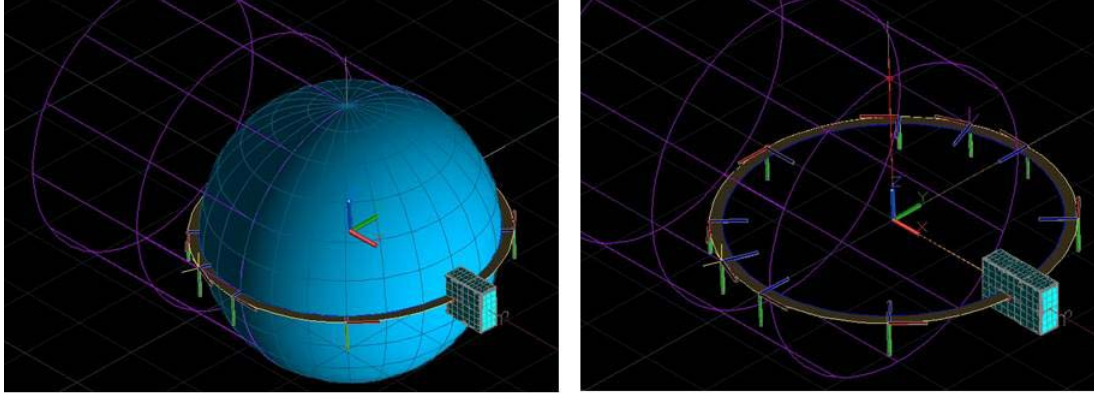


**Figure 35: Two views of the 0° Beta Angle Orbit, The Sample Cold Case**

The radiator is on the 3U face (10 cm x 30 cm face) and facing  $-Z$  direction on this orbit. The sun is in  $+X$  direction and the purple circles indicates the shadow of the Earth. In the second view in Figure 35, the Earth model was turned off to get a better view of the orbit. Three tests were conducted with this orbit: CS-P, CS-Q, and CS-R. In CS-P, the sample CubeSat model was used without the heat dissipater and the radiator. 4.5W of power applied to heaters. The purpose of this simulation was to determine the thermal behavior of the sample CubeSat with THCB in the sample cold case orbit. In CS-Q, basic configuration of the heat dissipater (with 1U size black tape covered radiator) was used to get the effectiveness of the heat dissipater in the cold case orbit. First, 4.5W of power was applied to be able to make comparison with CS-P and then, the power was increased to acquire the same temperature on the circuit board with the CS-P simulation. In CS-R simulation, the black tape covered 3U size radiator was used with the heat dissipater to determine the effect of the radiator size. Again, 4.5W was used for comparison, and the power level was increased to acquire the same temperature on the circuit board with the CS-P simulation.



The second orbit was modeled with a  $90^\circ$  beta angle for a sample hot case, which is shown in Figure 36. The radiator is on the 3U face (10 cm x 30 cm face) and facing  $-Y$  direction in the Figure 36. To simulate better a hot case, 6U face (20 cm x 30 cm face) of the CubeSat was oriented to the sun direction. The sun is in  $+X$  direction. The Earth model was turned off in the second view. Three simulations were conducted with this orbit: CS-S, CS-T, and CS-U.

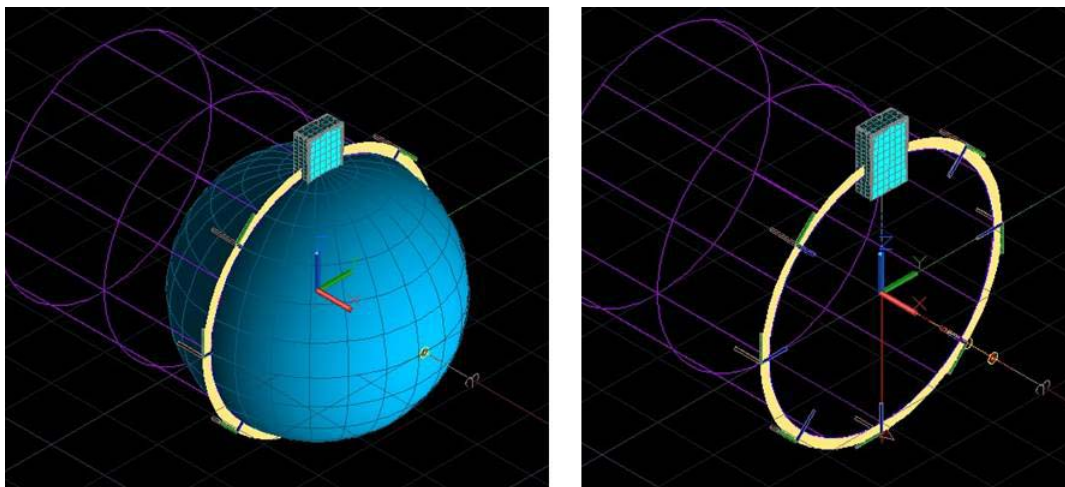


**Figure 36: Two views of the  $90^\circ$  Beta Angle Orbit, the Sample Hot Case**

In CS-S, the heat dissipater model and the radiator were not used. Thermal behavior of the sample CubeSat with THCB in the sample hot case orbit was determined in CS-S with applying 4.5W power to heaters. In CS-T, 4.5W power was applied to heaters using the basic configuration of the heat dissipater with the purpose of determining the effectiveness of the heat dissipater on the sample hot case orbit. After 4.5W simulation, the power level was increased to acquire the same temperature on the circuit board with CS-S to provide the improvement in power capacity with the same

maximum temperature. In CS-U, the black tape covered 3U size radiator was used to provide the effect of radiator size with two power levels: 4.5W and 22W.

### **Summary**

This chapter provided the descriptions of the methodologies used in this research. Both experimental and computational methodologies of the thesis were introduced and a brief experiment procedure was presented for both of them. The test articles were presented and all experiments and computational simulations conducted in this research were discussed in detail. Finally, the heat dissipater design process was introduced and the factors that drove the process were expressed.

## IV. Analysis and Results

This chapter provides the data collected from the experiments and predictions computed in simulations. The summary of the experiments and the simulations is presented in Table 1. As explained previously, in this thesis, *experimental test* is abbreviated as *ET*, *computational simulation* is abbreviated as *CS*, and all experiments and simulations were named with a letter to prevent confusion. For example chassis-only experimental test was named as experimental test-A , *ET-A*, and chassis-only computational simulation was named as computational simulation-A, *CS-A*.

The results of ET-A and CS-A provided data for further validation for the previously created TVAC computational model. ET-B provided data about THCB thermal behavior under vacuum. ET-C data were used to determine power levels for the subsequent experiments. ET-D and CS-D experiment results were used to acquire a validated sample CubeSat model, which was used to create a heat dissipation model. Lastly, all other data are presented in this chapter provided essential data for the objective of this thesis, which is developing a modular approach to dissipate heat from heat sources on a circuit board in a CubeSat.

### **Results of Chassis Only Experiment and Simulation (ET-A and CS-A)**

These tests included three steady state temperature set points, -10, 30, and 60 °C, which were selected within the TVAC's temperature envelop. ET-A data were used to determine the thermal behavior of the chassis in TVAC. In CS-A, the chassis were modeled on TD and the results were used for validation.

Five thermocouples were used to collect temperature data from the chassis. For the computational simulations, the nodes were determined which are at the same location

as the thermocouples. Selected thermocouple positions are shown in Figure 37. Temperature color post-processing figures of the -10 °C CS-A are shown in Figure 38. Since there are some energy losses because of the opening to solar simulator gate (shown in Figure 3), which is in the +X direction in Figure 38, the temperatures are slightly different around the chassis. There are also some losses from the front door, -Y direction, which can be detectable from the color difference on the chassis between the -Y side and +Y side. Even though there are losses from the walls of the shroud, these losses can be assumed to be compensated since the walls, except the front wall, have active temperature control with the engaged thermal media loop piping. Result comparison of the -10 °C ET-A and CS-A is providing in Table 2.

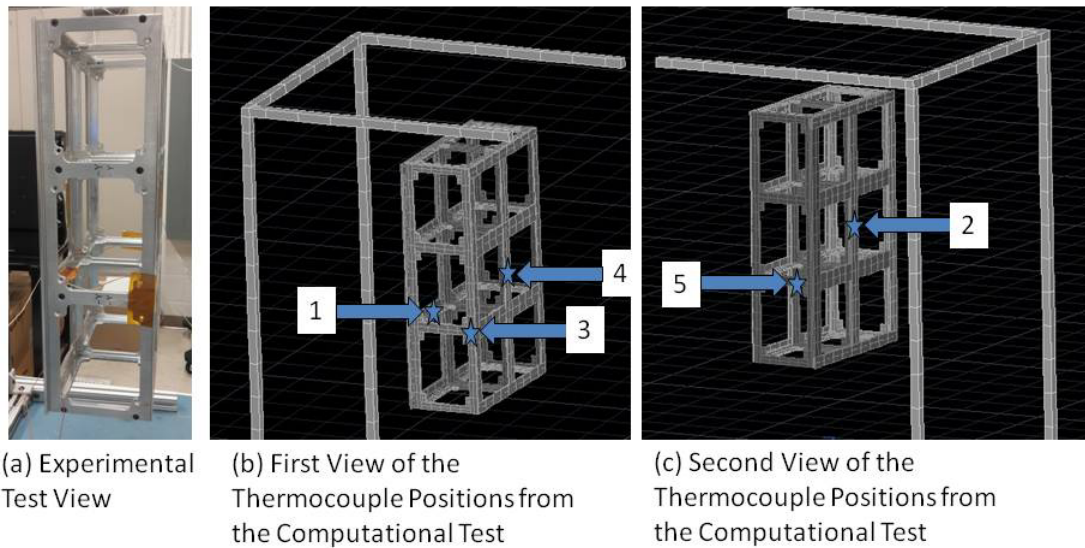


**Figure 37: Thermocouple Positions for ET-A and CS-A**

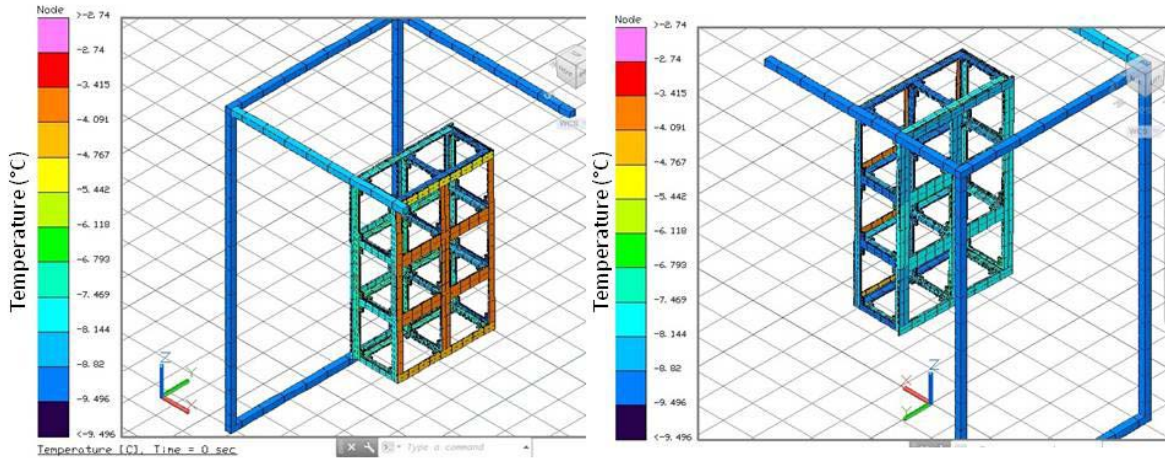


**Figure 38: Temperature Color Post-processing Figures of the -10 °C CS-A**

**Table 2: T= -10 °C ET-A and CS-A Steady State Temperature Result Comparison**

TVAC Plate and Shroud Temperature T = -10 °C			
	Experimental Results (°C)	Computational Results (°C)	Temperature Error (°C)
1 <sup>st</sup> Thermocouple	-6.43	-7.04	0.61
2 <sup>nd</sup> Thermocouple	-6.45	-7.79	1.34
3 <sup>rd</sup> Thermocouple	-5.89	-7.73	1.84
4 <sup>th</sup> Thermocouple	-5.43	-3.81	1.62
5 <sup>th</sup> Thermocouple	-6.16	-8.84	2.68

Table 2 shows that, there is a good validation for the model, with an error below 2.7 °C.

Temperature color post-processing figures of the 30 °C CS-A are shown in Figure 39, result comparison of the 30 °C ET-A and CS-A is providing in Table 3.

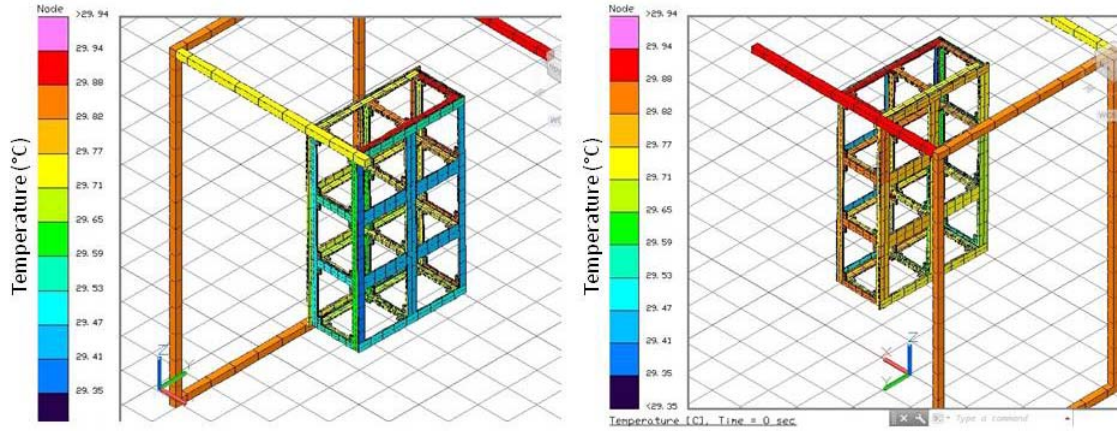


**Figure 39: Temperature Color Post-Processing Figures of the 30 °C CS-A**

**Table 3: T= 30 °C ET-A and CS-A Steady State Temperature Results Comparison**

TVAC Plate and Shroud Temperature T = 30 °C			
	Experimental Results (°C)	Computational Results (°C)	Temperature Error (°C)
1 <sup>st</sup> Thermocouple	30.27	29.73	0.54
2 <sup>nd</sup> Thermocouple	29.71	29.75	0.04
3 <sup>rd</sup> Thermocouple	30.46	29.51	0.95
4 <sup>th</sup> Thermocouple	30.83	29.76	1.07
5 <sup>th</sup> Thermocouple	30.03	29.85	0.18

It makes sense that the energy losses from the shroud were small in the 30 °C test, which is close to room temperature. As a result, the error possibility of the computational

model was small and the validation for the model was very good with an error below 1.1 °C.

Figure 40 shows the temperature color post-processing figures of the 60 °C ET-A and CS-A. Since the energy losses are more in the directions of +X (solar simulator gate) and -Y (front door), as expected, the temperatures of the chassis are relatively cooler at those sides. Table 4 provides the result comparison of the 60 °C ET-A and CS-A. Result comparison of the 60 °C ET-A and CS-A is providing in Table 4.

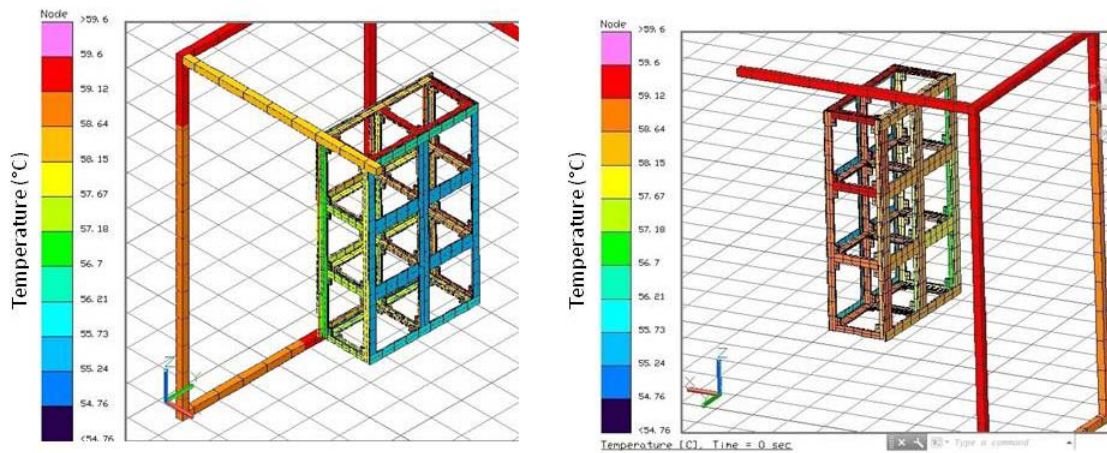


**Figure 40: Temperature Color Post-Processing Figures of the 60 °C ET-A and CS-A**

**Table 4: T= 60 °C ET-A and CS-A Steady State Temperature Results Comparison**

TVAC Plate and Shroud Temperature T = 60 °C			
	Experimental Results (°C)	Computational Results (°C)	Temperature Error (°C)
1 <sup>st</sup> Thermocouple	58.88	58.09	0.79
2 <sup>nd</sup> Thermocouple	59.60	58.26	1.34
3 <sup>rd</sup> Thermocouple	59.33	58.32	1.01
4 <sup>th</sup> Thermocouple	58.13	58.28	0.14
5 <sup>th</sup> Thermocouple	59.71	59.02	0.69

As shown in Table 4, correlation between the computational and experimental 60 °C tests was done with a temperature error below 1.4 °C. Temperature errors for all steady state set points are provided below in Table 5 for an easier evaluation.

**Table 5: Temperature Errors of the ET-A and CS-A for All Steady State Test Points**

Temperature Errors of ET-A and CS-A (°C)			
Steady State Set Point	T = -15 °C	T = 30 °C	T = 60 °C
1 <sup>st</sup> Thermocouple	0.61	0.54	0.79
2 <sup>nd</sup> Thermocouple	1.34	0.05	1.34
3 <sup>rd</sup> Thermocouple	1.84	0.95	1.01
4 <sup>th</sup> Thermocouple	1.62	1.07	0.14
5 <sup>th</sup> Thermocouple	2.68	0.18	0.69



Table 5 shows that the correlation was done for all steady state set points with an error below 2.7 °C. As the main result of ET-A and CS-A, the greater validation of the previously generated TVAC environment computational model was provided by conducting experiments of a sample 6U CubeSat chassis.

### **Results of Chassis with Heaters Experiment (ET-B) and Sample CubeSat Power Level Determination Experiment (ET-C)**

In ET-B, the TVAC was set to -15 °C and the experiment was started with a power level of 1.8 W. When steady state was achieved, the power was increased to 2.7 W, 4.5 W, and 6.3 W and data were collected at each new level.

In ET-C, the TVAC was set to -15 °C and 1.8 W, 2.7 W, and 4.5 W power levels were applied to observe the effect of high reflectivity of the aluminum covers with respect to black paint coated TVAC shroud. In this experiment, different from the chassis with heaters experiment, powers greater than 4.5 W were not pursued to prevent damage.

When there is a heat source inside the TVAC, the temperatures of the shroud and the plate change slightly during long experiments such as 24 hours or longer. If the temperature inside of the TVAC is relatively large, such as a resistor at 100 °C, the change of the TVAC temperature also becomes large ( $\pm 5$  °C in 24 hours). For this reason, since most of the experiments in this research were longer than 24 hours, plate and shroud temperatures of the TVAC were also presented with thermocouple data. For example, even though the set temperature of TVAC was -15 °C in ET-B, shroud temperature increased to -0.6 °C when the steady state was achieved at the 6.3W level. Table 6 shows the steady state results for each power level.

**Table 6: Steady State Result Comparison of the ET-B and ET-C**

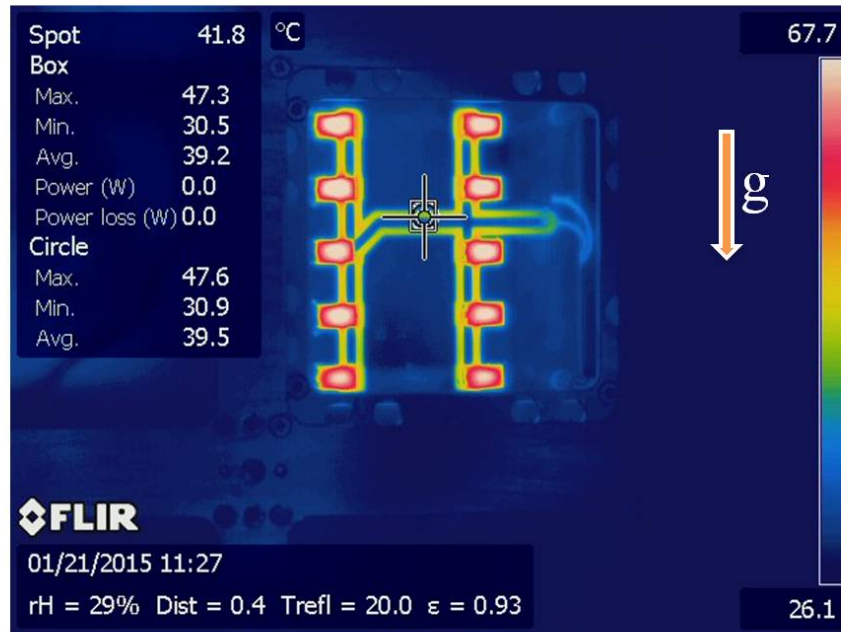
		ET-B	ET-C
1.8W Power	TVAC Plate / Shroud Temperature	-14.3°C / -12.4°C	-9.1°C / -4.3°C
	Circuit Board Temperature	31.3°C	52.3°C
2.7W Power	TVAC Plate / Shroud Temperature	-10.3°C / -5.5°C	-7.0°C / -1.9°C
	Circuit Board Temperature	51.9°C	75.0°C
4.5W Power	TVAC Plate / Shroud Temperature	-7.6°C / -2.0°C	-5.5°C / -0.4°C
	Circuit Board Temperature	74.1°C	102.0°C
6.3W Power	TVAC Plate / Shroud Temperature	-6.0°C / -0.6°C	-
	Circuit Board Temperature	92.2°C	-

Table 6 shows that temperatures increased faster in the sample CubeSat experiment as expected. Resistors in the aluminum-covered chassis heated the circuit board to 102 °C with 4.5W, although in ET-B, 6.3W was needed to reach to the 92.2 °C temperature level.

Two power levels, 1.8W and 4.5W, were selected for the subsequent experiments to decrease the experiment time, taking into consideration the results of ET-C.

### **Results of Sample CubeSat Tests (ET-D and CS-D)**

Before the ET-D experiments, thermal image of the circuit board was taken to ensure the uniformity of heat distribution on the circuit board, as shown in Figure 41.



**Figure 41: Thermal Image of the Circuit Board in Ambient Pressure and Room Temperature**

It should be noted that, the circuit board was perpendicular to the ground. Upper heaters seem warmer because of natural convection effect; however, it is apparent that, there is horizontally uniform heat dissipation. Consequently, the thermal image showed that there was a roughly uniform heat distribution on the circuit board and all resistors dissipate approximately the same amount of heat. Therefore, in the case of acquiring different temperatures from two thermocouples on the circuit board's top face in the same experiment, assuming uniform heat dissipation on the board, it was known that there was an error with measurements.

Six ET-D experiments were conducted with 1.8W and 4.5W power levels. In CS-D, the same experiments were conducted in TD as well. Steady state result comparison for 1.8W ET-D and CS-D is shown in Figure 42. Steady state result

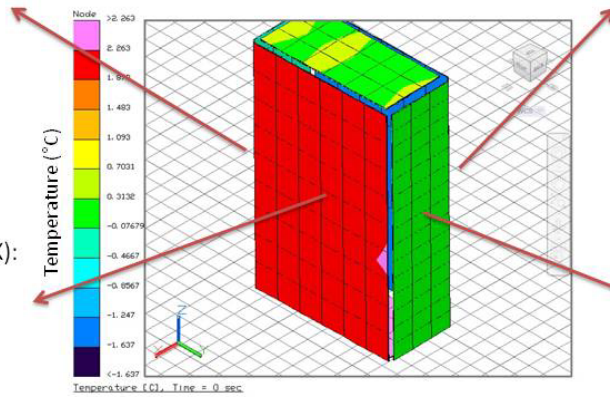
comparison for 4.5W is shown in Figure 43. Some layers of the CubeSat thermal model were turned off to get a better view of the salient features in Figure 42 and Figure 43.

Front Cover (-Y):  
 Experimental Result (ER): -2.1°C  
 Computational Result (CR) : -0.2°C

Left Cover (-X):  
 Experimental Result (ER): -1.0°C  
 Computational Result (CR): -1.6°C

Right Cover (+X):  
 ER: 0.1°C  
 CR: 2.2°C

Back Cover (+Y):  
 ER: -1.5°C  
 CR: 0.2°C



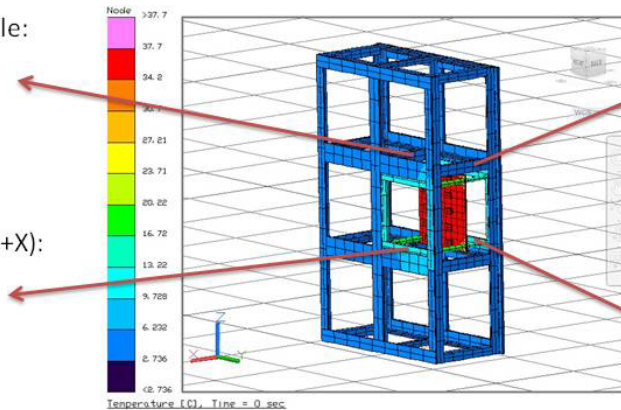
(a) Outside View

Chassis Middle:  
 ER: 2.7°C  
 CR: 5.0°C

Chassis Back (+Y):  
 ER: 0.3°C  
 CR: 3.5°C

1U Stack Top (+X):  
 ER: 7.0°C  
 CR: 9.0°C

1U Stack Bottom (-X):  
 ER: 5.5°C  
 CR: 8.0°C



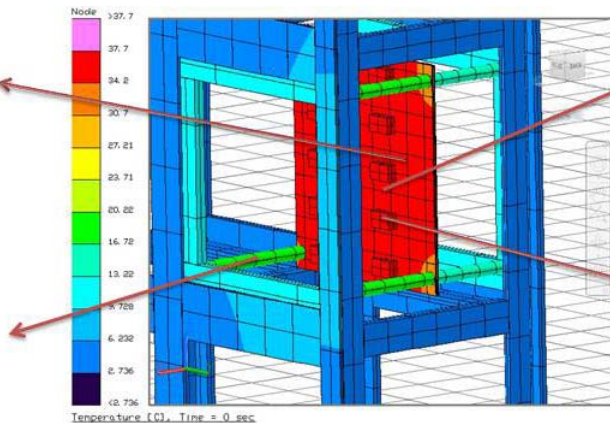
(b) Inside View-1

Circuit Board  
 Top Face:  
 ER: 39.0°C  
 CR: 37.0°C

Circuit Board  
 Back Face :  
 ER: 37.5°C  
 CR: 36.0°C

Spacer:  
 ER: 14.0°C  
 CR: 15.4°C

Heater:  
 ER: 40.0°C  
 CR: 38.0°C



(c) Inside View-2

**Figure 42: Steady State Test Result Comparisons for the 1.8W ET-D and CS-D**

Front Cover (-Y):  
 Experimental Result (ER): 10.3°C  
 Computational Result (CR) : 13.0°C

Left Cover (-X):  
 Experimental Result (ER): 13°C  
 Computational Result (CR): 11.2°C

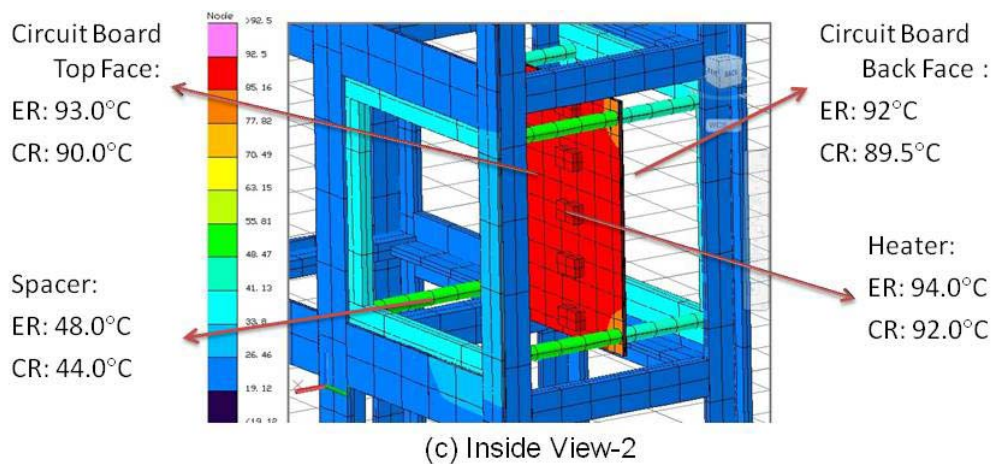
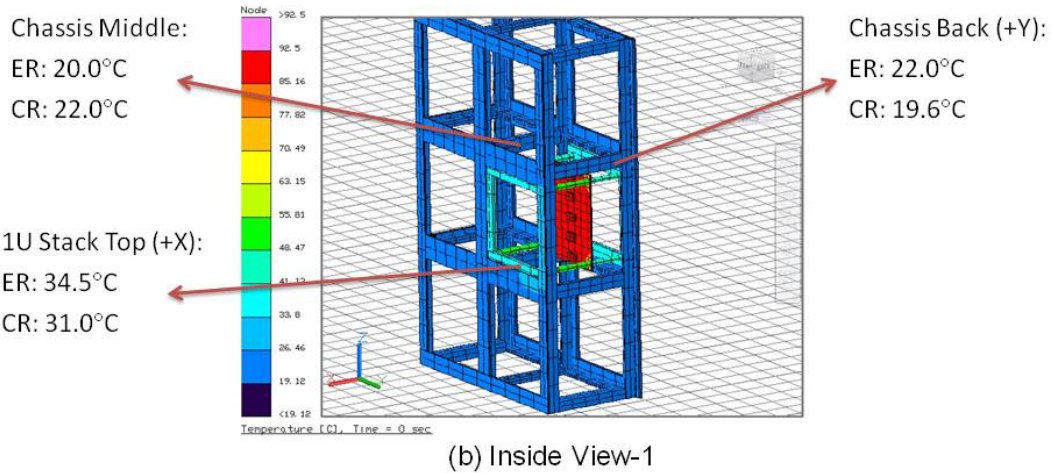
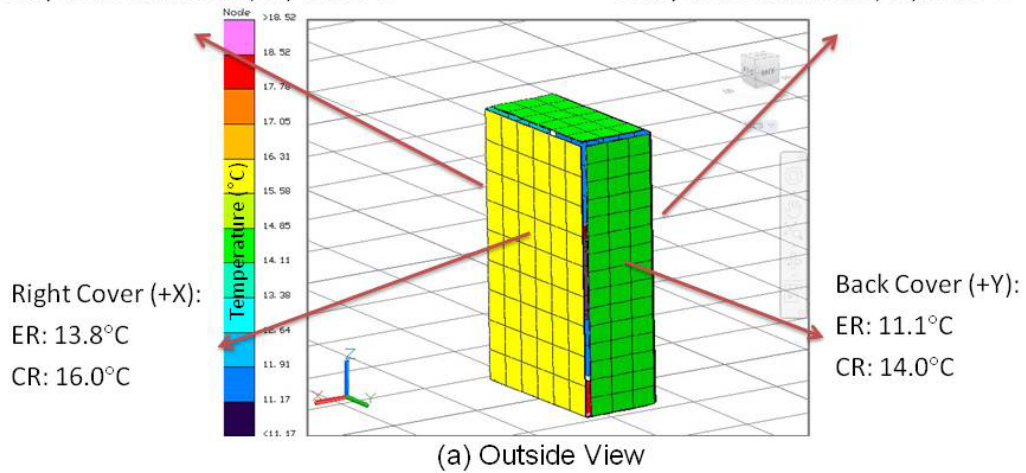


**Figure 43: Steady State Test Result Comparisons for the 4.5W ET-D and CS-D**

Table 7 shows the result comparison for 1.8W and Table 8 for 4.5W ET-D and CS-D. Each measurement point, e.g. front cover, back cover, or chassis middle, is represented with a number in the tables.

**Table 7: 1.8W ET-D and CS-D Steady State Result Comparison**

<b>Power Level P=1.8W</b>								
<b>TVAC Plate Temperature T = -14 °C, TVAC Shroud Temperature T= -13°C</b>								
Measurement Point	Experimental Results (°C)	Computational Results (°C)	Error (°C)		Measurement Point	Experimental Results (°C)	Computational Results (°C)	Error (°C)
1	-0.2	-2.1	<b>1.9</b>		7	3.5	0.3	<b>3.2</b>
2	-1.6	-1.0	<b>0.6</b>		8	9.0	7.0	<b>2.0</b>
3	2.2	0.1	<b>2.1</b>		9	8.0	5.5	<b>2.5</b>
4	0.2	-1.5	<b>1.7</b>		10	37.0	39.0	<b>2.0</b>
5	5.0	2.7	<b>2.3</b>		11	15.4	14.0	<b>1.4</b>
6	38.0	40.0	<b>2.0</b>		12	36.0	37.5	<b>1.5</b>

**Table 8: 4.5W ET-D and CS-D Steady State Result Comparison**

<b>Power Level P=4.5W</b>								
<b>TVAC Plate Temperature T = -15 °C, TVAC Shroud Temperature T= -14°C</b>								
<b>Measurement Point</b>	<b>Experimental Results (°C)</b>	<b>Computational Results (°C)</b>	<b>Error (°C)</b>		<b>Measurement Point</b>	<b>Experimental Results (°C)</b>	<b>Computational Results (°C)</b>	<b>Error (°C)</b>
1	13.0	10.3	<b>2.7</b>		7	90.0	93.0	<b>3.0</b>
2	11.2	13.0	<b>1.8</b>		8	89.5	92.0	<b>2.5</b>
3	16.0	13.8	<b>2.2</b>		9	48.0	44.0	<b>4.0</b>
4	14.0	11.1	<b>2.9</b>		10	92.0	94.0	<b>2.0</b>
5	22.0	20.0	<b>2.0</b>		11	22.0	19.6	<b>2.4</b>
6	34.5	31.0	<b>3.5</b>					

Table 7 and Table 8 show that maximum steady state temperature error between ET-D and CS-D was  $T_{error} \leq 4$  °C, which is within the acceptable error value determined for this research. Consequently, physical shape and thermo-optic properties of the computational model were close enough to physical tests and the computational model was dependable for a heat dissipater design.

### **Experimental and Computational Results of the Heat Dissipater Design**

Steady state temperature results of the heat dissipater validation experiments with the THCB are shown in Table 9 for 4.5W and 1.8W power levels.



**Table 9: Steady State Temperature Results of the Heat Dissipater Validation Experiments with THCB**

Power Level P=4.5W									
Thermocouple	ET-E (°C)	ET-F (°C)	ET-G (°C)	ET-H (°C)	ET-I (°C)	ET-J (°C)	ET-K (°C)	ET-O (°C)	ET-D (°C)
Circuit Board Top Face (Two Thermocouples)	103.1/ 105.4	56.1/ 57.4	46.5/ 47.8	34.4/ 34.9	43.9/ 44.4	26.4/ 27.3	30.0/ 31.5	69.5/ 67.5	93.0
Heat Dissipater Top Face	(Failed)	46.4	36.9	33.7	39.2	22.0	23.3	42.5	-
Heat Dissipater Bottom Face	90.8	49.3	40.0	31.8	36.7	19.3	28.6	-	-
Radiator (Outside Face)	22.1	23.3	16.4	18.1	26.6	9.3	10.1/3.8 (Deployed)	14.8	14.0 (Aluminum cover)
TVAC Plate	-15.1	-15.3	-15.3	-15.3	-14.1	-15.3	-14.8	-13.5	-15.0
TVAC Shroud	-14.7	-15.0	-13.0	-15.0	-15.1	-14.9	-13.2	-13.0	-14.0

Power Level P=1.8W									
Thermocouple	ET-E (°C)	ET-F (°C)	ET-G (°C)	ET-H (°C)	ET-I (°C)	ET-J (°C)	ET-K (°C)	ET-O (°C)	ET-D (°C)
Circuit Board Top Face (Two Thermocouples)	46.5/ 47.5	18.9/ 19.5	14.0/ 14.6	13.7/ 13.9	12.8/ 13.2	3.7/ 4.1	9.1/ 9.8	27.4/ 28.6	39.0
Heat Dissipater Top Face	(Failed)	15.0	10.2	13.7	11.2	2.3	6.5	16.2	-
Heat Dissipater Bottom Face	41.6	16.3	11.6	12.6	10.3	1.3	8.5	-	-
Radiator (Outside Face)	4.9	5.1	1.9	7.4	6.5	-2.2	1.4/-2.2 (Deployed)	3.7	-1.5 (Aluminum cover)
TVAC Plate	-13.4	-14.9	-14.6	-9.3	-13.9	-15.1	-13.0	-12.0	-14.0
TVAC Shroud	-12.9	-14.0	-13.8	-5.6	-12.6	-14.3	-11.8	-11.5	-13.0

Since both power level experiments resulted in similar consequences, only 4.5W results are discussed in this chapter. ET-E results showed that, as expected, the circuit board temperature was higher with respect to ET-D, because the black heaters' view to aluminum of the CubeSat was blocked by bare copper, top face of the heat dissipater, which has lower infrared emissivity and absorptivity. In addition to that, a 1U size bare copper radiator was placed instead of a same size aluminum plate, as shown in Figure 26 (a), which has lower IR emissivity than the aluminum. Since the conduction between the heat dissipater and the radiator was not created using braids in this experiment, as explained in the previous chapter, the circuit board temperature was increased to 105 °C from the 93 °C (ET-D) at the 4.5W power level.

In ET-F, copper braids were soldered between the heat dissipater and the 1U size radiator as shown in Figure 25. The conduction through copper braids reduced the circuit board temperature from 105.4 °C to 57.4 °C. Since copper has a very low IR emissivity ( $\epsilon_{\text{copper}}=0.04$ ), in ET-G, the radiator was covered with black tape which has a much higher IR emissivity ( $\epsilon_{\text{black tape}}=0.9$ ). This configuration reduced the temperature an additional 10 °C, from 57.4 °C to 47.8 °C. It must be noted that, in ET-F and ET-G, the top face of the heat dissipater is cooler than the bottom face, which indicates that there is not good conduction between the bottom face of the heat dissipater and the radiator. Since the heaters were hotter than the bottom face of the circuit board in ET-D, it should be expected that the top face of the heat dissipater must be warmer than the bottom face, because the heaters were in direct contact with the top face using a thermal conductive pad. Thus, it can be deduced that, there was a poor conduction between the bottom face of the heat dissipater and the radiator.

In ET-H, braids are soldered at a very high temperature using a blowtorch instead of soldering iron to create better conduction. Black tape covered 1U size radiator was used, which is the same configuration with ET-G. Results of ET-H showed that this soldering technique was better, as expected. The temperature difference between the top and bottom faces of the heat dissipater was reduced to 1.9 °C from 3.1 °C, which shows that there is very good conduction between the radiator and both faces of the heat dissipater through copper braids. Additionally, the temperature difference between the heat dissipater and the radiator was reduced to 13.7 °C from ET-G result of 20.5 °C, which is another indicator of better conduction through braids. Furthermore, in ET-G, the top face of the heat dissipater was hotter than the bottom face, which shows that the conduction from both faces of the heat dissipater to radiator was relatively equal. Consequently, ET-H results showed that the connection technique of the thermal straps is very effective to determine the achievement of the heat dissipation. ET-H heat dissipater configuration was named as basic configuration as explained in the previous chapter.

As the last step in ET-H, the power level was increased to acquire a circuit board top face temperature of 93 °C (ET-D result). The purpose was to determine how much power increase could be achieved by using the heat dissipater, assuming the ET-D result, 93 °C, is the maximum operating temperature.

**Table 10: The Comparison of ET-D and ET-H for Different Power Levels**

	ET-D	ET-H	ET-H
Power (W)	4.5	4.5	11
Circuit Board Top Face Temperature (°C)	93.0	34.9	89.0
TVAC Plate Temperature (°C)	-15.0	-15.3	-13.2
TVAC Shroud Temperature (°C)	-14.0	-15.0	-11.2

Table 10 shows that, THCB power level could be increased to 11W using the heat dissipater assuming the maximum temperature allowed is 93 °C. It should be noted that, in 11W ET-H experiment TVAC was warmer than ET-D experiment, which indicates that, actual power increase capability of the heat dissipater is a more than 11W for basic configuration. Consequently, the heat dissipater basic configuration is capable to allow an increase of power more than 240% on the circuit board, without exceeding the temperature level without a heat dissipater.

In ET-I, 3U size bare copper radiator made cooler all measured temperatures on the CubeSat with respect to ET-F as shown in Table 9. In ET-J, the 3U size radiator was covered with black tape and the circuit board temperature was measured as 27.3 °C, which was 93.0 °C in ET-D without the heat dissipater.

In ET-K, a 1U size deployable radiator was added to basic configuration, and the circuit board temperature was measured as 31.5 °C, which is a better result with respect to ET-H result of 34.9 °C. The top face of the heat dissipater was colder than the bottom face, which shows the braids between the deployable radiator and the top face of the heat dissipater achieved their design goal. However, it is obvious that the deployable radiator

did not improve significantly the heat dissipation capability of the design. Even though the side radiator was 10.1 °C, the deployable radiator was 3.8 °C, which shows that there is not enough conduction between the top surface of the heat dissipater and the deployable radiator. The conduction between the deployable radiator and the side radiator was minimized using black tape, kapton tape, and plastic washers as shown in Figure 30 (b) to simulate a real hinge as discussed in the previous chapter. It can be deduced that the effectiveness of the design with deployable radiator can be improved by increasing the conduction between the deployable radiator and the heat dissipater. It should also be noted that in ET-K, the shroud temperature is 1.8 °C warmer than ET-H, which is another reason for not having a noteworthy result from ET-K.

**Table 11: Steady State Temperature Results of ET-L, ET-M and ET-N**

	ET-L	ET-M	ET-N
Heat Dissipater	-	✓	✓ (w/o Edges)
Power	3.3W	3.3W	3.3W
Circuit Board Temperature	100.7 °C	37.7 °C	25.2 °C
TVAC Plate Temperature	-13.7 °C	-14.7 °C	-14.9 °C
TVAC Shroud Temperature	-12.9 °C	-13.4 °C	-13.4 °C

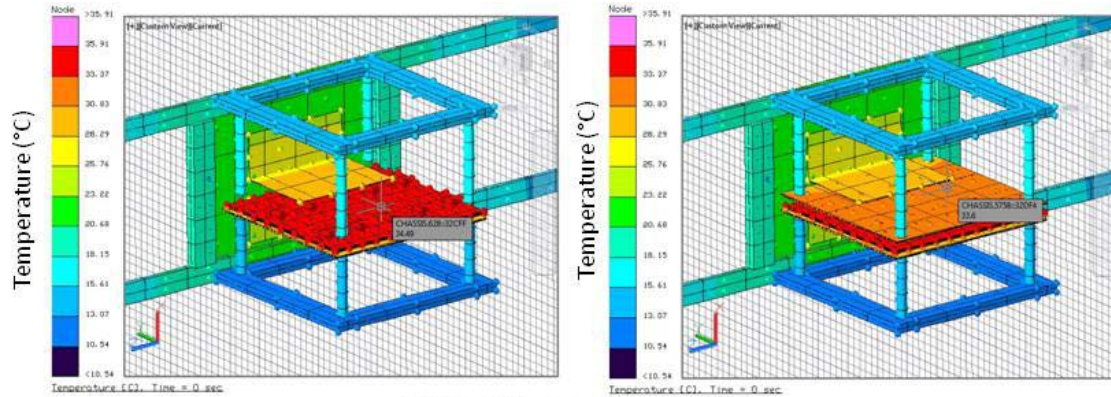
Steady state temperature results of ET-L and ET-M are presented in Table 11. In ET-L and ET-M, the SHCB was used to determine the effectiveness of the design when a direct connection between the heat source and the top face of the heat dissipater is not possible, as discussed in the previous chapter. First, in ET-L, the CubeSat with SHCB was tested in -15 °C TVAC. The experiment was terminated at the 3.3W power level, when the circuit board reached to 100.7 °C steady state temperature to prevent damage to

circuitry. In ET-M, aluminum edges were added to basic configuration of the heat dissipater and braid pieces were squeezed between the heater and the top face of the heat dissipater as shown in Figure 33. The temperature of the circuit board was reduced to 37.7 °C with an indirect contact. This result shows that, the heat dissipater design is very effective to reduce the heat by an indirect contact between the heat source and the heat dissipater.

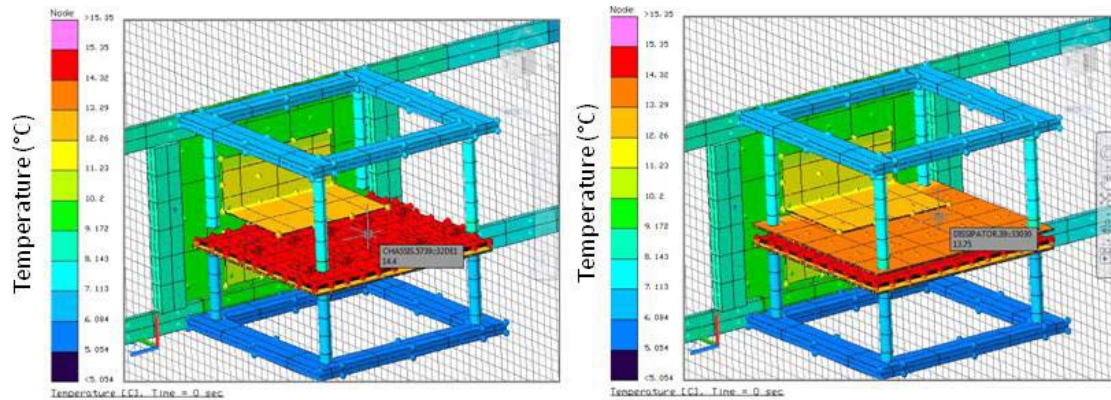
In ET-N, basic configuration of the heat dissipater was used and top face of the heat dissipater was placed directly on top of the single heater using a thermal conductive pad. The purpose was to determine the heat transfer effectiveness of the basic configuration in case of a concentrated thermal load. Table 11 shows that circuit board's temperature was measured as 25.2 °C in ET-N and it can be deduced that the basic configuration of the heat dissipater is very effective on concentrated thermal loads.

In ET-O, only the top face of the heat dissipater was used with THCB. The bottom face of the heat dissipater was removed from the basic configuration. The purpose was to determine the effectiveness of the heat dissipater's box shape with a comparison with ET-H. As discussed previously, the basic configuration of the heat dissipater reduced the circuit board temperature to 34.9 °C from 93.0 °C. However, temperature decreased to 69.5 °C in ET-O. Since the bottom face of the heat dissipater caused an additional 34.6 °C decrease in ET-H, it can be deduced that the box shape is very effective. The weight of one face of the heat dissipater with copper braids is 90 grams (a 10 cm x 10 cm x 0.1 cm copper plate, *bottom face*, and four 1.5 cm x 7 cm x 0.1 cm copper braids). Thus, it can be concluded that the increase in weight was worth the increase in capability of dissipating heat.

Since the ET-H design was assumed as the basic configuration with a black tape covered 1U size radiator, the thermal desktop model of the heat dissipater (CS-H) was adjusted to fit the ET-H data. The thermal braids were simulated as a one piece solid as shown in Figure 23 with the same length and the width of the real braids. Since four braids with 1.5 cm width used at the both faces, the braid model was created as one piece with 6 cm width. The thickness was reduced to simulate the effective thickness of the braids for conduction. Conductions were modeled using the contactor method with ray trace algorithm between the braids-the radiator and the braids-the heat dissipater. A ray trace algorithm shoots rays perpendicular from the “from surface” and deems the closest node to be whatever node ray first encounters as explained in the previous chapter. This algorithm is very fast and accurate between parallel surfaces. In view of the fact that the contactor calculates all surface area between the parallel surfaces for conduction, which is not realistic for this case, the conductivity values were determined less with respect to a contactor with solder intervening material. In ET-H, the soldered surface areas, which should be calculated for conduction, were smaller as shown in Figure 27 (b). Figure 44 shows the temperature color post-processing figures of CS-H and Table 12 presents the steady state temperature result comparison of ET-H and CS-H.



(a) Two Views of 4.5W CS-H



(a) Two Views of 1.8W CS-H

**Figure 44: The Temperature Color Post-Processing Figures of CS-H**

**Table 12: Steady State Temperature Result Comparison of ET-H and CS-H**

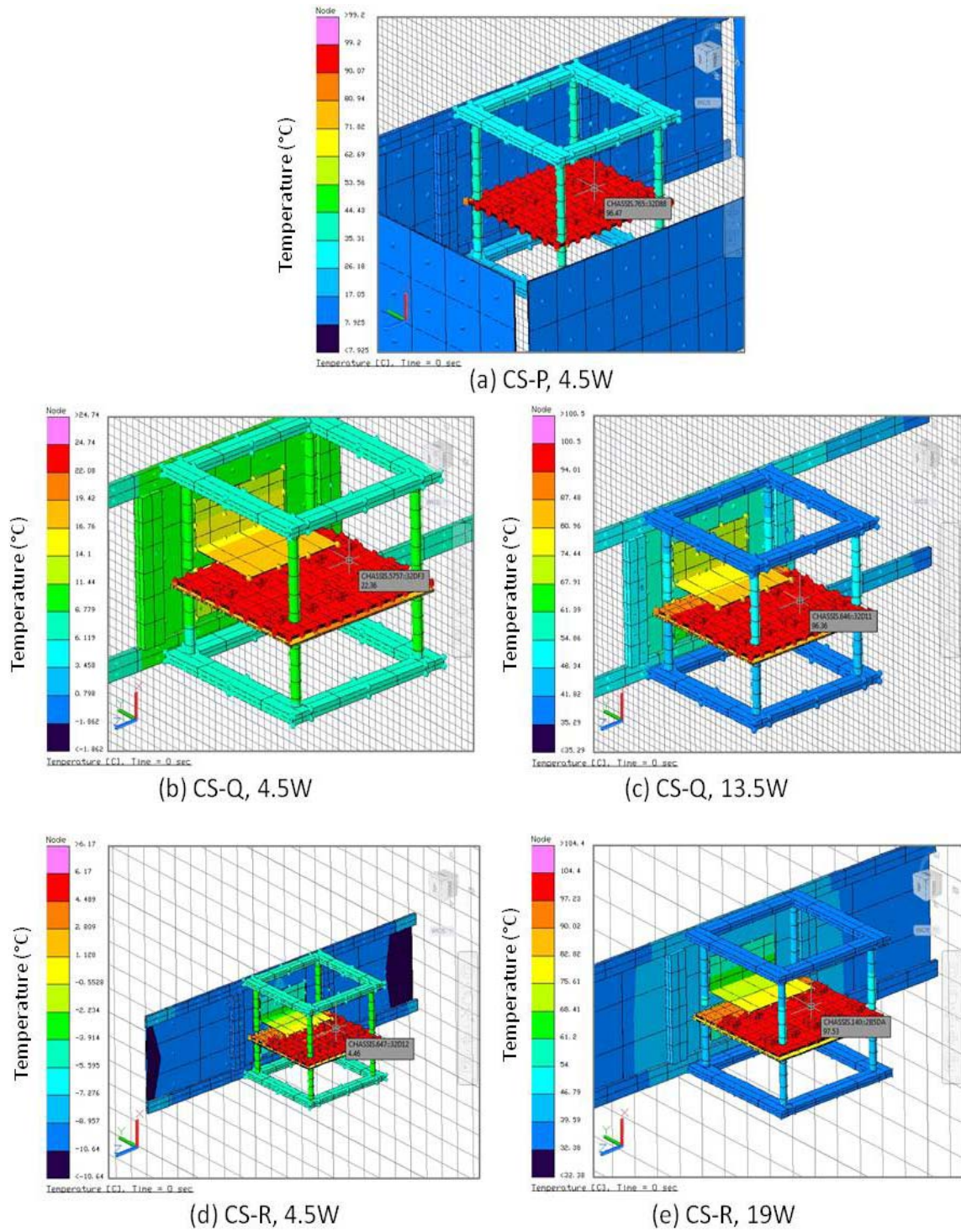
	ET-H at 4.5W (°C)	CS-H at 4.5W (°C)		ET-H at 1.8W (°C)	CS-H at 1.8W (°C)
Circuit Board Top Face	34.4/ 34.9	34.5		13.7/ 13.9	14.4
Heat Dissipater Top Face	33.7	33.6		13.7	13.8
Heat Dissipater Bottom Face	31.8	30.5		12.6	13.2
Radiator (Outside Face)	18.1	21.1		7.4	9.6
TVAC Plate	-15.3	-15.3		-9.3	-9.3
TVAC Shroud	-15.0	-15.0		-5.6	-5.6



Table 12 shows that the heat dissipater model was validated with an error below 3.0 °C at all power levels. This indicates that, the model is dependable to conduct further computational experiments such as orbit performance simulations.

### **Orbit Performance Simulation Results of the Heat Dissipater**

Two orbits were created and six orbital simulations were conducted on TD as explained in the previous chapter. Figure 45 shows the temperature color post-processing figures of CS-P, CS-Q, and CS-R and the circuit board steady state temperature predictions of the simulations are presented in Table 13.

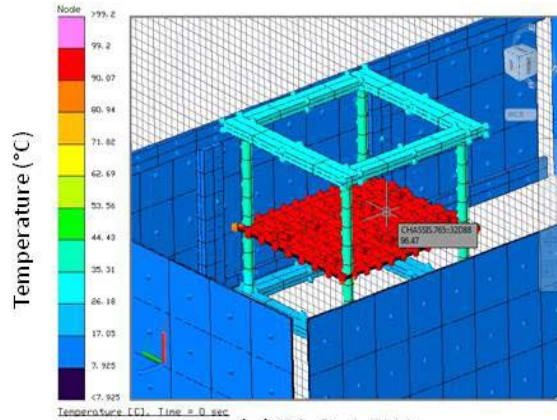


**Figure 45: Temperature Color Post-Processing Figures of CS-P, CS-Q, and CS-R**

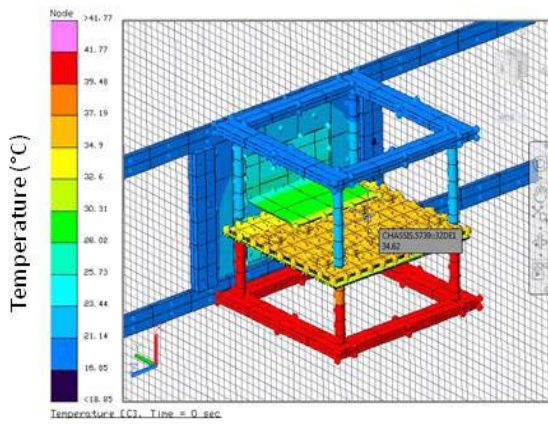
**Table 13: Steady State Temperature Predictions of CS-P, CS-Q, and CS-R**

	CS-P	CS-Q		CS-R	
Beta Angle	0°	0°		0°	
Heat Dissipater	-	✓		✓	
Radiator Size	-	1U (Black Tape Covered)		3U (Black Tape Covered)	
Power	4.5W	4.5W	13.5W	4.5W	19W
Circuit Board Temperature	96.5 °C	22.4 °C	96.4 °C	4.5 °C	97.5 °C

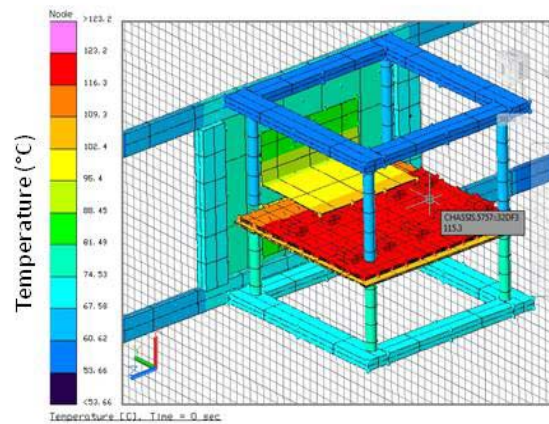
The temperature of the circuit board was predicted as 96.5 °C with 4.5W power on THCB, in the sample cold case orbit. In CS-Q, validated heat dissipater model was used and the circuit board temperature was decreased to 22.4 °C with 1U size black tape covered (black painted simulation) radiator. Assuming the 96.5 °C is the maximum operating temperature for this circuit board, the power can be increased to 13.5W using the heat dissipater, which means 300% increase in power capacity for this configuration. CS-P results shows that, using a 3U size black radiator, the circuit board temperature was reduced to 4.5 °C and the power can be increased to 19W without exceeding 96.5 °C. CS-P power result, 19W, is 420% of the original power. Figure 46 shows the temperature color post-processing figures of CS-S, CS-T, and CS-U and the circuit board steady state temperature predictions of the simulations are presented in Table 14.



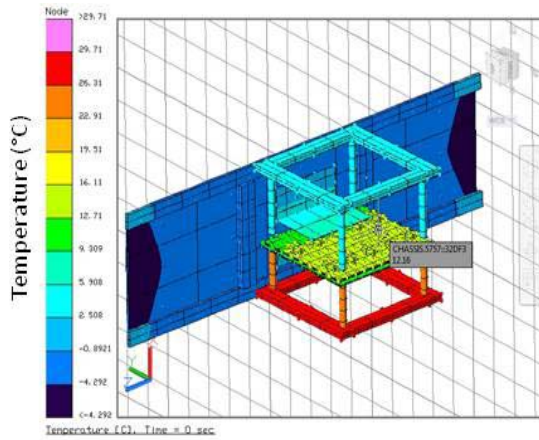
(a) CS-S, 4.5W



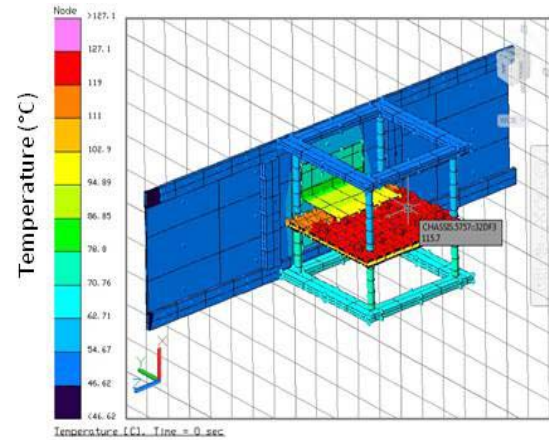
(b) CS-T, 4.5W



(c) CS-T, 15.5W



(d) CS-U, 4.5W



(e) CS-U, 22W

**Figure 46: Temperature Color Post-Processing Figures of CS-S, CS-T, and CS-U**

**Table 14: Steady State Temperature Predictions of CS-S, CS-T, and CS-U**

	CS-S	CS-T		CS-U	
Beta Angle	90°	90°		90°	
Heat Dissipater	-	✓		✓	
Radiator Size	-	1U (Black Tape Covered)		3U (Black Tape Covered)	
Power	4.5W	4.5W	15.5W	4.5W	22W
Circuit Board Temperature	116.8 °C	34.6 °C	115.3 °C	12.2°C	115.7°C

Three simulations were created with a sample hot case orbit. Circuit board temperature reached to 116.8 °C in this orbit without the heat dissipater. In CS-T, the circuit board temperature was reduced to 34.6 °C with the same power level of 4.5W. Assuming the maximum operating temperature is 116.8 °C, the power on the processors can be increased by 340% to 15.5W. In CS-U, the heat dissipater with 3U size radiator resulted in 12.2 °C temperature on the circuit board. Lastly, CS-U results showed that, assuming 116.8 °C is the maximum operating temperature in this case, power on the processors can be increased almost 490% to 22W level without exceeding the assumed maximum operating temperature.

### Summary

All data collected from the simulations and experiments were presented and the results were analyzed in this chapter. ET-A and CS-A results provided further validation to previously generated TVAC computational model. ET-D and CS-D results validated the sample CubeSat computational model. ET-E, F, G, H, I, J, K, L, M, and N results showed that the heat dissipater design is very effective in dissipating heat from various heat sources and it is possible to use the heat dissipater effectively with different

configurations, such as with various radiator sizes and with/without the aluminum edges. ET-O data showed that, the box shape heat sink design is much more effective than a design with only one plate on the heat source. ET-H and CS-H results validated the heat dissipater computational model. Finally, CS-P, Q, R, S, T, and U simulations proved that this heat dissipater gives valuable results on orbit, which is also a proof of the achievement of the objective of the thesis.

## **V. Conclusions and Recommendations**

This chapter presents the conclusions of the research. The objective is reviewed, demonstrating that it has been met. Advantages and weak points of the heat dissipater design are discussed. Finally, the recommendations for future work are presented.

### **Conclusions of Research**

The objective of this thesis was to develop a modular approach to dissipate heat from high power heat sources on a circuit board by using thermal control hardware in a sample CubeSat.

Since the previously generated TVAC environment computational model was validated only by using a 10 in x 10 in aluminum plate [Hatzung, 2014], this research provided data by conducting experiments and computational simulations with a more realistic test article, a sample 6U CubeSat chassis, (ET-A and CS-A) within TVAC. The steady state test points covered a large range of temperatures (-10 °C to 60 °C) within TVAC's temperature envelope. Experiment and simulation results were validated with a maximum steady state temperature error below 2.7 °C for all steady state test points. Thus, further validation for the TVAC model was provided.

Later, a circuit board with ten resistors (THCB) was placed in chassis and an experiment conducted in -15 °C TVAC (ET-B). Then, the same experiment was re-conducted with a sample CubeSat (ET-C). The chassis was covered with aluminum plates to simulate a fully enclosed sample CubeSat with heat sources. These two experiments showed that, expectedly, the resistors became much hotter when their open view to highly absorptive black painted TVAC shroud was obstructed by highly reflective aluminum plates. For example, even though the temperature of the top face of

the circuit board was measured as 92.2 °C at 6.3W power level in ET-B, it reached to 102.0 °C at 4.5W power in ET-C.

IR images of the THCB in ambient pressure showed that there was a roughly uniform heat distribution on the circuit board face, so two thermocouples were used in many experiments to acquire dependable temperature measurements of the circuit board face. The circuit board top face temperature was assumed as reference value in many experiments and simulations. The first reason was the difficulties of taking temperature measurements from the resistors, because of their sizes and shapes. The second reason, experiments showed that the resistor and the circuit board temperatures were very close to each other in steady state results. The sample CubeSat with THCB was modeled and validated by data of ET-D and CS-D, with a maximum steady state temperature error below 4 °C for two different power levels. These results showed that the sample CubeSat model was dependable to model a heat dissipater design.

Since the experiment results showed that the circuit board bottom face's temperature is very close to the top face, the heat dissipater was designed as a box shape to remove the heat using both faces. Additionally, this heat dissipater was designed to minimize or eliminate the high power heat sources thermal effect on the satellite's overall thermal management by preventing heat flow from the bottom face of the circuit board to other components of the CubeSat. Furthermore, ET-O results proved that, removing heat from a circuit board using both faces is much more effective than doing it with single face as expected.

The heat dissipater's top and bottom faces were made of copper, because of the advantage of thermal conductivity. They were designed as 10 cm x 10 cm x 1 cm plates.



Even though computational simulation results for the thicker plates were relatively more effective at dissipating heat, weight and mechanical strength were other factors that should be considered. When the copper plates were designed thicker, the weight became much higher because of the high density of copper. Since the main purpose of the edges is supporting the faces of the heat dissipater, instead of removing heat from the heat source, they were designed as aluminum to take advantage of the aluminum's low density and superior mechanical strength with respect to copper.

The heat dissipater box was connected to a radiator using copper braids, which are commonly used for ground wire applications. In this research, four braids with 1.5 cm width were used between each face of the heat dissipater box and the radiator. Braid amount can be adjusted for various cases with different power levels. Since many experiments were conducted with the heat dissipater, braids were designed relatively long (7 cm each) to simplify assembly. Since the soldered parts were no longer than 2 cm at each side (soldered parts between braids-radiator and braids-heat dissipater faces), this length was obviously a disadvantage for the heat transfer.

Even though the prototype was built using commercial copper plates and copper braids using for ground wire applications, and the computational models were designed based on these material properties, the experiment results showed that, the heat dissipater is very effective to dissipate heat from a circuit board containing heat sources in a CubeSat. For example, the design reduced the temperature of a circuit board with ten resistors from 93 °C to 34.4 °C at the 4.5W power level, with 1U size (10 cm x 10 cm) radiator, in -15 °C TVAC. In addition to this, it reduced the temperature of a circuit board with a single resistor simulating a concentrated heat load, with 3.3W applied of power,

from 100.7 °C to 25.2 °C, with 1U size radiator, in -15 °C TVAC. Undoubtedly, using higher thermally conductive materials, such as OFHC copper or graphite composites, can improve the results.

The connection technique of the thermal straps is also very important, as the comparison of ET-G and ET-H results showed. In the first place, thermal straps were soldered using a soldering iron. The circuit board temperature was reduced from 93 °C to 47.8 °C using the heat dissipater in a test configuration. However, when the braids were soldered with high temperature, using a blowtorch, the temperature was measured as 34.9 °C with the same test configuration, which is a proof of the importance of the connection quality of the thermal straps.

The design is also very effective when a direct contact between a face of the heat dissipater and the heat source is not possible. Using some thermally conductive materials, such as squeezed copper braid pieces, gave very good results. For example, first, a test conducted with a single resistor gave 100.7 °C on the circuit board without the heat dissipater. Then the heat dissipater reduced the temperature to 37.7 °C in the same test configuration, with an indirect contact between the resistor and the heat dissipater box. Since the heat dissipater gave the temperature result of 25.2 °C with a direct contact for the same heat source, it can be deduced that, better results can be acquired from indirect contact with intervening materials with higher conductivity.

The faces of the heat dissipater and the radiator inside the CubeSat were determined as bare copper because of the low IR optic properties of the copper. The reason was to minimize the heat flow into the CubeSat. On the other hand, some of the experiments were conducted to determine the effectiveness of surface finish of the

outside face of the radiator. As expected, the results showed that, optical properties of the outside surface of the radiator are very effective for the design success. For example, even though bare copper 1U size radiator resulted in 56.1 °C circuit board temperature for a test configuration, black tape covered same size radiator reduced the temperature 46.5 °C. Similarly, covering the 3U size radiator with black tape to simulate a black painted surface reduced temperature to 26.4 °C, from the bare copper radiator result of 43.9 °C. Even though the black photographic tape was used for this research to simulate black paint and improve the optical properties of the radiator, it is expected that, a polyurethane black paint coated surface minimizes the contact resistance and can yield better results.

Radiator size is another important factor for the design. ET-H and ET-J results showed that, if the CubeSat mission allows, the radiator size could be increased, such as 2U or 3U, to acquire better results for higher power processors. Even though it was not tested in this research because of the time constraints, more than one face of the CubeSat can be used for radiators and the heat dissipater can be connected to those radiators using thermal straps to deal with very high heat levels. It is also proved in the research that, using a deployable radiator is another alternative in case of high heat levels. However, it should be noted that, assuming there is very low conductivity through deployable radiator hinges, increasing the conductivity between the deployable radiator and the heat dissipater box is essential for better results. If relatively long straps are to be used between the heat dissipater box and the deployable radiator, materials with very high thermal conductivity may be selected to increase the performance.

Finally, orbit simulation predictions proved that the heat dissipater design is very successful to remove the heat in both sample cold case and hot case scenarios. The design is flexible enough to let the designer to pick a radiator size and number of straps, which gives the best results for the situation. In case of very high heat levels, deployable radiators are also preferable. The design is also very effective when a direct contact is not possible between the high power processor and the heat dissipater box. Consequently, this design is a modular approach to dissipate heat from high power heat sources on a circuit board in a CubeSat. It is capable to prevent excessive temperature condition for the heat-generating component and to minimize heat flow into the satellite. Due to its modularity, this design can be used in any 1U stack in a CubeSat.

### **Recommendations for Future Research**

The design could not be tested with various materials. Using materials with higher thermal conductivity, such as OFHC copper, instead of commercial copper plates in the box and radiator design would be a better option. Additionally, straps with higher thermal performance than copper ground wire braids would improve the affectivity of the design.

All experiments were conducted with 1 mm thick copper radiators in this research. Thicker radiator performance, especially for larger scale radiators, *2U and 3U*, and surface finish effect of the radiator are also important factors should be examined.

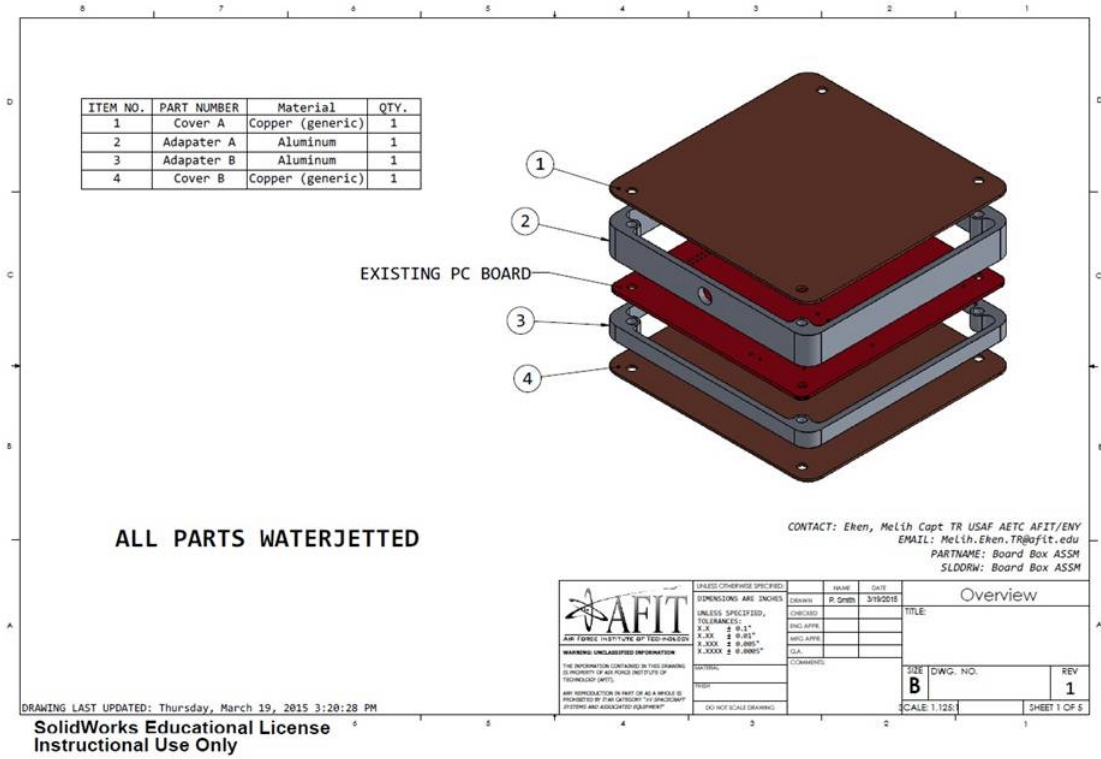
Thermal strap connections, such as bolting the straps using a highly conductive intervening material or using thermal paste, are another aspect would be searched. Using radiators on more than one CubeSat face to deal with very high temperatures would provide greater confidence to design. However, the thermal performance of relatively long straps would be another challenge in this configuration.

The heat dissipater design performance was determined only by using two different circuit boards in a sample 6U CubeSat. Experiments with various payloads in different size CubeSats would assure the modularity of the design.

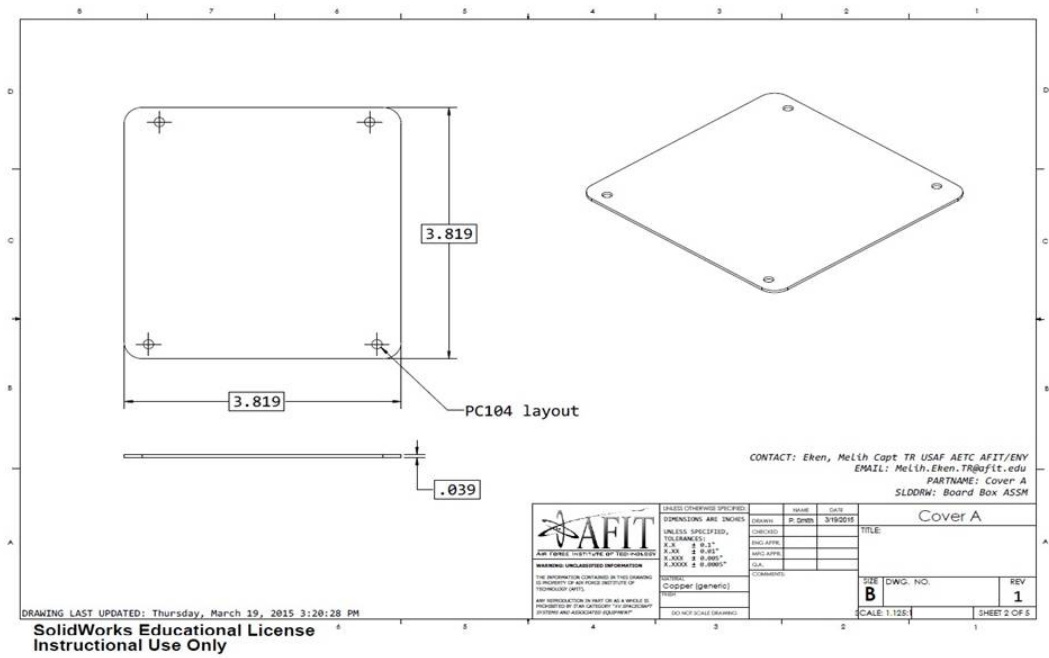
Finally, since a few computational simulations were conducted only to determine the mechanical strength of the heat dissipater design, it should undergo detailed computational mechanical analysis and physical testing to determine the flight acceptance level and the ability to operate on orbit.

## Appendix A: Technical Drawing of the Heat Dissipater Box

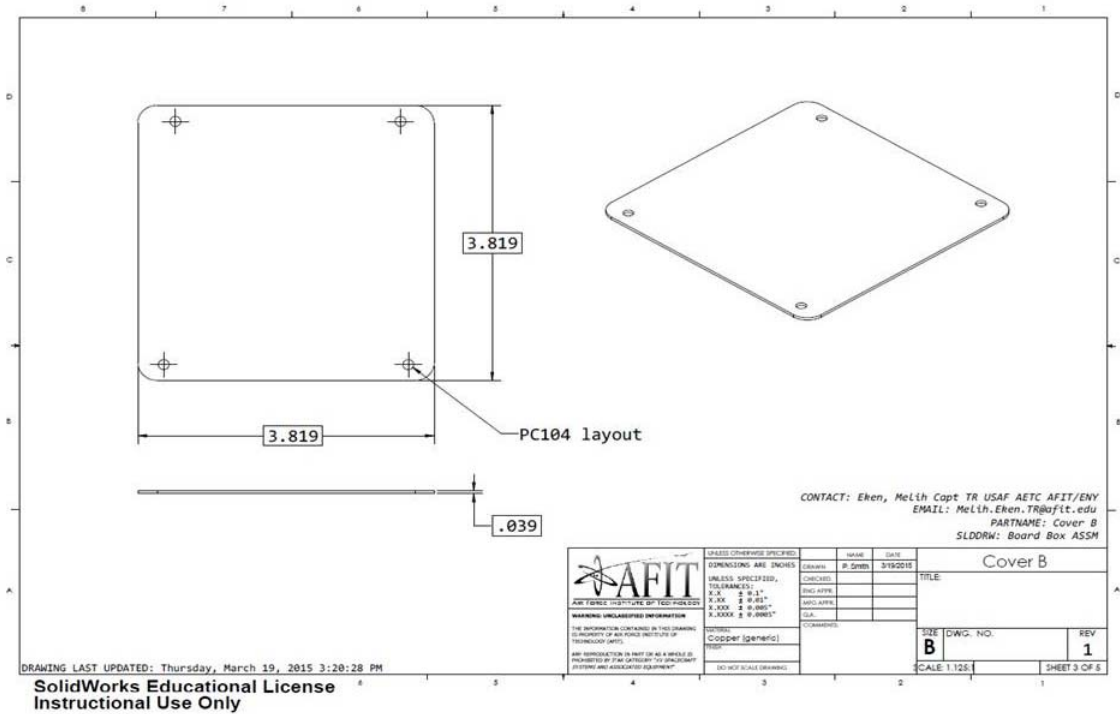
Technical drawing of the heat dissipater box is shown in Figure 47. All dimensions are in inches. Material of the faces (1 and 4) are copper and the edges (2 and 3) are aluminum.



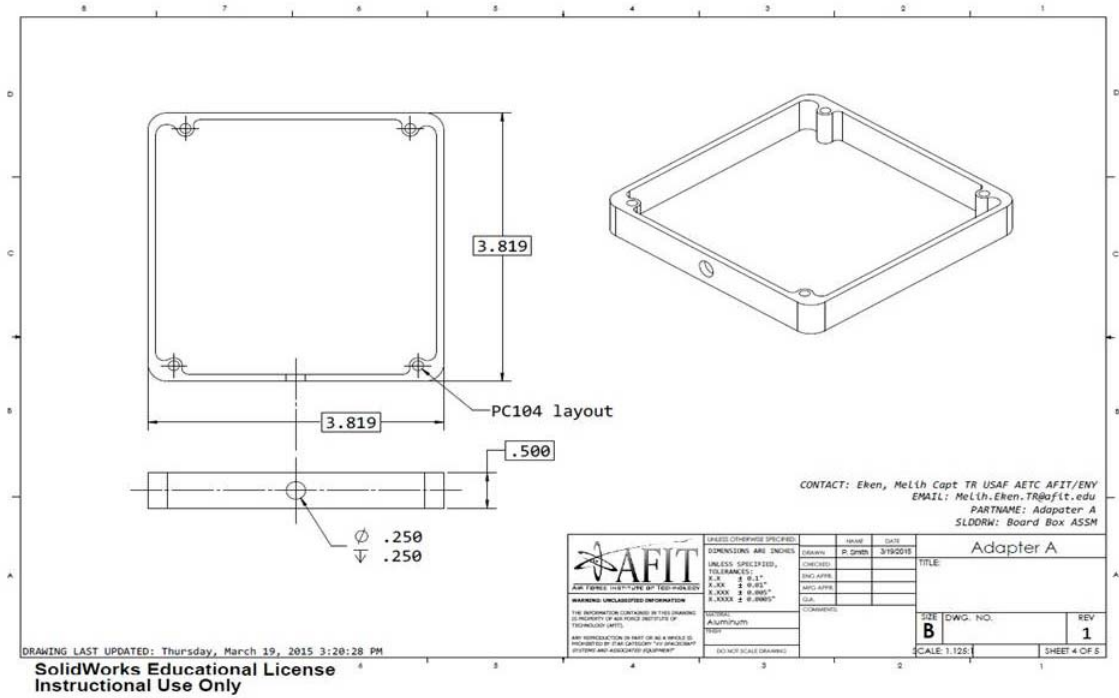
(a) Exploded View of the Heat Dissipater Box



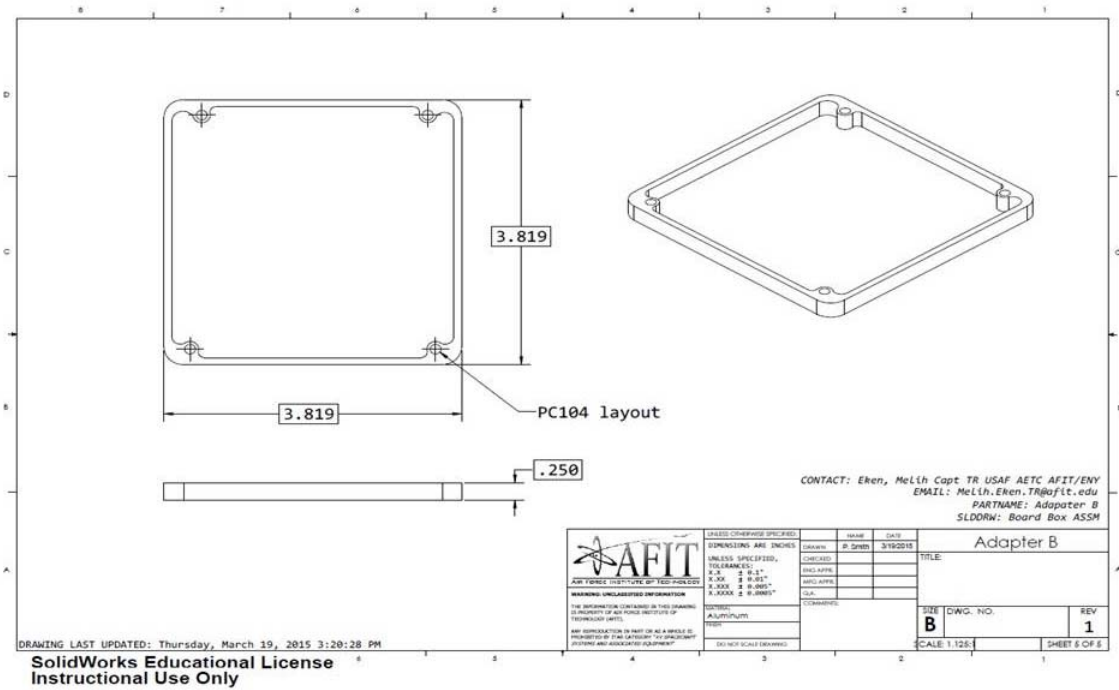
(b) The Top Face of the Heat Dissipater Box



(c) The Bottom Face of the Heat Dissipater Box



(d) The First Edge of the Heat Dissipater Box



(e) The Second Edge of the Heat Dissipater Box

Figure 47: Technical Drawing of the Heat Dissipater Box



## References

- 88<sup>th</sup> Air Base Wing. "Air Force, Small Business Developing Critical Processors for Satellites", *88<sup>th</sup> Air Base Wing Public Affairs*, January 2015.
- Asundi, Sharan A. and Fitz-Coy, Norman G. "CubeSat Mission Design Based on a Systems Engineering Approach," *Aerospace Conference*, 1-9. IEEE, 2013.
- Banks, B.A., De Groh, K.K., Miller, S.K., "Low Earth Orbital Atomic Oxygen Interactions with Spacecraft Materials." *Materials Research Society Symposium Proceedings*, 851: 331-342 (2004)
- Birur, G.C., Siebes, G., Swanson, T.D., *Spacecraft Thermal Control*, Lavergne: Academic Press, 2014.
- C&R Technologies. *Thermal Desktop® User's Manual: Version 5.6*. (April 2013)
- Czernik, S., *Design of the Thermal Control System for Compass-1*, MS Thesis, University of Applied Sciences, Aachen, Germany, August 2004.
- Diaz-Aguado, M. F., "Small Class-D Spacecraft Thermal Design, Test and Analysis – PharmaSat Biological Experiment," *Aerospace Conference*, 1-9. IEEE, 2009.
- Dinh, D.Q., *Thermal Modeling of NanoSat*, MS thesis, San Jose State University, San Jose CA, May 2012.
- Elhady, A.M., "Design and Analysis of a LEO Micro-Satellite Thermal Control Including Thermal Contact Conductance," *Aerospace Conference*, 1-11. IEEE, 2010.
- Evans, H., Lange, J., and Schmitz, J., *The Phenomenology of Intelligence-focused Remote Sensing 1<sup>st</sup> ed.*, Riverside Research, 2014.
- Gilmore, D. G. *Spacecraft Thermal Control Handbook Volume I: Fundamental Technologies*, El Segundo: The Aerospace Press, 2002.
- Grossman, E., Gouzman, I., Verker, R., "Debris/Micrometeoroid Impacts and Synergistic Effects on Spacecraft Materials." *MRS Bulletin*, 35: 41-47 (January 2010)
- Hatzung, D., *Thermal Characterization of the Air Force Institute of Technology Solar Simulation Thermal Vacuum Chamber*, MS thesis, Air Force Institute of Technology, Wright-Patterson AFB OH, March 2014.

- Heidt, H., Puig-Suari, J., Moore, A. S., Nakasuka, S., and Twiggs, R. J. "CubeSat - A new generation of picosatellite for education and industry low-cost space experimentation," *14<sup>th</sup> Annual/USU Conference on Small Satellites*, 2000 . [Online]. Available: <http://search.proquest.com/docview/27219077?accountid=26185> [Accessed 15 July 2014]
- Incropera, F. P., DeWitt, D. P., Bergman, T. L., and Lavine, A. S., *Fundamentals of Heat and Mass Transfer 6<sup>th</sup> ed.*, Hoboken: John Wiley & Sons, Inc., 2006.
- NASA Goddard Space Flight Center, *General Environmental Verification Standard*. GSFC-STD-7000A. Greenbelt: NASA Goddard, 2013.
- Ozisik, M. Necati, *Heat Transfer A Basic Approach*, McGraw-Hill, Inc. 1985
- Pumpkin Incorporated, CubeSat Kit Website, *Frequently Asked Questions*, 2013. [Online]. Available: <http://www.cubesatkit.com/content/faq.html> [Accessed 25 June 2015]
- Smith, K. D., *Environmental Testing and Thermal Analysis of the NPS Solar Cell Array Tester*, MS thesis, Naval Postgraduate School, Monterey, June 2011.
- Swartwout, M. "The First One Hundred CubeSats: A Statistical Look," *Journal of Small Satellites*, vol. 2, no. 2, 2014.
- Swartwout, M. *CubeSat Database Online*, 2015. [Online]. Available: <https://sites.google.com/a/slu.edu/swartwout/home/cubesat-database> [Accessed 14 April 2015]
- Wertz, J. R., Everett, D. F., and Puschell, J. J. *Space Mission Engineering: The New SMAD*, Hawthorne: Microprism Press and Springer, 2011.
- Wright-Patterson AFB. *Thermal /Vacuum Solar Simulation System Manual* (06 August 2013)

<b>REPORT DOCUMENTATION PAGE</b>				<i>Form Approved OMB No. 074-0188</i>	
<p>The public reporting burden for this collection of information is estimated to average 1 hour per response, including the time for reviewing instructions, searching existing data sources, gathering and maintaining the data needed, and completing and reviewing the collection of information. Send comments regarding this burden estimate or any other aspect of the collection of information, including suggestions for reducing this burden to Department of Defense, Washington Headquarters Services, Directorate for Information Operations and Reports (0704-0188), 1215 Jefferson Davis Highway, Suite 1204, Arlington, VA 22202-4302. Respondents should be aware that notwithstanding any other provision of law, no person shall be subject to a penalty for failing to comply with a collection of information if it does not display a currently valid OMB control number.</p> <p><b>PLEASE DO NOT RETURN YOUR FORM TO THE ABOVE ADDRESS.</b></p>					
<b>1. REPORT DATE (DD-MM-YYYY)</b> 28-07-2015		<b>2. REPORT TYPE</b> Master's Thesis		<b>3. DATES COVERED (From – To)</b> Sep 2013 – Jul 2015	
<b>TITLE AND SUBTITLE</b>  Modular Heat Dissipation Technique for a CubeSat				<b>5a. CONTRACT NUMBER</b>	
				<b>5b. GRANT NUMBER</b>	
				<b>5c. PROGRAM ELEMENT NUMBER</b>	
<b>6. AUTHOR(S)</b>  Eken, Melih, Captain, TurAF				<b>5d. PROJECT NUMBER</b>	
				<b>5e. TASK NUMBER</b>	
				<b>5f. WORK UNIT NUMBER</b>	
<b>7. PERFORMING ORGANIZATION NAMES(S) AND ADDRESS(S)</b> Air Force Institute of Technology Graduate School of Engineering and Management (AFIT/ENY) 2950 Hobson Way, Building 640 WPAFB OH 45433-8865				<b>8. PERFORMING ORGANIZATION REPORT NUMBER</b>  AFIT-ENY-15-S-73	
<b>9. SPONSORING/MONITORING AGENCY NAME(S) AND ADDRESS(ES)</b>  Intentionally left blank				<b>10. SPONSOR/MONITOR'S ACRONYM(S)</b>	
				<b>11. SPONSOR/MONITOR'S REPORT NUMBER(S)</b>	
<b>12. DISTRIBUTION/AVAILABILITY STATEMENT</b> <b>DISTRUBTION STATEMENT A.</b> APPROVED FOR PUBLIC RELEASE; DISTRIBUTION UNLIMITED.					
<b>13. SUPPLEMENTARY NOTES</b> This material is declared a work of the U.S. Government and is not subject to copyright protection in the United States.					
<b>14. ABSTRACT</b> <p>In recent years, due to their many advantages, interest in larger scale CubeSats, such as 3U and 6U, has been increased. Correspondingly, dissipating the heat from the heat generating components in the CubeSat has become a challenge for thermal control. In this research, a modular approach was developed to dissipate heat from the overheating components in a CubeSat. To accomplish this, both experimental and computational methodologies were used. A 6U CubeSat was computationally modeled and the model correlated by experimental test results. Subsequently, validated CubeSat thermal model was used to design a modular heat dissipater. Validation and performance experiments of the heat dissipater were conducted by using prototypes of the design. Finally, using the validated heat dissipater model, orbit performance predictions of the heat dissipater were conducted computationally. This heat dissipation technique was designed to prevent excessive temperatures for the heat-generating components and to minimize the heat flow into the CubeSat. Due to its modular approach, this design can be used in any 1U stack in a CubeSat.</p>					
<b>15. SUBJECT TERMS</b> CubeSat, Thermal Model, Thermal Vacuum Chamber, Heat Dissipation, Thermal Management, Modular, Small Satellite					
<b>16. SECURITY CLASSIFICATION OF:</b>			<b>17. LIMITATION OF ABSTRACT</b>  UU	<b>18. NUMBER OF PAGES</b>  129	<b>19a. NAME OF RESPONSIBLE PERSON</b> Maj James L. Rutledge, AFIT/ENY
<b>a. REPORT</b>  U	<b>b. ABSTRACT</b>  U	<b>c. THIS PAGE</b>  U			<b>19b. TELEPHONE NUMBER</b> (937) 255-6565, ext 4734 (james.rutledge@us.af.mil)